SECOND LAW ANALYSIS OF PREMIXED COMPRESSION IGNITION COMBUSTION IN A DIESEL ENGINE USING A THERMODYNAMIC ENGINE CYCLE SIMULATION

A Thesis

by

SUSHIL S. OAK

Submitted to the Office of Graduate Studies of
Texas A&M University
in partial fulfillment of the requirements for the degree of

MASTER OF SCIENCE

August 2008

Major Subject: Mechanical Engineering

SECOND LAW ANALYSIS OF PREMIXED COMPRESSION IGNITION COMBUSTION IN A DIESEL ENGINE USING A THERMODYNAMIC ENGINE CYCLE SIMULATION

A Thesis

by

SUSHIL S. OAK

Submitted to the Office of Graduate Studies of
Texas A&M University
in partial fulfillment of the requirements for the degree of

MASTER OF SCIENCE

Approved by:

Co-Chairs of Committee,	Timothy J. Jacobs
	Jerald A. Caton
Committee Members,	Adonios Karpetis
Head of Department,	Dennis O'Neal

August 2008

Major Subject: Mechanical Engineering

ABSTRACT

Second Law Analysis of Premixed Compression Ignition Combustion in a Diesel Engine Using a Thermodynamic Engine Cycle Simulation. (August 2008)

Sushil S. Oak, B.E., University of Mumbai

Co-Chairs of Advisory Committee: Dr. Timothy J. Jacobs
Dr. Jerald A. Caton

A second law analysis of compression ignition engine was completed using a thermodynamic engine cycle simulation. The major components of availability destruction and transfer for an entire engine cycle were identified and the influence of mode of combustion, injection timing and EGR on availability balance was evaluated.

The simulation pressure data was matched with the available experimental pressure data gathered from the tests on the Isuzu 1.7 L direct injection diesel engine. Various input parameters of the simulation were changed to represent actual engine conditions.

Availability destruction due to combustion decreases with advanced injection timing and under premixed compression ignition (PCI) modes; but it is found to be insensitive to the level of EGR. Similarly, trends (or lack of trends) in the other components of availability balance were identified for variation in injection timing, EGR level and mode of combustion. Optimum strategy for efficient combustion processes was proposed based on the observed trends.

DEDICATION

I would like to dedicate this thesis to my parents who have continuously provided encouragement to me. Their support has been instrumental in all of my endeavors. I would also like to dedicate this thesis to my brother who has been a source of motivation for me.

ACKNOWLEDGEMENTS

I would like to thank my committee chairs, Dr. Jacobs, and, Dr. Caton, for providing their useful views and comments during the completing of this work. Their guidance throughout the course of this project was instrumental in a timely completion of this work.

I would also like to thank my other committee member, Dr. Karpetis, for his cooperation that helped me in finishing this thesis.

TABLE OF CONTENTS

Page

Page

LIST OF FIGURES

FIGURE Page

FIGURE Page

FIGURE Page

FIGURE Page

FIGURE Page

FIGURE Page

LIST OF TABLES

1. INTRODUCTION

Internal combustion engines have a long history of development. Since their first use in a vehicle in 1886, there has been a growing number of vehicles and even off-road machines that have used internal combustion engines as the prime mover. Even though the earlier efforts in the development of engines were focused on efficiency and increasing power output, more recently the efforts have been aimed at reducing emissions. With more stringent emissions regulation of future, new modes of combustion are being sought to effectively reduce engine-out emissions with as little penalty on other performance parameters as possible.

Even though conventional compression ignition engines have thermodynamically superior efficiency than the spark ignition engines, diesel engines produce more nitric oxides (NOx) and particulate matter (PM) emissions. It is known that better fuel-air mixing helps in reducing PM emissions while lowering of combustion temperatures helps in reducing NOx emissions. New combustion modes attempt to achieve both these conditions simultaneously.

This thesis follows the format and style of *Journal of Automobile Engineering.*

1.1 New modes of combustion

The new modes of combustion that have caught attention of the recent researchers are homogeneous charge compression ignition (HCCI) combustion and premixed charge compression ignition (PCI) combustion modes.

In HCCI combustion mode, fuel and air are completely mixed prior to ignition. This is similar to the SI engine. But the ignition is initiated by compressing the cylinder charge to the temperatures above auto-ignition temperatures similar to the CI engines. As a result ignition occurs simultaneously at multiple locations inside the cylinder. The control of combustion process is more challenging in case of HCCI combustion mode.

In PCI combustion, air and fuel are not completely premixed, but the fuel is injected sufficiently before the desired start of combustion to create an all-premixed burn. Higher levels of EGR and leaner air-fuel mixtures are employed to increase ignition delay. Injection timing and injection pressures are adjusted such that they assist in achieving higher ignition delays. More fuel injected during longer ignition delay also gets more time to mix with the cylinder charge. Hence longer ignition delay assists in obtaining more premixed air-fuel mixtures. It is noted that even though initial burning takes place through premixed mechanism, the combustion is not entirely homogeneous. The fuel and air are not completely mixed prior to the start of combustion and hence even though PCI mode tends to be premixed, some very small fraction of diffusion controlled burning may also take place.

1.2 Implementation of exhaust gas recirculation (EGR)

This project is focused on PCI mode and hence application of EGR in relation to achieving PCI combustion mode is discussed in this section. As seen earlier, longer ignition delays are necessary in achieving PCI combustion mode. EGR is used as a primary means to achieve longer ignition delays.

EGR introduces inert species of exhaust products and at the same time lowers the oxygen concentration inside the cylinder. These two factors have pronounced effect on overall engine combustion and emissions. These two factors are instrumental in achieving more premixed burning and achieving low temperature combustion. As a result, application of EGR has been demonstrated by many researchers to reduce PM and NOx emissions significantly. The current study attempts to answer the aspects of application of high levels of EGR related to combustion efficiency from second law perspective.

1.3 Second law analysis of engine processes

Second law analysis gives a more complete analysis of engine processes as it helps in identifying the sources of irreversibilties. Second law analysis of an engine helps in quantifying these irreversibilities by introducing the concept of availability. Availability transfer and destruction in the engine processes and effects of various engine parameters on the availability balance gives additional insight into various losses and indications for improvements can be extracted from the second law parameters.

It is important to exploit second law parameters along with first law analysis for correct analysis of engine processes. For example first law analysis alone favors the use of excess air in spark ignition engines. This is because, the thermodynamic efficiency of the engine cycle increases with use of excess air. Excess air on the contrary makes the combustion conditions leaner and reduces the combustion temperatures. Hence less excess air is favorable from the second law perspective. As a result it is noted that, use of second law for engine analysis provides an added dimension to the study of the influence of an engine parameter on overall performance results.

Another important aspect of application of second law to engines is that it provides useful information which may not be obtained from the first law analysis alone. For example, use of turbocharger to increase pressure and temperature is found to decrease combustion availability destruction. Turbocharger thus offers a good means of extracting some fraction of exhaust availability.

2. MOTIVATION AND OBJECTIVES

Availability of experimental data for different modes of combustion was one of the motivations for selecting Isuzu 1.7 L direct injection engine for the current study. The experiments were conducted at the test cell of the Engine Systems Research of the General Motors Collaborative Research Laboratory at WE Lay Automotive Laboratory of the University of Michigan **[1]**.

The ability of the simulation to calculate second law parameters was another motivation, as it provided an opportunity to investigate the engine combustion processes from second law perspective to gain additional insight into the effects of mode of combustion, injection timing and EGR.

The objective of the current work is to complete a second law analysis of a compression ignition engine using a thermodynamic engine cycle simulation. Availability destruction and transfer during the entire engine cycle is calculated to quantify the results. Major sources of availability transfer and destruction are identified to be availability transfer through heat transfer and the exhaust, availability destruction due to combustion, availability destruction through intake mixing and availability unused due to unburned fuel. The remaining availability gets converted into indicated work. Analysis is carried out for two different modes of combustion, namely lean conventional (LC) and premixed compression ignition (PCI) combustion. Five LC and fifteen PCI cases are studied. The various tasks completed to achieve the overall objectives of this project are summarized below:

1. The first step involves matching the simulation parameters to closely resemble actual in-cylinder conditions. Thus, experimental pressure data is matched as closely as possible with the simulation pressure data to ensure same thermodynamic states between experiment and simulation.

2. Parametric sweeps of the relevant parameters are carried out to evaluate the influence of individual parameters on engine combustion processes and to gain insight into the differences between simulation model and actual engine combustion processes.

3. Finally, influences of EGR, injection timing and mode of combustion are evaluated from the second law perspective. Based on the above results, an optimum combustion strategy is proposed to reduce availability destruction due to combustion.

3. LITERATURE REVIEW

The effect of mode of combustion, EGR and injection timing on the availability balance for a compression ignition engine is the main objective of this project. All of the above factors play an important role in controlling the combustion process. Both the nature of combustion and the rate of combustion are affected by these factors. Hence the information about their individual effects on engine combustion can assist in determining the optimum combination of these parameters. In the past, attempts have been made to evaluate the effect of these parameters on the combustion characteristics such as ignition delay, combustion duration, peak temperature and premixed and diffusion controlled combustion fractions. These past efforts are summarized below.

Ignition delay is a very critical characteristic that affects engine performance and emissions characteristics. Naturally, many researchers have worked on evaluating the influence of ignition delay in altering the combustion process in an engine. EGR is demonstrated to have changed the length of ignition delay by some of the investigators. Zhang et al. **[2]** noted that EGR increases the ignition delay. They varied EGR levels from 0% to 45%. Dilution effect of EGR and lowered oxygen concentration were sought to be the major factors responsible for the increased ignition delay. They also noted that increased ignition delay increases the fraction of premixed burning and thereby affects the combustion characteristics. On the contrary a few researchers (Desantes et al. **[3]** and Jacobs et al. **[4]**) have found that the ignition delay is not varied by the change in EGR level. But they varied the EGR level from 0% to 20%. Thus it could be said that the

change in the ignition delay at lower EGR levels is smaller while ignition delay increases rapidly at higher EGR levels. This may be because of the increasing intake temperature offsetting the dilution effect caused by low EGR level. Nitu et al. **[5]** found that the ignition delay almost doubled when the EGR level was increased from 0% to 45%. Thus, it seems that higher EGR levels are required to achieve significant lengthening of ignition delay period.

Peak combustion temperature affects the emissions characteristics of an engine. The use of EGR in internal combustion engines is primarily used as a strategy to reduce nitric oxide (NOx) emissions. As there exists a close relationship between the combustion temperatures and emissions, efforts have been directed to determine the effect of EGR on peak temperatures. Desantes et al. **[3]** have shown that the peak temperature decreases with increasing EGR level primarily because of presence of exhaust gases that reduce the combustion rate. Presence of exhaust gases also decrease the ratio of specific heats (γ) thereby indirectly decreasing the temperature of the compressed gases.

EGR is found to decrease the heat release rate. Desantes et al. **[3]** found almost linear increase in combustion duration with increase in EGR level. EGR also affects the fraction of premixed and diffusion controlled burning. Nitu et al. **[5]** have shown that the combustion is predominantly premixed when the EGR level is around 45%. On the contrary, Desantes et al. **[3]** noted that the fractions of premixed and diffusion are not affected by the EGR level. Again it is worth noting that, the EGR levels studied by them are as low as 20%. But even with the low EGR levels they found that the peak heat

release rate decreases with increasing EGR level for both premixed and diffusion controlled burn periods.

Injection timing is also a critical parameter in controlling the combustion in an engine. Also it can be varied independently of EGR level. It controls the peak cylinder temperature and pressure by controlling the location of start of combustion. Influence of injection timing on the combustion process is analyzed by McTaggart-Cowan et al. **[6]**. They have noted that the late injection timing results in ending the combustion process sooner because of the low temperatures and pressures prevailing during the expansion stroke. They also suggested that the advanced injection timings are more suited for higher EGR levels as it achieves better emissions results along with higher efficiency.

Second law analysis for engine cycle processes was firstly used at around 1960. But most of the work related to second law analysis is carried out after around 1980s. Some of the efforts aimed at second law analysis of engine cycle are mentioned below. Rakopoulos and Giakoumis **[7]** showed that most of the in-cylinder availability destruction is associated with combustion availability destruction while availability destruction due to mixing processes account for less than 5% of the in-cylinder availability destruction. They also found that around 80% of the combustion availability destruction is associated with the heat transfer from hot reacting gases to the surrounding low temperature mixture. As a result, higher combustion temperatures reduce the fraction of availability destruction due to combustion. Flynn et al. **[8]** mentioned that combustion availability destruction is influenced by the timing and rate of heat release rate. Thus, injection timing and EGR level (as it affects rate of heat release) are two

important parameters that influence the availability destruction during combustion. Primus and Flynn **[9]** showed that the availability destruction increases with retarded injection timing and also with increasing combustion duration. Van Gerpen and Shapiro **[10]** on the contrary found that the combustion duration and shape of heat release curves have little impact on the total availability transfers and destructions. Some of the researchers have used Wiebe function for obtaining heat release profile and have studied the influence of Wiebe parameters on the availability balance. Gallo et al. **[11]** found that there is a reduction in irreversibility with increase in Wiebe parameter 'm'. Irreversibilities are also affected by the equivalence ratio. Kyritsis and Rakopoulos **[12]** demonstrated reduced combustion related availability destruction with leaner operations. They also found that the decrease in the combustion availability destruction results in corresponding increase in availability transfer either due to heat transfer or through exhaust.

The previous works on application of second law to engine processes are summarized below:

Combustion availability destruction was found to be the dominant source of in-cylinder availability destruction and hence most of the efforts are directed on reducing the combustion availability destruction. It has been shown that the combustion availability destruction is not affected significantly by the factors such as combustion duration, fraction of premixed burning and injection timing. Any decrease in combustion availability destruction was seen to accompany larger availability transfer due to heat transfer or exhaust and hence very little gain in indicated work could be realized.

None of these prior works have evaluated the effect of mode of combustion on the availability balance. The present study then aims at evaluating the comparison of different modes of combustion (Best BSFC, LC and PCI) along with the influence of EGR and injection timing from second law perspective. Thus, the present study offers a comprehensive analysis of engine combustion process.

4. OVERVIEW OF THERMODYNAMIC ENGINE CYCLE SIMULATION

A thermodynamic engine cycle simulation is used in the present work to analyze the various engine processes and to evaluate thermodynamic properties. It also generates the information necessary for a second law analysis and gives availability parameters for the different engine processes. The details about the formulation and solution algorithm used in the simulation can be found elsewhere **[13]**. This section is intended to present a brief summary of these details.

4.1 Theme of the simulation

The simulation is based on the zero dimensional thermodynamic model of the engine. The simulation relies extensively on the first law of thermodynamics and equation of state to correlate thermodynamic properties with different engine operating and design parameters. Being a zero dimensional model, the simulation does not give any spatial information such as concentration gradients or property gradients. But multiple zones are incorporated for the evaluation of thermodynamic properties during intake process and combustion process to enhance accuracy. The description of these zones is provided later in this section. Some of the key assumptions used in the simulation are:

1. The engine is assumed to be in a steady state. As a result, the same thermodynamic state is reached after one complete cycle. This fact is then

utilized during the iterative solution procedure to match the initial and final values.

2. The cylinder contents are assumed perfectly homogeneous for the compression, late expansion and exhaust processes.
3. During intake, the cylinder contents are assumed to be divided into two homogeneous zones – one containing a fresh charge while the other consisting of a residual charge.
4. Combustion process leads to the heterogeneity. Not only does it lead to new species but it also leads to property and concentration gradients. Hence it is assumed that the three zone model is more appropriate than a two zone model to represent the combustion process (Even though more zones are expected to generate more accurate solutions. In two-zone model, the cylinder contents are divided into two homogeneous parts, while in three-zone model, the cylinder contents are divided into three homogeneous parts. Hence dividing cylinder contents in multiple zones would help to take into account the steep property gradients).
5. All the gases occupying any zone at any stage in an engine cycle are assumed to obey ideal gas equation.
6. Combustion efficiency is assumed to be 100%.

4.2 Description of different zones used in the simulation

4.2.1 One-zone formulation

As stated above, one zone formulation is applied to compression, late expansion and exhaust processes. The first law of thermodynamics for one-zone formulation is given as:

$$\frac{dE}{dt} = \frac{\delta Q}{dt} - \frac{\delta W}{dt} + \frac{d\,\mathrm{m}_{\mathrm{in}}}{dt} h_{in} - \frac{dm_{out}}{dt} h_{out} \tag{1}$$

The above equation is expanded to get the expression for the bulk gas temperature which in turn is used to get the pressure using ideal gas equation.

4.2.2 Two-zone formulation for intake process

A two zone formulation is used during the intake process. One zone is used for the fresh charge and the other for the residual gases. The energy equations used in this case are essentially the same as equation (1) above. But the presence of two zones makes the expression for the bulk gas temperature more complex. In addition to the energy equation, mass conservation equation is used to derive the instantaneous mass contained in each zone. Mixing of the fresh charge with the residual gases is dictated by the inlet flow rate.

4.2.3 Two-zone formulation for combustion process

Before applying energy and mass conservation equation to the three-zone model, the equations are applied to the two-zone model. The two zones considered are burned zone and an unburned zone. The burned zone consists of the products of combustion. As

the flame propagates forward, more and more of the cylinder charge is combusted, and as a result, the burned zone mass increases while the unburned zone mass decreases. Hence the process can be viewed as a mass transfer from the unburned zone to the burned zone.

Hence the energy equations for these two zones can be written as:

$$\frac{d(mu)_b}{d\theta} = \frac{\delta Q_b}{d\theta} - \frac{dV_b}{d\theta} + \frac{dm_b}{d\theta} h_u \tag{2}$$

$$\frac{d(mu)_u}{d\theta} = \frac{\delta Q_u}{d\theta} - p\frac{dV_u}{d\theta} + \frac{dm_u}{d\theta} h_u \tag{3}$$

Above two equations along with the conservation of mass and ideal gas equation lead to the expressions for the derivatives of temperatures and volumes of these two zones as well as the derivative of the pressure. Hence the solution to the set of five simultaneous ordinary differential equations is sought.

4.2.4 Three-zone formulation for combustion process

As discussed above, the combustion process leads to the heterogeneity. This is a primary motive for using three zones for the combustion process. In this approach, the burned zone is further subdivided into two zones – an adiabatic core zone and a boundary layer zone that surrounds the adiabatic core zone. Even though these two sub-zones are assumed to be homogeneous, this formulation helps the accuracy of the calculations primarily because of the two reasons. Boundary layer zone surrounds the adiabatic core zone and mainly occupies the region close to cylinder wall. Hence the temperature of the boundary layer zone (which is lower than the temperature of the

adiabatic core zone) influences the amount of heat transfer. Thus, this helps in better accounting of heat transfer. Secondly, the adiabatic core zone being at the higher temperature and also being responsible for the NO formation, this formulation leads to more accurate NO emission calculations. The mass transfer takes place from the unburned zone to the adiabatic core zone (as flame propagates) and from the adiabatic core zone to the boundary layer zone. The energy equations for these two sub-zones thus take the following form:

$$\frac{d(mu)_a}{d\theta} = -p\frac{dV_a}{d\theta} + \frac{dm_b}{d\theta}h_u - \frac{dm_{bl}}{d\theta}h_a \tag{4}$$

$$\frac{d(mu)_{bl}}{d\theta} = \frac{\delta Q_b}{\delta\theta} - p\frac{dV_{bl}}{d\theta} + \frac{dm_{bl}}{d\theta}h_a \tag{5}$$

The mass transfer from the adiabatic core zone to the boundary layer zone is dictated by the energy conservation equations (equation (4) and (5)) and mass conservation equations. The temperature of the boundary layer zone is arrived at by using the logarithmic relation as follows:

$$T_{bl} = \frac{T - T_{wall}}{\ln(T_a / T_{wall})} \tag{6}$$

Finally, use of ideal gas equations for these sub-zones along with mass and energy conservation equations lead to the set of six ordinary differential equations. Even though these ordinary differential equations can be formed so as to solve for different combinations of the unknowns, the most stable set of ordinary differential equations are solved for derivative of temperatures, volumes and mass of these two sub-zones. Thus

the solution to the set of six simultaneous ordinary differential equations is sought. The sub-models and the solution procedure are described in the subsequent sections.

4.3 Sub-models used for solving the set of ordinary differential equations

4.3.1 Chemical kinetics

It is essential for the accuracy of the solution that the correct thermodynamic property values are used. These properties include specific internal energy, specific entropy, specific gas constants etc. Hence in order to ensure that the correct thermodynamic property values are used, one must ensure that the correct composition of the cylinder content is evaluated. Equilibrium concentrations of the different species are determined for temperatures above a certain value (typically, 1200 K). If the temperature is below this value then it is assumed that the concentrations of the species are not affected by the chemical reactions as these reactions either stop or proceed very slowly at lower temperatures. Once the composition is determined accurately, the thermodynamic properties for every species can be determined from the thermodynamic data. The bulk properties can then easily be evaluated.

4.3.2 Combustion model

The simulation uses the Wiebe function for heat release modeling. The Wiebe function relates the fraction of fuel mass consumed to the burn duration as follows:

$$x_b = 1 - \exp(-ay^{m+1}) \tag{7}$$

where,

$$y = \frac{\theta - \theta_0}{\theta_b} \tag{8}$$

θ is an instantaneous crank angle location

θ_0 is the crank angle corresponding to the start of combustion, and

θ_b is the burn duration.

And,

$$x_b = \frac{(m_f)_{burned}}{(mf)_{total}} \tag{9}$$

i.e. x_b shows the fraction of total fuel mass burned from start of combustion to the present time step.

Parameters "a" and "m" are used to control combustion rate. A detailed description of Wiebe function and influence of the parameters used in this function are given in section 3.

4.3.3 Heat transfer model

The heat transfer to or from the cylinder is given as:

$$\frac{\delta Q}{d\theta} = h_c A(\theta)(T_{wall} - T_{avg}) \tag{10}$$

For two or three zone model, the heat transfer from the individual zones is calculated using the same equation. But the area term ($A(\theta)$) is calculated for each zone separately based on the volume occupied by the zone.

Also, in order to take into consideration the differences in the temperature of different zones, a formulation is presented such that the zones with lower temperatures are assigned smaller fraction of the total heat transfer. For example, for unburned zone heat transfer this results into:

$$\frac{\delta Q_b}{d\theta} = \frac{\delta Q_u}{d\theta} - \frac{\delta Q_{total}}{d\theta} \tag{11}$$

The convective heat transfer coefficient (h_c) in equation (10) is determined using Woschni correlation **[14]**.

4.3.4 Fluid mechanics model

The flow through the intake and exhaust manifolds is assumed to be one-dimensional and isentropic. An empirical discharge coefficient is used to simulate practical losses during the flow. Open flow area is calculated from the valve diameter and valve lift profile.

For this study, the simulation makes use of sinusoidal valve lift profile. Maximum lift for the inlet valves is 7.8 mm and that for the outlet valves is 8 mm. There are two inlet valves and two outlet valves per cylinder. The simulation also needs the timing of the valve opening and closing periods to calculate the instantaneous flow rate. For this study, the inlet valves open at 354° aTDC and close at -136° aTDC. Exhaust valves open at 122° aTDC and close at 366° aTDC. This gives rise to a valve overlap period of 12 degrees.

4.4 Solution procedure

Application of mass and energy conservation equations along with the equation of state to different zones in the cylinder results in a set of simultaneous ordinary differential equations. In addition to that, various thermodynamic property variables appearing in these equations are dependent on the solution to these ordinary differential equations. This calls for the iterative solution procedure. The simulation makes use of iterative Euler technique. The boundary conditions are specified through inlet and exhaust temperature and pressure. Some of these values are not known beforehand. Thus simulation uses the guessed starting values to begin iterations. Based on the steady state assumption, the iterations are terminated when the start and end thermodynamic states are within specified tolerance.

5. OVERVIEW OF DIESEL ENGINE OPERATING PARAMETERS

The experimental data used for the comparison with the simulation results in this project is obtained from the experiments conducted on an Isuzu 1.7 liter direct injection diesel engine. Even though the results from the experiments are compared in the subsequent sections, performing the experiments were not part of the project and hence only a description of the engine relevant to the current work is provided without reference to the experimental set up. Only a brief description of the experimental measurements of the relevant properties and parameters is described in the present section. A reader can refer to the dissertation **[1]** for more information on the engine and the experimental set up. On the contrary, a more detailed description of the simulation input parameters and their influence on the pressure trace is given in this section and in section 3.

5.1 Diesel engine specifications

The geometric and other operating parameters of the engine are listed in Table 1. The engine is 4-cylinder in-line engine with direct injection. Other hardware used in the experiments includes fuel injection system, turbocharger and instrumentation for experimental measurements. A brief description of these components is presented in this section.

5.1.1 Fuel injection system

This engine made use of a common rail fuel system. The rail pressure can be varied between 100 bar to 1400 bar. A rail pressure of 100 bar is employed for lean conventional (LC) combustion and that of 1000 bar is employed for premixed compression ignition (PCI) combustion. Single injection was used in all the experiments. The injector is centrally located in a cylinder.

Table 1 Diesel engine specifications

Item	Value
Number of cylinders	4
Bore (mm)	79
Stroke (mm)	86
Displaced Volume (dm^3)	1.7
Compression Ratio	16
Inlet Valves (2/cyl):	
Diameter (mm)	27.5
Max Lift (mm)	7.8
Opens (°CA aTDC)	354
Closes (°CA aTDC)	-136
Exhaust Valves (2/cyl):	
Diameter (mm)	26.5
Max Lift (mm)	8.0
Opens (°CA aTDC)	122
Closes (°CA aTDC)	366
Valve Overlap (degrees)	12°
Fuel	Swedish Diesel
AF_{stoich}	14.73
Fuel System	Direct-Injection Common Rail
Injector Location	Centrally mounted
Injector Nozzle Number of Holes	6
Injector Nozzle Spray Angle (deg)	150
Turbocharger	Variable Geometry Turbocharger

5.1.2 Variable geometry turbocharger (VGT)

A VGT is used to control the exhaust gas recirculation (EGR) level. Changing the position of vanes of the VGT offers variable flow area. This helps in developing desired pressure difference between the exhaust and inlet manifold necessary to route required amount of EGR back into the cylinder. Hence EGR is an addition to the inlet fresh air supply. PCI cases are exceptions to this, as inlet air flow rate is slightly reduced in these cases in order to achieve a high EGR level employed in PCI cases (PCI cases use around 40% EGR)

5.1.3 Experimental measurements

Table 2 summarizes various parameters measured along with the type of equipment used for corresponding measurements. The calculated uncertainties are also provided in this table. A reader can refer to the dissertation **[1]** for the details of these uncertainty calculations and for additional information on the equipments used.

5.2 Nomenclature

Three different types of cases are analyzed in the present work. The description of these cases is provided later. The nomenclature used to identify these cases is described in this section.

The three different types (modes) of combustion are Best BSFC, LC and PCI modes. Among these three types, LC cases are subdivided based on injection timing and PCI cases are subdivided based on the injection timing and the exhaust gas recirculation

(EGR) level used. Thus, there is a need of a systematic naming scheme to identify each individual case uniquely and clearly. The scheme followed is explained through the examples. Consider a case named PCI_42_9. This shows that the case is of PCI type. Further, the first number (42 in this case) represents the percentage of EGR used. The second number shows the injection timing in degrees before top dead center (bTDC). In case of LC, only one number (indicating the injection timing) is necessary to identify each individual case. Thus a case of LC type with injection timing of 15° before TDC would be designated as LC_15.

Table 2 Summary of experimentally measured parameters

Item	Instrument	Uncertainty
Speed	Eddy Current Sensor	+/- 5 RPM
Torque	Load Transducer	+/- 2.48 N-m
Fuel Flow Rate	Frequency Pulse	+/- 2.7×10^{-3}
Air Flow Rate	Laminar Flow Element & Differential Pressure Sensor	+/- 0.516 g/s
Non-cylinder Pressures	Strain Gauge Pressure Transducer	+/- 4.14 kPa
Temperatures	K-Type Thermocouples	--
Exhaust Species Measurement:		
CO	NDIR (AVL CEB II)	< 7%
CO2	NDIR (AVL CEB II)	< 7%
O2	Paramagnetic (AVL CEB II)	< 7%
NOx	Chemiluminescent (AVL CEB II)	< 7%
NO	Chemiluminescent (AVL CEB II)	< 7%
HC	FID (AVL CEB II)	< 7%
CH4	FID (AVL CEB II)	< 7%
In-cylinder Pressure	Piezoelectric Transducer	+/- 0.25 bar

5.3 Set of inputs for the simulation

Some of the inputs used in the simulation are selected based on the measured values from the corresponding experiments, for example geometrical parameters, EGR level used, etc. But for some of the inputs, values are selected so as to represent actual experimental conditions as closely as possible. Table 3 shows these input and other parameters used in the simulation.

It is noted that the difference exists between the actual fuel used (Swedish fuel) and the fuel type used for simulation calculations (C_7H_{14}). Thus, it is essential to compare the critical properties of these fuels that may influence combustion calculations. Table 4 presents the comparison of selected properties of these two fuels. It is seen that the lower heating value, density and stoichiometric air-fuel ratio of these two fuels are very close. Most importantly, the lower heating value and stoichiometric air-fuel ratio affect combustion calculations. Hence it can be assumed that the modeling of actual fuel as C_7H_{14} would not introduce major errors in overall combustion calculations. Even though no information on the Cetane number is obtained for C_7H_{14}, any difference in the Cetane number, if exists, would not affect combustion calculations as the simulation does not incorporate the influence of Cetane number (which is manifested in the ignition delay). The simulation on the contrary, uses Wiebe function and burn duration to calculate the instantaneous heat release. This difference is highlighted in the next section in relation to the discussion on the mode of combustion.

Table 3 Input and operating parameters used in the simulation

Item	Value	Description
Fuel (approximate average)	C_7H_{14}	Actual Fuel would be more complex in terms of chemical structure. The actual fuel would be a mixture of several hydrocarbons. But C_7H_{14} is used in the simulation as a fuel so as to closely follow the actual fuel type.
AF_{stoich}	14.71	As per the choice of the fuel as C_7H_{14}
Inlet Pressure (kPa)	Varies	Inlet pressure is chosen such that the simulation pressure trace closely follows the experimental pressure trace for the motoring portion of the curve.
Exhaust Pressure (kPa)	Varies	Known from the experimental measurements.
Engine Speed (rpm)	1500	Known from the experimental measurements
CA of combustion start, θ_0	Varies,	It is varied to obtain the best fit to the experimental pressure trace.
Combustion duration (°CA)	Varies	It is varied to obtain the best fit to the experimental pressure trace.
Wiebe Parameters ("a" and "m")	Vary	Wiebe parameters are chosen as per the mode of combustion to vary the combustion rate.
Exhaust Gas Recirculation	Varies	It is a known quantity for every case.
Cylinder Wall Temp(K)	500	Known from the experimental measurements.
Fuel LHV (kJ/Kg)	43,545	Fixed for a chosen fuel (i.e. C_7H_{14})
Equivalence Ratio	Varies	Known from the experimental measurements
EGR Inlet Temperature	Varies	Known from the experimental measurements
Inlet Air Temperature	Varies	Known from the experimental measurements.
Compression Ratio	16	It is fixed for the given engine and hence same for all the cases. The actual value is determined by matching the motoring portion of the experimental pressure trace.

Table 4 Comparison of properties of actual fuel with C_7H_{14}

Property	Swedish Diesel	C_7H_{14}
Cetane Number	51.6	unknown
Lower Heating Value (MJ/Kg)	43.48	43.54
A/F Stoichiometric	14.74	14.71
Density(Kg/m^3)	810	758

It is seen from Table 3 that the parameters that are not fixed (i.e. either not known from the operating conditions or the experimental measurements) are:

i. Inlet pressure

Inlet pressure affects the inflow of fresh air charge in the cylinder. This in turn affects the actual air-fuel ratio inside the cylinder. The air-fuel ratio is an important parameter in the control of combustion processes and hence modification in the inlet pressure can help in achieving desired combustion strategy. For example, in the context of this study, the LC cases have higher inlet pressure than the PCI cases. Lower inlet pressures are used for PCI cases in order to decrease air flow rate slightly in order to achieve higher EGR levels.

ii. Start of combustion

Simulation uses start of combustion to mark the commencement of combustion processes. As the simulation is used for the analysis of diesel engine combustion in this study, the start of combustion is not known beforehand. The ignition delay follows the commencement of fuel injection. The ignition delay depends on several different parameters such as EGR level, equivalence ratio, injection pressure, injection timing.

iii. Combustion duration

The simulation uses a Wiebe function for heat release modeling. A feature of the Wiebe function is that it gives almost 100% fuel burning. The combustion duration represents the duration from the start of combustion to the crank angle corresponding to almost 100% fuel burning. It is to be noted that the combustion duration is a user input and the use of Wiebe function results in a small fraction of unburned fuel at the end of the combustion duration. Hence it can be seen that the combustion duration has a significant effect on the rate of heat release making it a critical parameter in combustion modeling.

iv. Wiebe parameters

Simulation uses the Wiebe function introduced in the earlier section (equation 7). The Wiebe function always gives an 'S' shaped mass fraction burn curve. The Wiebe parameters are used to modify the "shape" of this curve. The instantaneous heat release is obtained from the derivative of mass fraction burn curve. Hence by modifying the "shape" of the mass fraction burn curve, the Wiebe parameters change the distribution of the heat released during the combustion duration.

Parametric sweeps of these variables are carried out to determine their influence on the predicted in-cylinder pressure. In addition to the above parameters, sweeps for compression ratio are also carried out to confirm the actual compression ratio (As there is some uncertainty involved in deciding the actual compression ratio by experimental

tests). The discussion of the Wiebe parameters will be provided after different modes of combustion are introduced, in the next section.

5.4 Results for parametric sweeps

As discussed above, the values of some of the variables are not known beforehand. Thus, it is possible to have a number of different combinations of these parameters. It is thus beneficial to distinguish the individual effects of these input parameters on the pressure trace. This helps one to select the set of optimum values for these parameters depending upon the operating conditions. The results for these parametric sweeps are shown in the following figures. Results obtained for only five of the total 21 cases are shown for each parameter sweeps. Best BSFC, two LC and two PCI cases are chosen as representative cases.

5.4.1 Influence of start of combustion location

Figures 1 – 5 show the variation of pressure trace with change in start of combustion location. It is seen that in all the cases, retarding the start of combustion by 3° decreases the peak pressure by around 500 kPa. Similarly, advancing the start of combustion by the same margin increases the peak pressure by around 500 kPa. But the start of combustion does not affect the rate of rise of pressure. This is a direct consequence of the use of Wiebe function for the calculation of heat release. Equation 7 represents the Wiebe function.

It can be seen from equation 7 that the burn rate is governed by the burn duration θ_b and the instantaneous crank angle position θ. The start of combustion θ_0 does not have any influence on the rate of heat release. It only changes the location of the start of combustion thereby advancing or retarding the heat release. The selection of appropriate start of combustion would be dictated by the injection timing but it will not have significant influence on rate of combustion once combustion commences.

Slight variation in the rate of rise of pressure as seen from these figures may be attributed to the fact that, the in-cylinder conditions for a major portion of combustion process vary significantly with the change in start of combustion location. This fact has a direct consequence on the increase in pressure realized due to ongoing heat release. For example, the start of combustion close to TDC would result in higher rate of increase in pressure with the same heat release rate in comparison to rate of increase in pressure accompanying the heat release occurring further down the expansion stroke. During the expansion stroke, the increasing volume decreases the pressure and temperature. The heat being released by combustion would thus be utilized in heating the surrounding gases which are at comparatively lower temperatures. Hence, the retarded start of combustion would result in slightly lower rate of increase in pressure even though the heat release rates are equal for all start of combustion locations. Figures 1 – 5 support this notion.

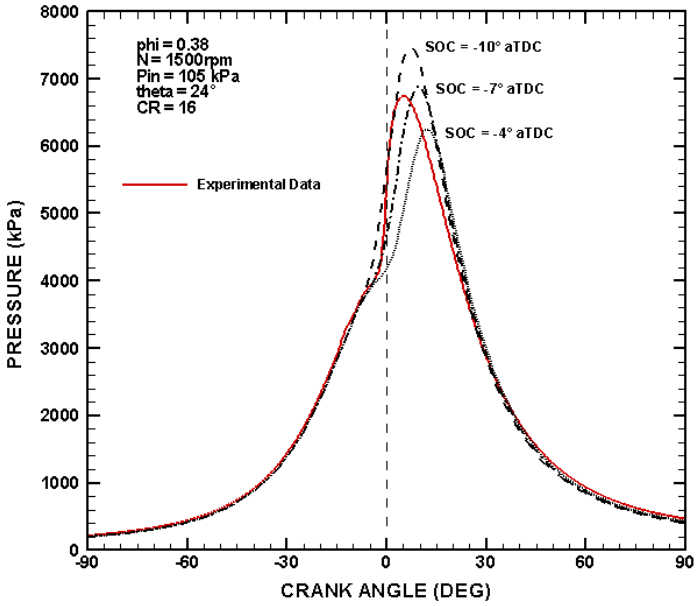

Fig. 1 Variation of pressure trace with change in start of combustion location for Best BSFC case.

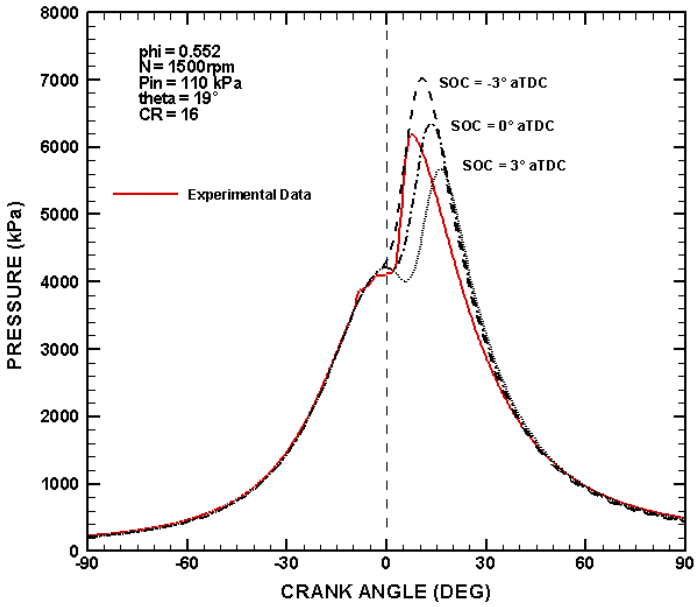

Fig. 2 Variation of pressure trace with change in start of combustion location for LC_10.

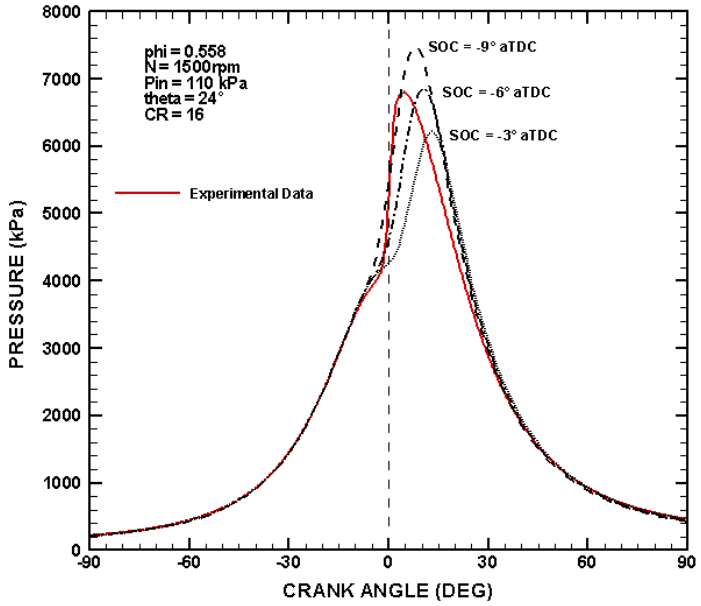

Fig. 3 Variation of pressure trace with change in start of combustion location for LC_15.

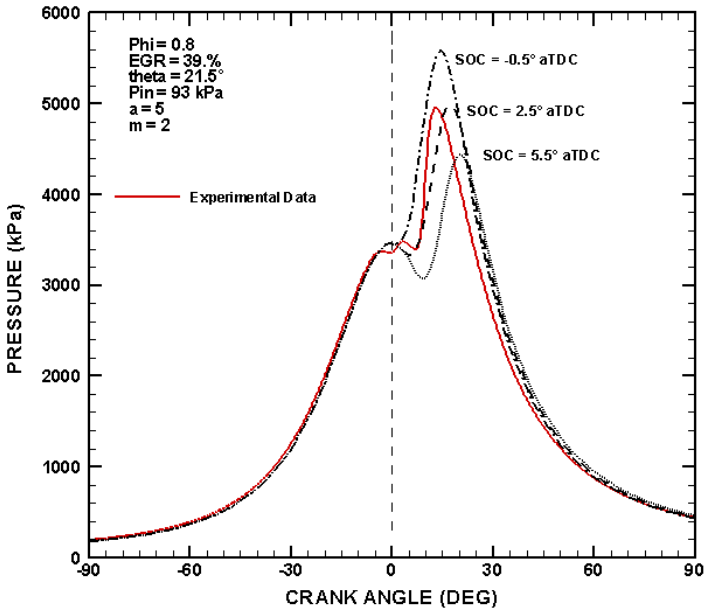

Fig. 4 Variation of pressure trace with change in start of combustion location for PCI_39_9.

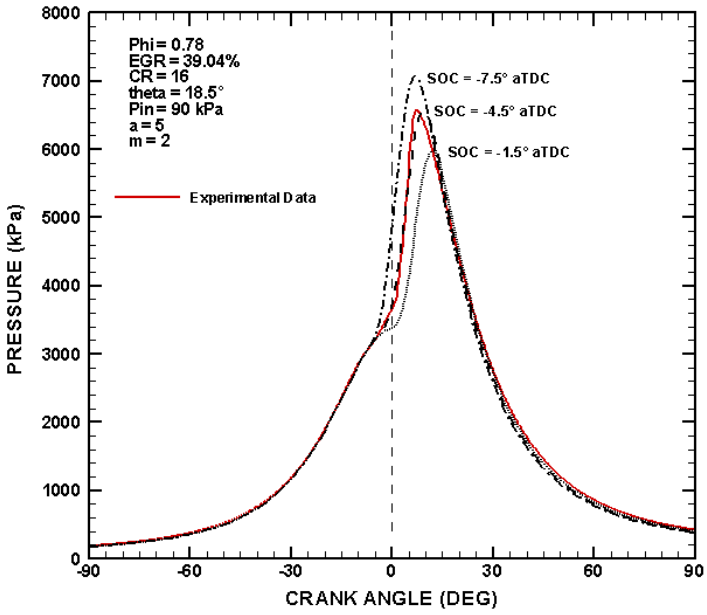

Fig. 5 Variation of pressure trace with change in start of combustion location for PCI_39_15.

5.4.2 Influence of burn duration

Figures 6 – 10 show the variation of pressure trace with burn duration. It is seen that when the burn duration reduces by 5°, the peak pressure increases by around 500 kPa. Increase in the burn duration by the same margin reduces the peak pressure by around 500 kPa. In addition to its effect on peak pressure, it is seen that, change in burn duration also affects the rate of rise of pressure. Thus burn duration influences rate of combustion. This again follows from the Wiebe function (equation 7). The observation of the Wiebe function suggests that the increasing burn duration decreases the heat release rate. This not only lowers the rate of rise of pressure but also reduces the peak pressure as seen from the figures 6 – 10. Another consequence of a lower heat release is

that, the total heat released is spanned over longer duration. Thus, the location of peak pressure is retarded with increasing burn duration.

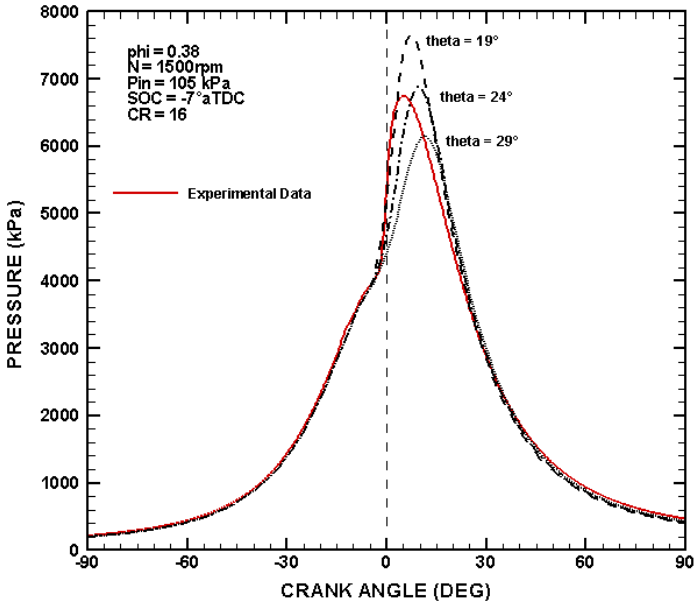

Fig. 6 Variation in pressure trace with burn duration for Best BSFC case.

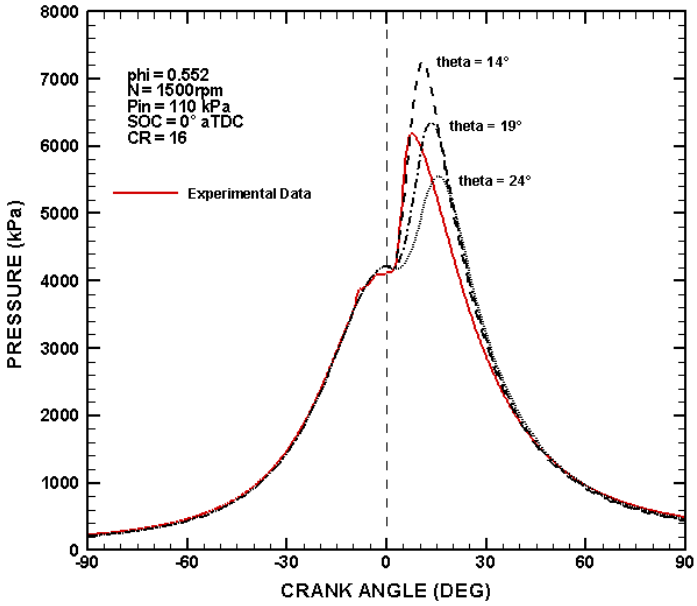

Fig. 7 Variation in pressure trace with burn duration for LC_10.

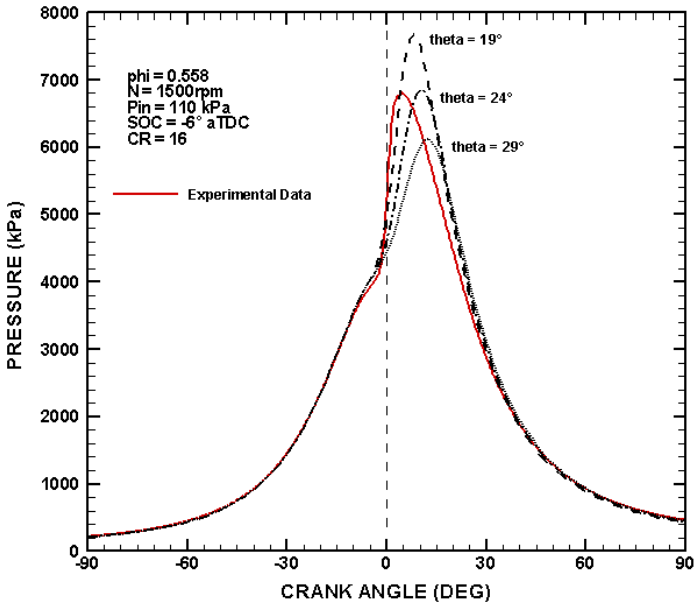

Fig. 8 Variation in pressure trace with burn duration for LC_15.

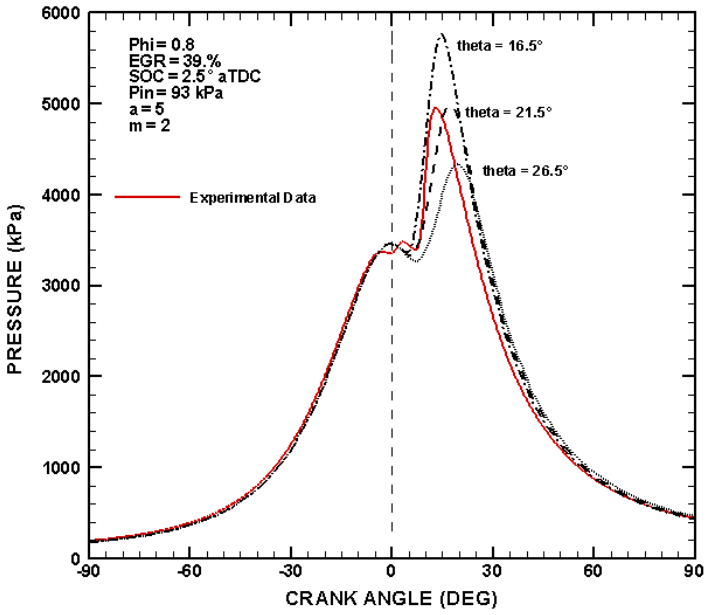

Fig. 9 Variation in pressure trace with burn duration for PCI_39_9.

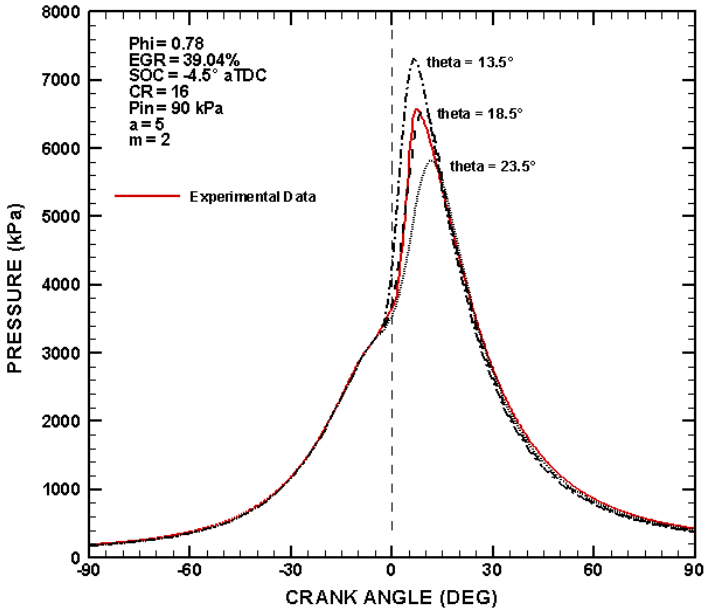

Fig. 10 Variation in pressure trace with burn duration for PCI_39_15.

5.4.3 Influence of compression ratio

The influence of compression ratio is shown in Figures 11 – 15. As expected, the peak pressure increases as compression ratio increases. The rate of pressure rise after the start of combustion though is same for all compression ratios, as compression ratio does not affect the rate of combustion. Also, as compression ratio is fixed by the geometry of the cylinder, it is essentially the same for all cases (Best BSFC, LC, PCI etc.). After trial and error procedure it is observed that compression ratio of 16 gives the best match to the experimental trace in all cases and hence the tested compression ratio (See Table 1) is found to be correct.

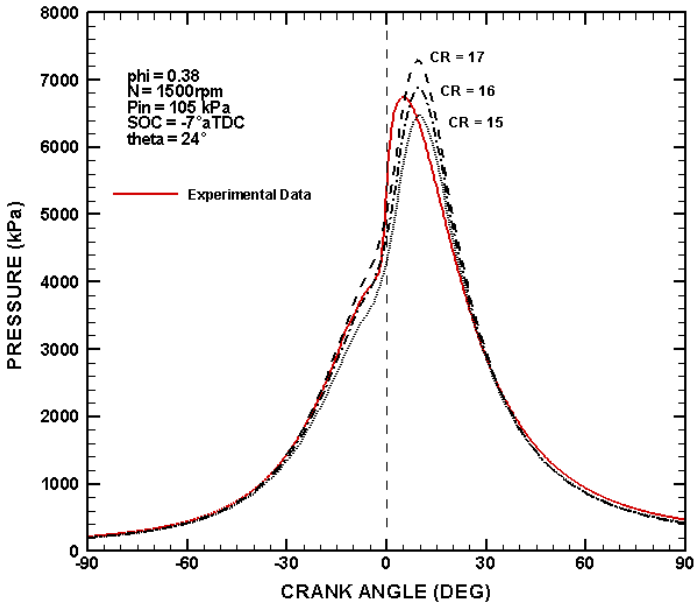

Fig. 11 Variation of pressure trace with compression ratio for Best BSFC case.

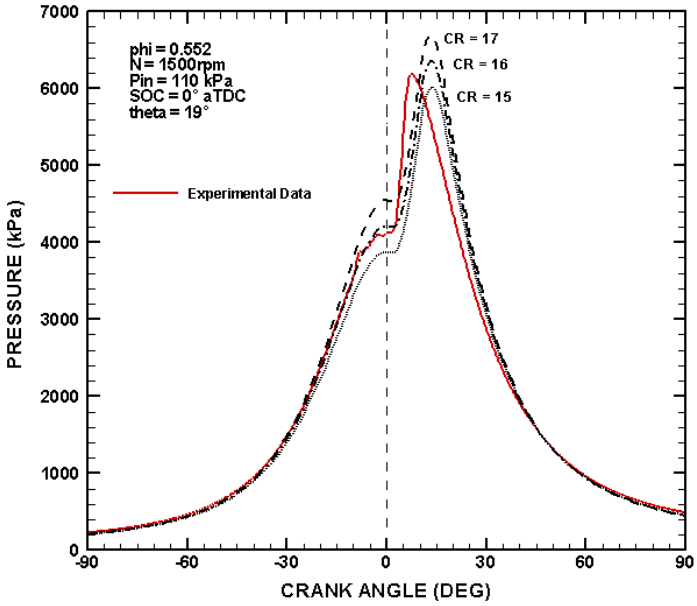

Fig. 12 Variation of pressure trace with compression ratio for LC_10.

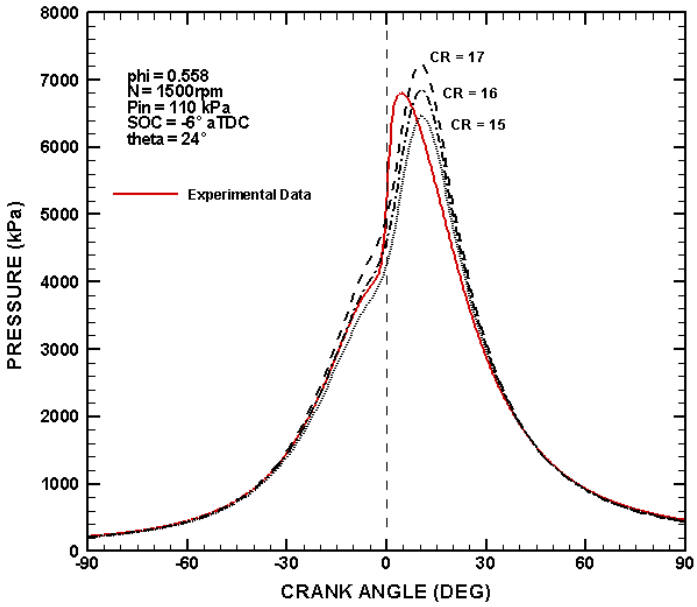

Fig. 13 Variation of pressure trace with compression ratio for LC_15.

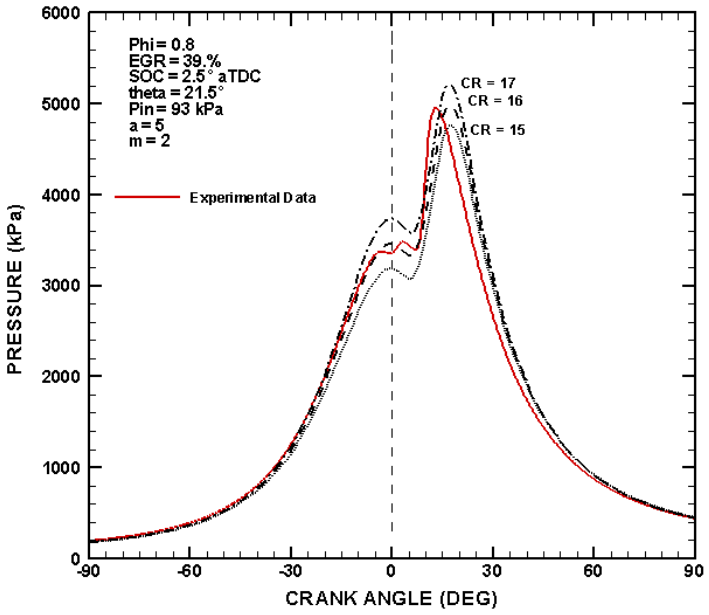

Fig. 14 Variation of pressure trace with compression ratio for PCI_39_9.

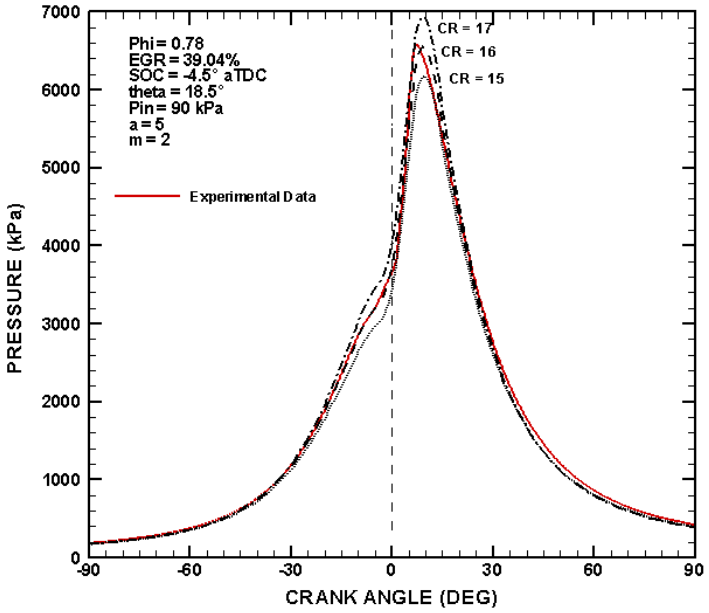

Fig. 15 Variation of pressure trace with compression ratio for PCI_39_15.

5.4.4 Influence of inlet pressure

Figures 16 – 20 show the variation of pressure trace with the inlet pressure. The effect of increasing inlet pressure is to "lift up" the pressure trace. In that sense, effect of inlet pressure seems to be similar to the effect compression ratio has on the pressure trace. Inlet pressure has only negligible effect on the combustion process and hence optimum inlet pressure is determined by matching the motoring portion of the engine cycle.

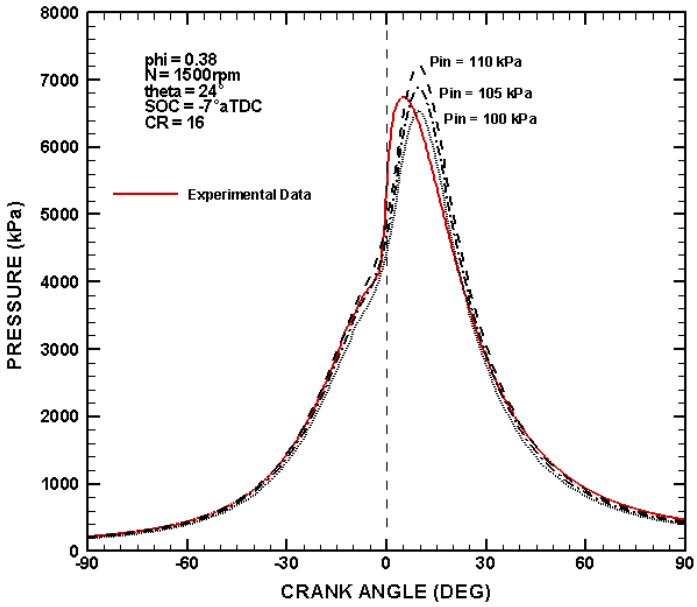

Fig. 16 Variation of pressure trace with change in inlet pressure for Best BSFC case.

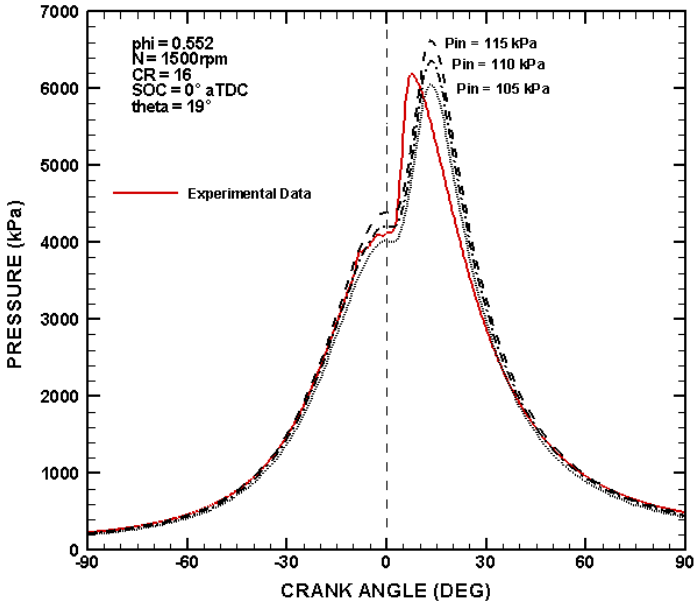

Fig. 17 Variation of pressure trace with change in inlet pressure for LC_10.

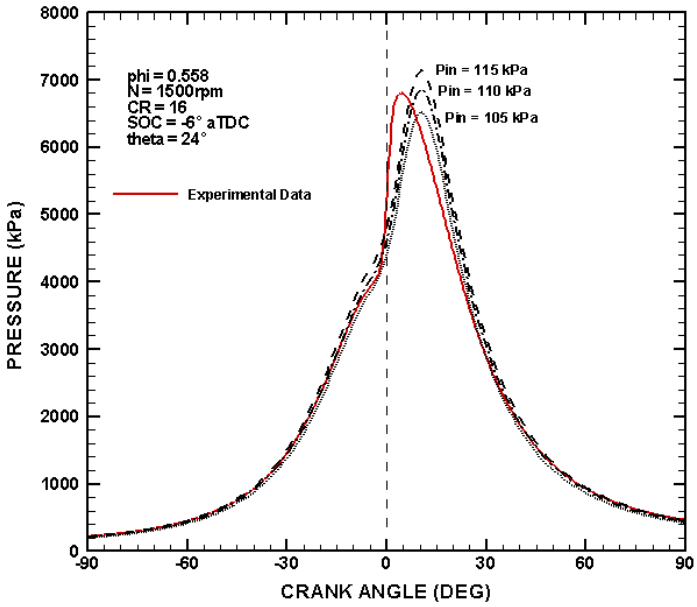

Fig. 18 Variation of pressure trace with change in inlet pressure for LC_15.

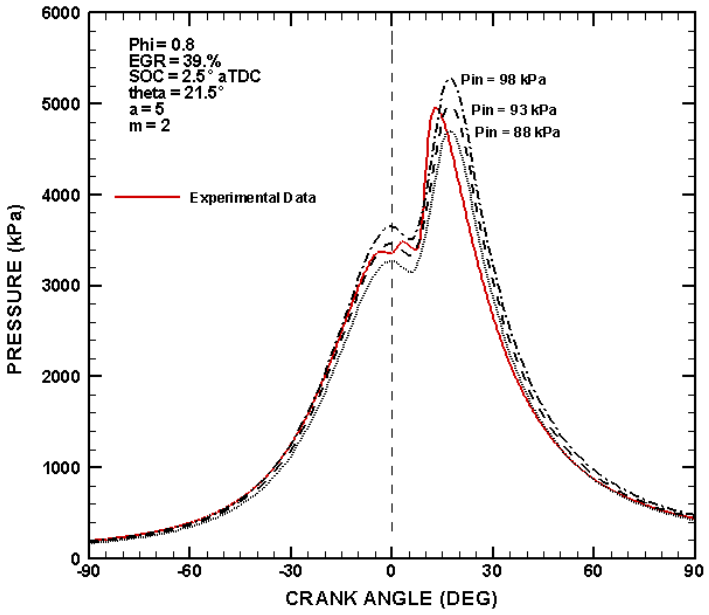

Fig. 19 Variation of pressure trace with change in inlet pressure for PCI_39_9.

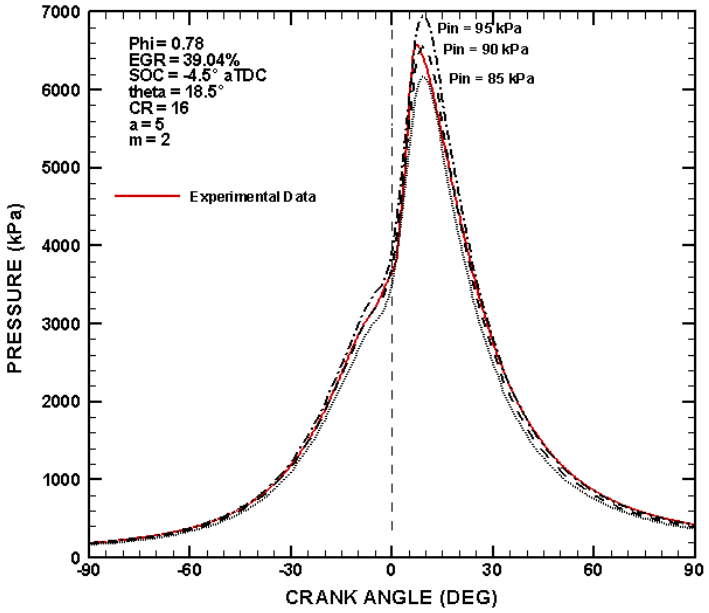

Fig. 20 Variation of pressure trace with change in inlet pressure for PCI_39_15.

6. INTRODUCTION TO DIFFERENT MODES OF COMBUSTION

Three different modes of combustion are studied in the present work. These modes are designated as Best BSFC, lean conventional (LC) and premixed compression ignition (PCI) cases. The most significant parameter triggering the change in the mode of combustion is the EGR level. Apart from the EGR level, injection timing and inlet pressure are adjusted to achieve the required mode of combustion. Injection timing helps in achieving a certain mode of combustion through altering the ignition delay. Inlet pressure affects the mass flow rate and thus affects the oxygen concentration inside the cylinder. EGR affects the combustion process in many different ways. It affects the ignition delay by altering the composition of the cylinder contents – EGR changes the equivalence ratio and introduces inert species of product of combustion. EGR also reduces combustion temperatures. Because of the several different ways in which EGR affects combustion, separate subsection is devoted at the end of the present section to discuss the influence of EGR in detail.

6.1 Different modes of combustion

Basic criterion to distinguish between different modes of combustion is the fraction of premixed and diffusion control burning. In premixed burning, the fuel and air are mixed sufficiently well so that the chemical mechanisms (i.e. reaction kinetics) limit the reaction. When mixture temperatures are suitable for ignition, combustion takes place quite rapidly. On the contrary, fuel and air are not thoroughly mixed in diffusion

controlled (or mixing controlled) burning. Hence in this mode, the combustion rate is limited by the entrainment of air (oxygen to be more specific) into the flame. As the reaction progresses, the rate of oxygen entrainment increases as reaction temperatures, Turbulence and other combustion enhancement increase. Hence the sustainability of the flame and thus the rate of combustion are determined by the diffusion of oxygen to the flame front.

Conventional diesel engine combustion consists of two phases of combustion. As the fuel injected during the ignition delay period is mixed with the air, this initial mass of fuel burns with premixed mechanism. This initial premixed burning is marked by the peak in the heat release rate curve. The remaining fuel then burns with mixing controlled mechanism. Hence ignition delay, injection characteristics, equivalence ratio all affect the rate of heat released during premixed and diffusion combustion phases. Based on the above discussion, Best BSFC, LC and PCI modes are distinguished and their peculiarities are discussed below.

1. Best BSFC mode: This mode of combustion has the highest fraction of diffusion controlled burning among three modes considered. It uses negligible EGR level. The injection timing is optimized to give the maximum efficiency (Hence termed as Best BSFC mode). Negligible EGR implies higher combustion temperatures which increase the efficiency. Injection timing is adjusted such that the combustion occurs close to the TDC and thus overall combustion temperatures are higher. Ignition delay of this mode is relatively shorter thus the combustion is predominantly diffusion controlled. This is highlighted through the comparison of experimental heat release curve for Best BSFC

case with the corresponding curve for LC_10 in Figure 21. The heat release rates are calculated from the measurement of in-cylinder pressure. LC_10 is chosen for comparison so that both Best BSFC and LC case would have same injection timing (10° bTDC in this case). This eliminates the injection timing effects on heat release curves. Comparison of the heat release curves as shown in Figure 21 for these cases indicates that even though the injection timing is same for both these cases, LC_10 has delayed start of combustion, which is an indication of higher ignition delay achieved in LC_10 compared corresponding ignition delay in Best BSFC case. This ultimately results in higher amount of premixed burning in LC_10 case than Best BSFC case.

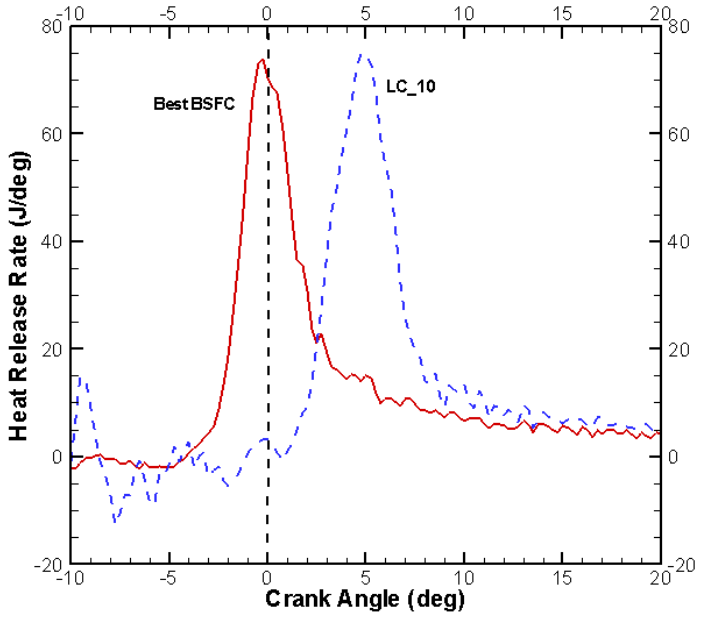

Fig. 21 Comparison of heat release rates between Best BSFC and LC_10 cases.

2. LC mode: This mode of combustion is achieved by using around 30% EGR. The use of higher percentage of EGR results in higher ignition delay. As a result, the fraction of premixed burning increases. Increased EGR level reduces the combustion temperatures. Use of EGR also reduces equivalence ratio making the combustion conditions leaner, hence the name lean conventional. Five different injection timings leading to five different operating points are studied under this mode of combustion.

3. PCI mode: This mode of combustion is achieved by using around 40% EGR. Effect of EGR is more pronounced at the higher EGR levels. At these levels, the ignition delay is longer (it is longer than that observed in LC cases by around 3° as found from simulation results, provided in next section) in case of PCI mode. Thus there would be more premixed burning than that observed in LC mode, hence the name premixed compression ignition. The comparison of the experimental heat release curves is made between LC_15 and PCI_39_15 to support this notion. Again, the experimental heat release rates are calculated from the measured in-cylinder pressure. These two cases are chosen so as to have same injection timing in both these cases. The result is shown in Figure 22. It is clear from this figure that even though the injection timing is same in both these cases, PCI_39_15 shows delayed start of combustion, indicating that it has higher ignition delay than that achieved in LC_15 case. This results in higher premixed burning. Also it is important to note that the peak heat release rate in PCI_39_15 is considerably higher than that attained in LC_15 case. This might be explained as follows. The higher ignition delay in PCI_39_15 leads to more fuel being injected before the combustion begins. Longer ignition delay also gives more time to injected fuel to

vaporize and mix with air before combustion begins. Hence larger fraction of injected fuel ignites simultaneously leading to higher peak heat release rates.

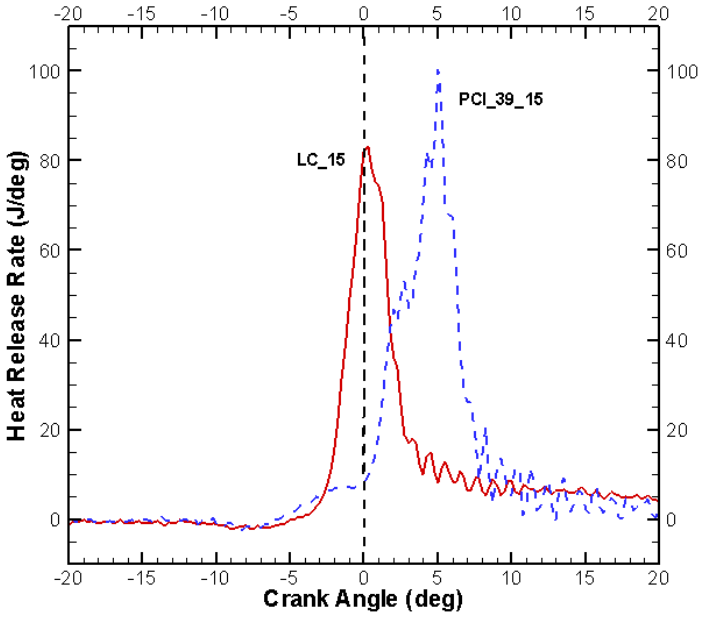

Fig. 22 Comparison of heat release rates between LC_15 and PCI_39_15 cases.

Also the inlet pressures for this mode of combustion are significantly lower than that of LC mode. Higher percentages of EGR are achieved not only by increasing the exhaust manifold pressure but also by reducing the air flow slightly. Hence the oxygen concentration inside the cylinder is lower than that realized in LC cases. Small variations in EGR levels (from around 38% to 42%) are carried out for PCI mode apart from the variation in injection timing. This leads to different combinations of EGR levels and injection timings. Fifteen such operating points are studied under this mode of combustion.

At this instant it is beneficial to recognize the difference in the actual modes of combustion and the combustion model used by the simulation. The simulation is based on the homogeneous combustion model. But as seen above, the modes of combustion for the experimental cases vary from predominantly diffusion controlled to combination of premixed and diffusion controlled burning. Hence fundamental difference exists in the combustion mechanisms of the simulation and experimental cases. Simulation uses Wiebe function to calculate the heat release rate which gives symmetric heat release rate, a characteristic common to homogeneous combustion. The Wiebe function and the effects of Wiebe parameters on combustion process are described in next sections.

6.2 Wiebe function and parameters

Wiebe function gives the rate of burning based on the parameters such as combustion duration, start of combustion and parameters ‘a’ and ‘m’. The mathematical expression for the Wiebe function is presented earlier (equation 7).

The simulation thus calculates the fuel mass burned from this equation and uses the lower heating value of the fuel to calculate the amount of heat released per crank angle. Thus the parameters – start of combustion, burn duration, ‘a’ and ‘m’ are important in controlling the heat release rate. The effects of start of combustion and burn duration on the pressure trace have already been demonstrated in the previous section. Effects of parameters ‘a’ and ‘m’ are discussed in this section.

6.3 How Wiebe parameters ‘a’ and ‘m’ reflect combustion behavior?

The effect of change in Wiebe parameters on combustion is demonstrated through their effect on the mass fraction burn curves and the pressure traces. The parametric sweeps of these parameters for selected cases are shown below.

6.3.1 Influence of Wiebe parameter ‘a’ on mass fraction burn

Figures 23 – 27 depict the effect of Wiebe parameter ‘a’ on mass fraction burn. It is noted that the rate of burning increases with increase in ‘a’. For all the results below, the start of combustion and burn duration is kept constant to evaluate the effect of Wiebe parameter ‘a’. The apparent decrease in burn duration with increase in ‘a’ is due to higher rates of initial burning rates. Thus, lesser and lesser fuel burns in the latter portion of combustion process with increase in ‘a’. The higher rates of initial burning are noticeable from the larger slopes of the mass fraction burn curves with higher values of ‘a’. It is also noted that all mass fraction burn curves appear to start at around the same time indicating that the combustion commences at the same time for all cases irrespective of parameter ‘a’.

Above observations are useful in terms of selecting a best value of ‘a’ based on the engine combustion processes. Higher rates of initial burning with higher ‘a’ values suggest that higher ‘a’ can be used for more premixed burning where higher heat release rates are achieved. In typical PCI mode of combustion, higher initial rates of burning are expected to occur due to large amount of initial burning, but the combustion would occur more slowly after this initial burning phase and the overall combustion duration would

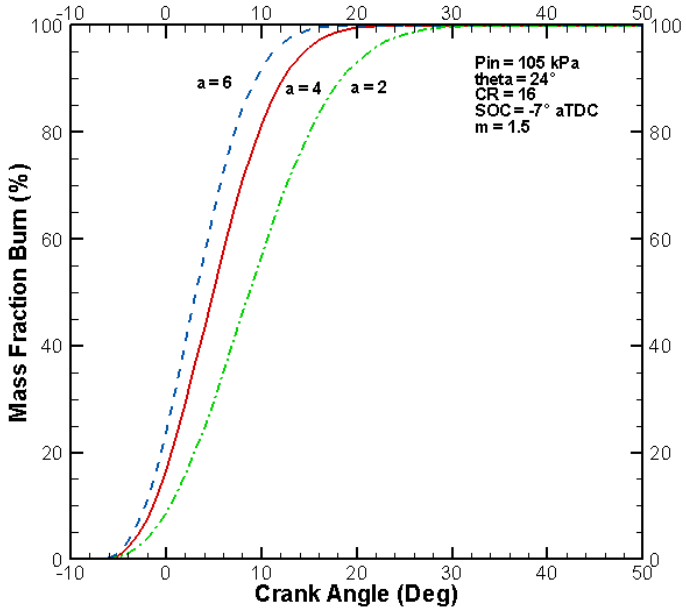

Fig. 23 Variation of mass fraction burn with Wiebe parameter 'a' for Best BSFC case.

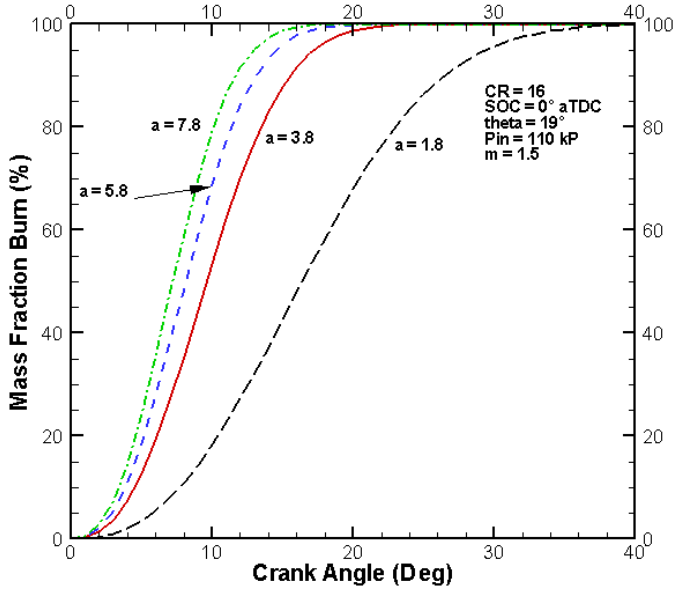

Fig. 24 Variation in mass fraction burn with Wiebe parameter 'a' for LC_10.

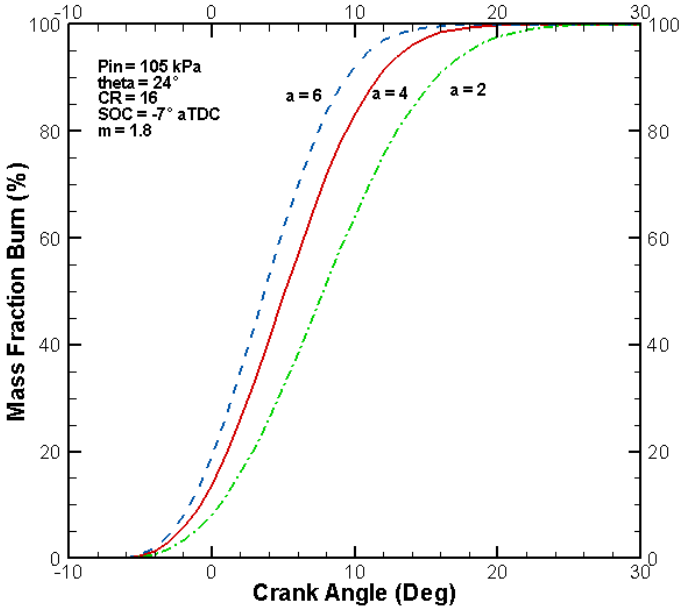

Fig. 25 Variation in mass fraction burn with Wiebe parameter 'a' for LC_15.

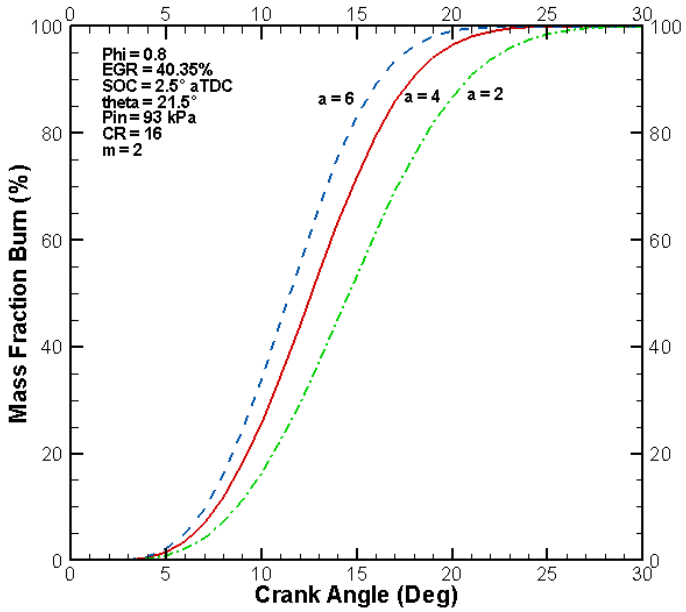

Fig. 26 Variation in mass fraction burn with Wiebe parameter 'a' for PCI_39_9.

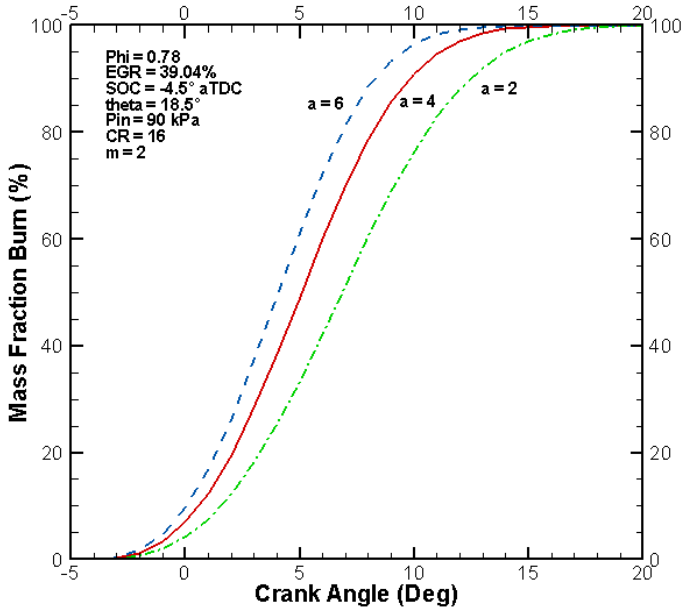

Fig. 27 Variation in mass fraction burn with Wiebe parameter 'a' for PCI_39_15.

get lengthened. This is because; the fuel that does not undergo the initial premixed burning would burn at the lower rate because of the lower combustion temperatures of PCI combustion mode. But higher ‘a’ values reduce the combustion duration and would contrast the actual PCI combustion.

6.3.2 Influence of Wiebe parameter ‘a’ on pressure trace

Observations made in section 6.3.1 are now extended to the pressure data. Figures 28 – 32 show the effect of Wiebe parameter ‘a’ on pressure traces. It is seen that the peak pressure increases with increase in ‘a’. Also increase in peak pressure progressively decreases with further increase in ‘a’. There is only a small variation in start of combustion location with change in ‘a’. Another important observation emerging from these results is that, the location of the peak pressure is advanced with higher values of ‘a’. This is consistent with higher burning rates observed with higher ‘a’ values. Through parametric sweeps, it was seen in section 6.3.1 that higher ‘a’ values not only increase initial burn rate but also decrease 10% to 90% burn duration. Higher initial burn rates typically associate with large initial premixed burning. This suggest the use of higher values of ‘a’ when fraction of premixed burning is expected to be higher.

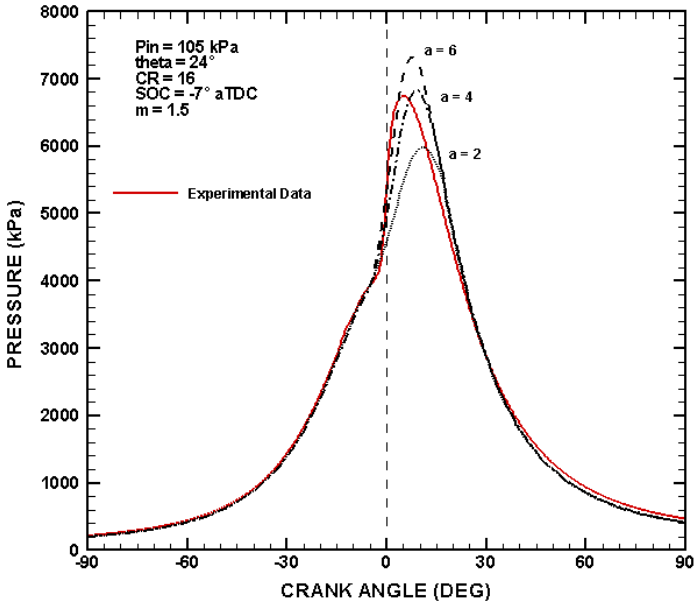

Fig. 28 Variation of pressure trace with Wiebe parameter 'a' for Best BSFC case.

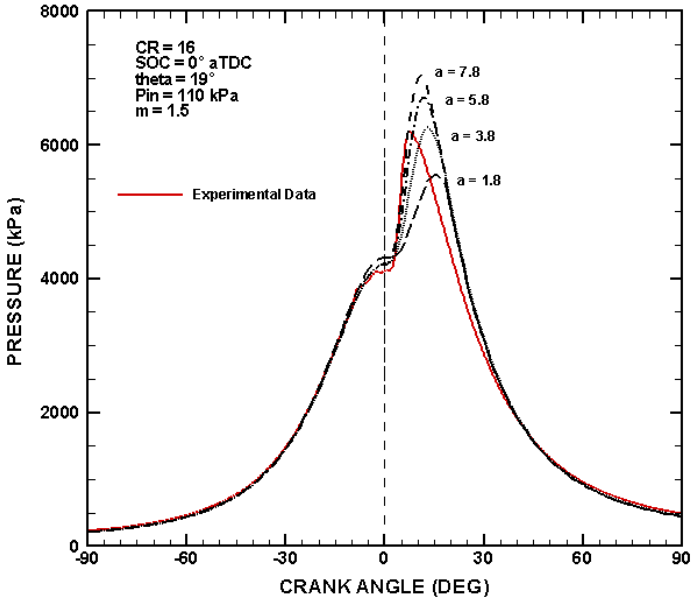

Fig. 29 Variation of pressure trace with Wiebe parameter 'a' for LC_10.

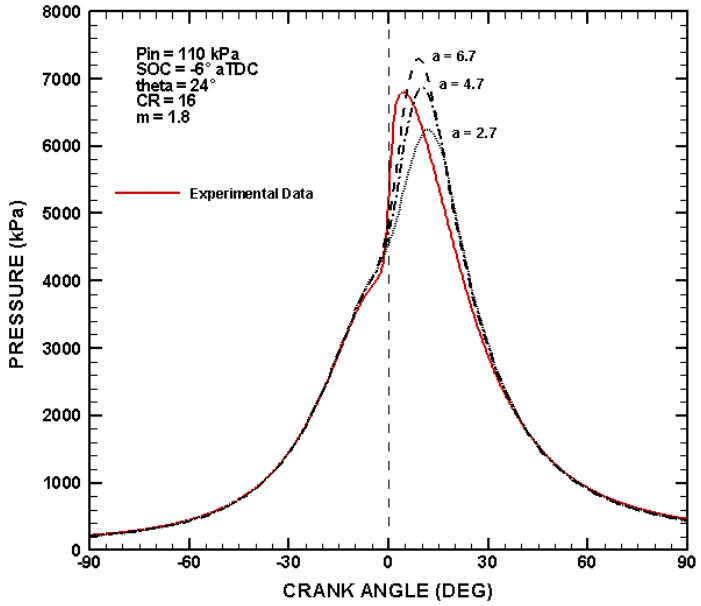

Fig. 30 Variation of pressure trace with Wiebe parameter 'a' for LC_15

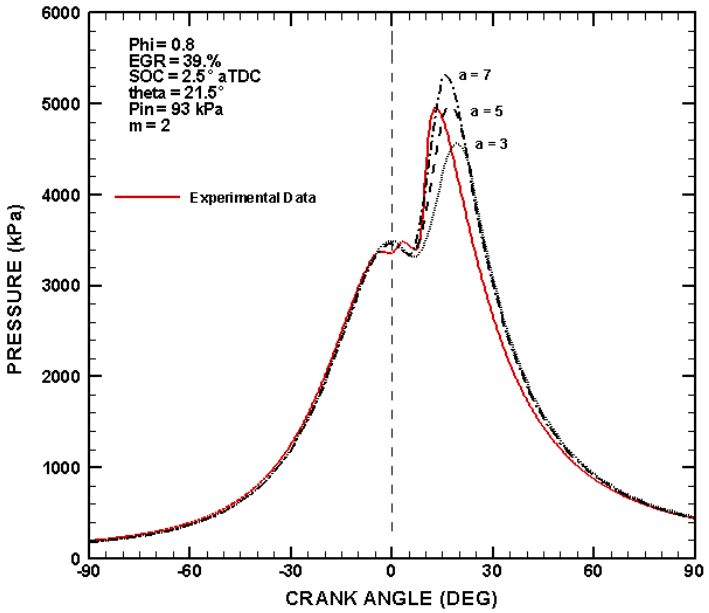

Fig. 31 Variation of pressure trace with Wiebe parameter 'a' for PCI_39_9.

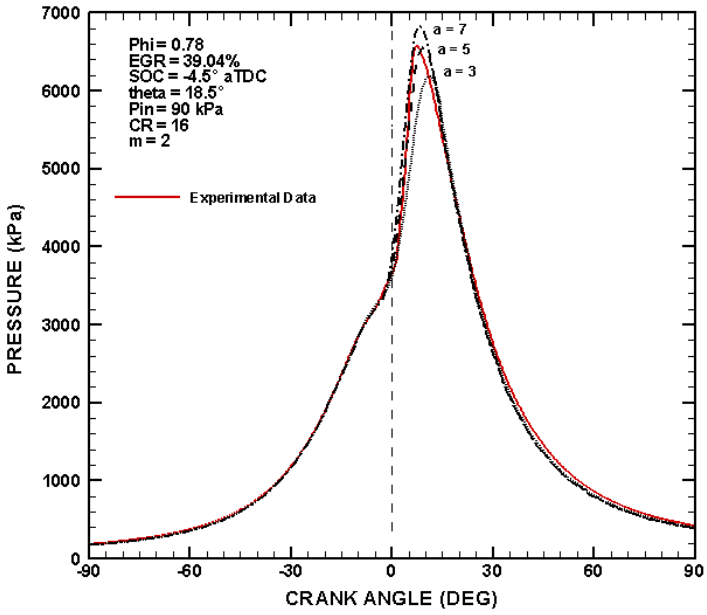

Fig. 32 Variation of pressure trace with Wiebe parameter 'a' for PCI_39_15.

6.3.3 Influence of Wiebe parameter 'm' on mass fraction burn

Figures 33 – 37 show the influence of Wiebe parameter 'm' on mass fraction burn. It is observed that increase in 'm' decreases initial burning rate (0% to 10% mass fraction burn takes longer). But the rates of burning are higher after this initial burning. Because of this higher burning rate with increase in 'm', the burn duration apparently decreases with higher 'm' even though the combustion starts late. It is important to note that change in 'm' apparently delays the start of combustion. Initial burning rates are very low with higher values of 'm' so that there is no apparent presence of burned mass fraction immediately after start of combustion (note that the start of combustion is kept constant) with higher values of 'm'.

Above observations are helpful to select the optimum value of ‘m’ for modeling the actual engine combustion process. Delayed start of combustion with higher ‘m’ suggests higher values of ‘m’ for combustion processes involving longer ignition delay that are typical to PCI mode. But very high values of ‘m’ decrease the overall burn duration quite rapidly unlike that attained PCI combustion.

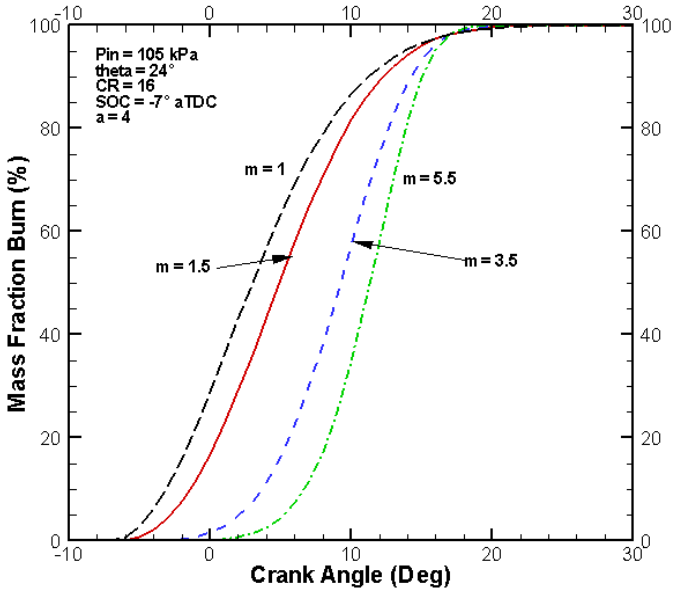

Fig 33 Variation in mass fraction burn with Wiebe parameter ‘m’ for Best BSFC case.

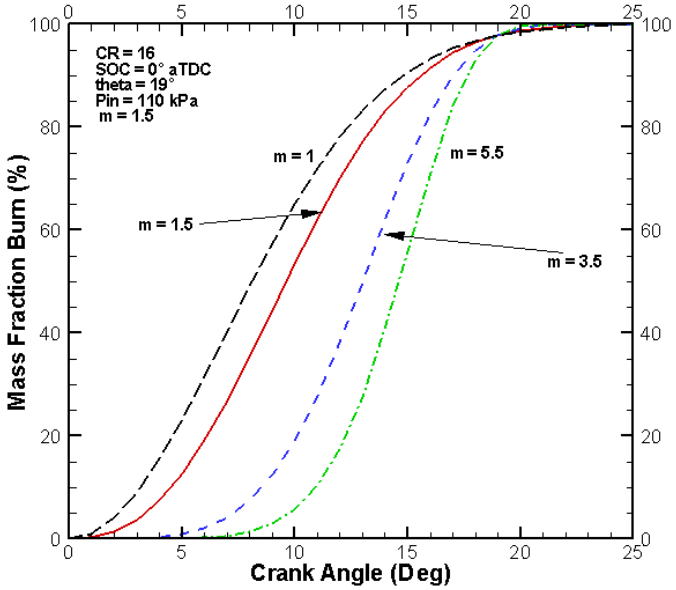

Fig 34 Variation in mass fraction burn with Wiebe parameter 'm' for LC_10.

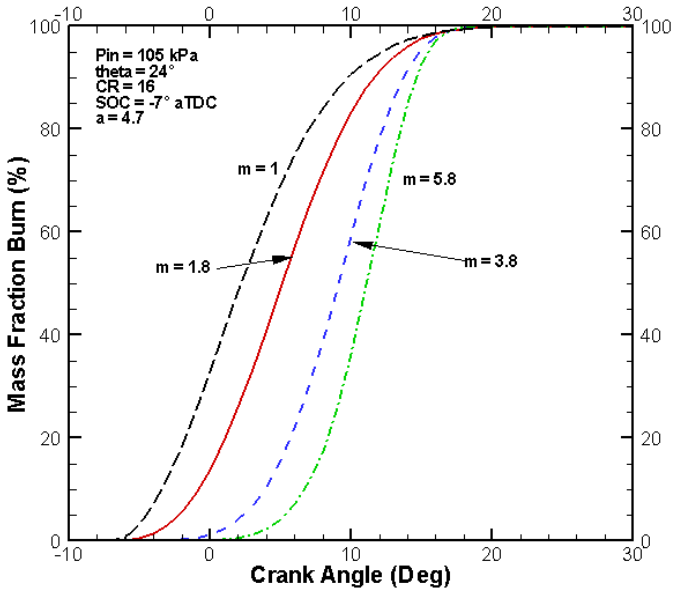

Fig 35 Variation in mass fraction burn with Wiebe parameter 'm' for LC_15.

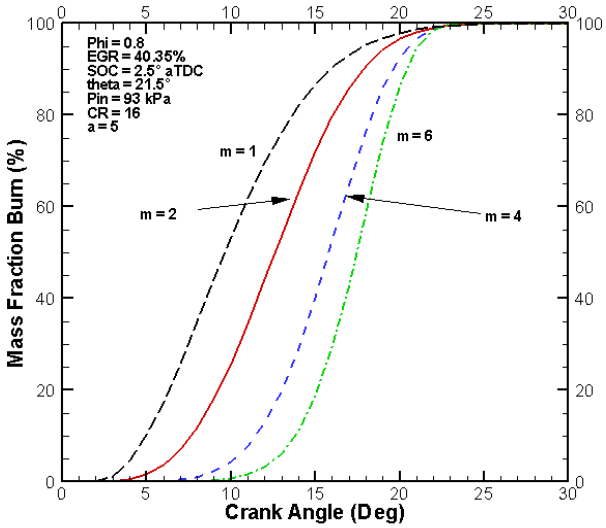

Fig 36 Variation in mass fraction burn with Wiebe parameter 'm' for PCI_39_9.

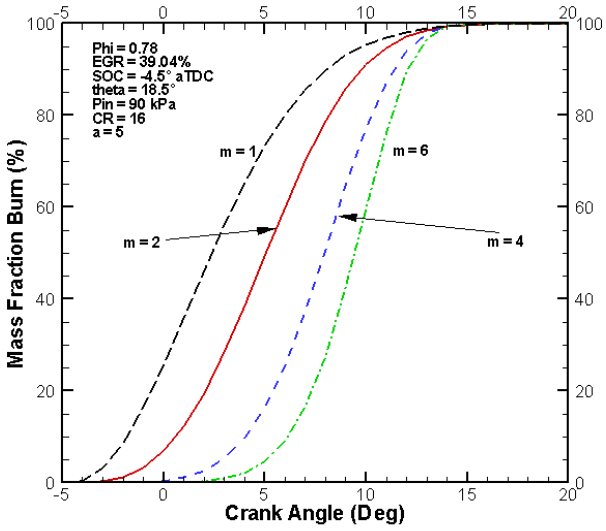

Fig 37 Variation in mass fraction burn with Wiebe parameter 'm' for PCI_39_15.

6.3.4 Influence of Wiebe parameter ‘m’ on pressure trace

Observations made in section 6.3.3 are now related to the pressure trace. Figures 38 – 42 show the influence of Wiebe parameter ‘m’ on pressure traces. It is seen that the effect of ‘m’ on peak pressure is opposite to the effect of parameter ‘a’. Increase in ‘m’ reduces the peak pressure, but the reduction in peak pressure with ‘m’ is much more significant than the increase in peak pressure with equal change in parameter ‘a’. This is a consequence of a delayed start of combustion with higher ‘m’ as seen in the section 6.3.3. Again, decrease in the peak pressure progressively diminishes as ‘m’ is increased further. Another significant influence of ‘m’ is that it changes the start of combustion location. This is unlike parameter ‘a’ which is observed to have very slight influence on start of combustion. It is also seen that ‘m’ reduces initial burn rate but increases the rate of burning after this initial burning is over.

Above observations provide some insight into how Wiebe parameters ‘m’ can reflect combustion behavior. Delay in the start of combustion by increasing ‘m’ can be thought to be equivalent to that introduced by the ignition delay. Thus higher values of ‘m’ should be used when longer ignition delay period exists. Higher ignition delay periods are typical of PCI mode.

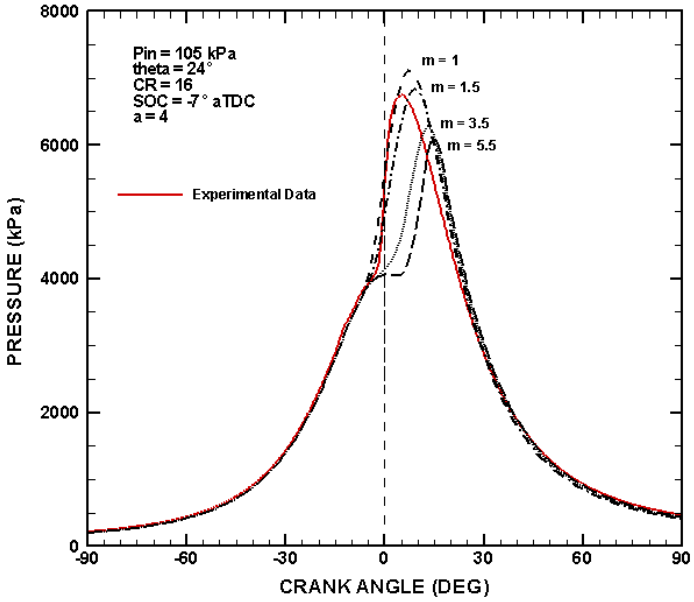

Fig. 38 Variation of pressure trace with Wiebe parameter 'm' for Best BSFC case.

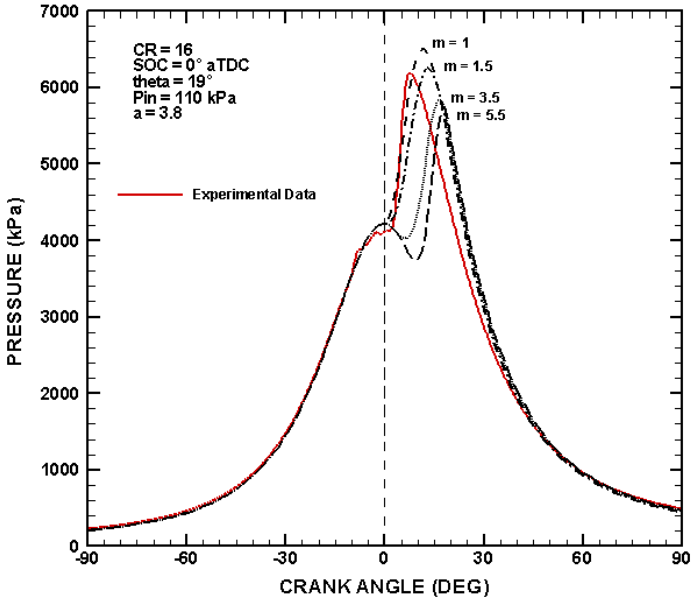

Fig. 39 Variation of pressure trace with Wiebe parameter 'm' for LC_10.

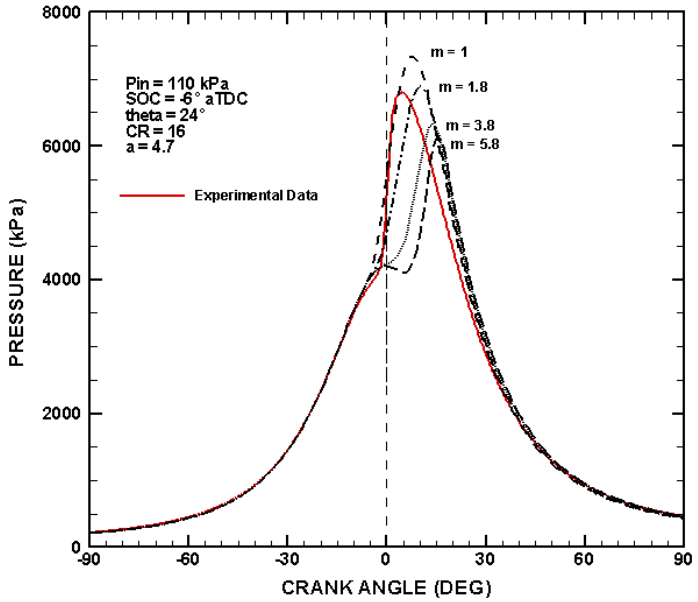

Fig. 40 Variation of pressure trace with Wiebe parameter 'm' for LC_15.

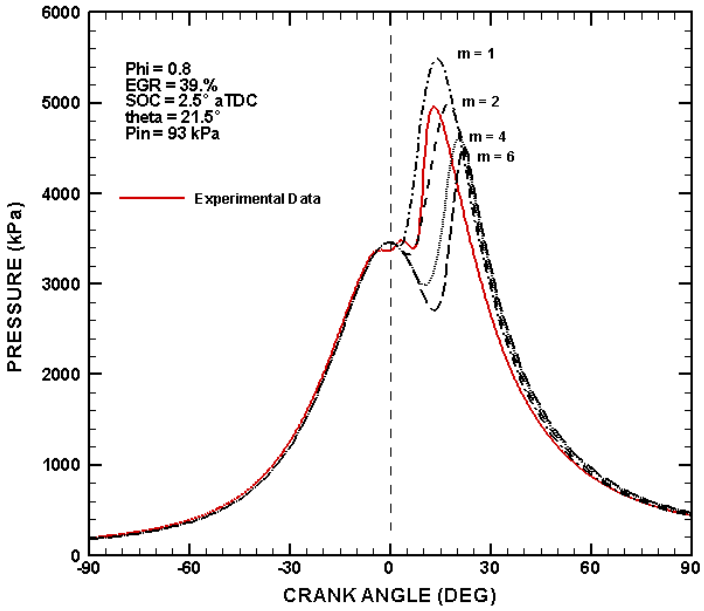

Fig. 41 Variation of pressure trace with Wiebe parameter 'm' for PCI_39_9.

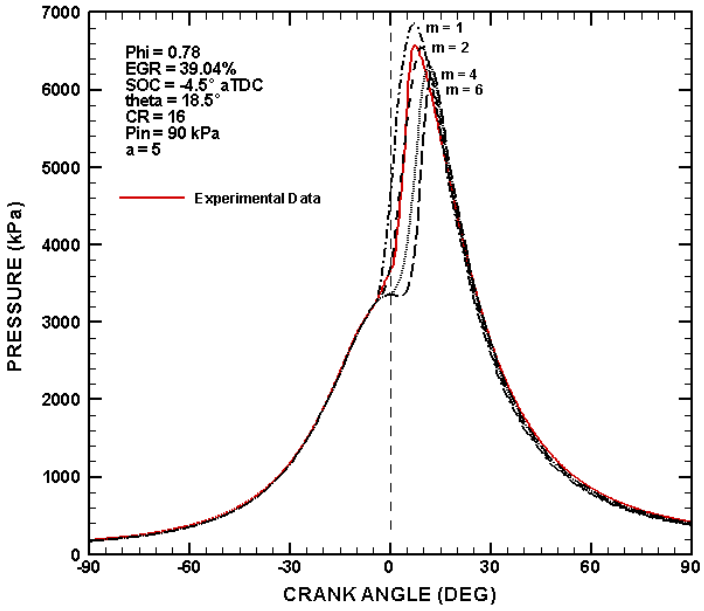

Fig. 42 Variation of pressure trace with Wiebe parameter 'm' for PCI_39_15.

6.3.5 Characterization of combustion modes by Wiebe parameters

This section summarizes the effects of parameters 'a' and 'm'. Higher 'm' delays the start of combustion while higher 'a' increases the initial burn rate. Both these factors are typical to increased ignition delay and more premixed burning resulting thereof. But higher 'a' and higher 'm' both increase 10% - 90% burn rate which is uncharacteristic to the higher premixed burning achieved by longer ignition delay. This is because, once the initial fuel mass has undergone premixed burning, the remaining fuel undergoes diffusion controlled burning. Also the leaner conditions of combustion and presence of higher amount of EGR lowers the combustion temperatures. Thus 10% - 90% burn rate is lowered. But, above discussion suggests that an astute choice of 'a' and 'm' would give more realistic view of actual in-cylinder combustion.

Above observations are checked with actual numbers obtained from the simulation results. At this point it is worth mentioning that the actual mass fraction burn curves for SI engine combustion have been fitted with a = 5 and m = 2 **[15]**. As SI engine combustion is homogeneous these values of 'a' and 'm' serve as benchmark values for completely homogeneous combustion. In the present study the optimum values of 'a' and 'm' found for different modes of combustion are listed in table 5.

Table 5 Optimum values of Wiebe parameters 'a' and 'm' for different operating points

Case Considered	Parameter 'a'	Parameter 'm'
Best BSFC	4	1.5
LC_10	3.8	1.5
LC_5	4.9	2
LC_3	4.8	1.85
LC_15	4.7	1.8
PCI (All 15 operating points)	5	2

The optimum values of Wiebe parameters are obtained from the curve fitting of experimental pressure data. It is seen that the optimum values of 'a' and 'm' are respectively 5 and 2 for all PCI cases. Hence this reflects that the PCI mode tends to undergo homogeneous combustion. LC mode on the contrary does not show uniformity in values of optimum Wiebe parameter. This could be attributed to the fact that the LC cases use around 30% EGR (PCI cases use around 40% EGR). Thus influence of EGR at this level is lower while influence of injection timing is also discernible. For example the Best BSFC case (which has injection timing 10° bTDC) and LC_10 case both have same injection timing. The injection timing in these cases is close to the TDC when the cylinder temperature and pressure are expected to be high. This must have reduced the

ignition delay for these two cases compared to other three LC cases. Thus these two cases have ‘a’ and ‘m’ as around 4 and 1.5 respectively. These lower values of ‘a’ and ‘m’ support the notion of using lower values of the Wiebe parameters for shorter ignition delays and for diffusion controlled burning.

The remaining three LC cases either have advanced or retarded injection timing which increases ignition delay. Thus the combustion in these three cases is expected to be more premixed than Best BSFC and LC_10. And the values of Wiebe parameters again reflect this combustion characteristic. Hence it is demonstrated that with proper choice of Wiebe parameters it is possible to differentiate different modes of combustion. EGR is used to alter the mode of combustion along with other parameters as described earlier. Hence it is important to evaluate the influence of EGR and to understand how the simulation accounts for the change in EGR level. Following section addresses this question.

6.4 Influence of EGR

6.4.1 Summary of EGR effects

EGR affects engine combustion process in many ways. These different ways and the combustion characteristics affected are summarized in Table 6.

Table 6 Various effects of EGR on different attributes of engine combustion processes

Various effects of EGR	Combustion characteristics			
	Ignition Delay	Combustion Duration	Peak Temperature	Fraction of Premixed Burning
Reduction in O_2 concentration (Dilution Effect)	Increases	Increases	Decreases	Increases
Introduction of CO_2 and H_2O which dissociate at higher temperatures (Chemical effect)	Negligible effect	Negligible effect	Decreases	Negligible Effect
Increase in the specific heat capacity of inlet charge (Thermal Effect)	Decreases	Negligible Effect	Decreases or increases	Negligible Effect
Increase in the inlet charge temperature	Decreases	Negligible Effect	Increases	Negligible Effect
Reduction in the inlet mass flow rate (Thermal Throttling)	Negligible Effect	Decreases	Increases	Negligible Effect

These effects are explained below

i. Dilution effect: Presence of EGR reduces the concentration of oxygen inside the cylinder. This is termed as the dilution effect. As the oxygen concentration decreases, the rates of pre-ignition reactions are lowered which results in higher ignition delay. Lower concentration of oxygen also influences the diffusion controlled portion of the combustion process. As oxygen entrainment rate controls the reaction rate in case of diffusion burning, lower oxygen concentration results in longer burn duration. Longer burn durations result in lower peak temperatures.

Higher ignition delay allows more time for the portion of a fuel mass injected during ignition delay to mix with the cylinder charge. This increases the fraction of premixed burning.

ii. Chemical effect: Even though the presence of CO_2 and H_2O affect the pre-ignition reactions, their effect on the ignition delay and corresponding effect on the premixed and diffusion controlled fractions are negligible. But their presence affects the peak temperature as both these components of EGR dissociate at higher temperatures (at around 2000 K). These dissociation reactions are endothermic and hence help in reducing the peak temperatures.

iii. Thermal effect: EGR introduces inert products of combustion into the cylinder. These species have higher specific heat capacity. Hence the pressure and temperature at the end of compression process are higher (This follows from the isentropic relation between the initial and final pressures and temperatures). The higher temperatures would tend to decrease the ignition delay by expediting the fuel vaporization and pre-ignition reactions. Hence the ignition delay tends to decrease. This tends to decrease the fraction of premixed burning. The higher initial temperatures at the start of combustion tend to increase the peak temperature but the higher heat capacity of the cylinder charge absorbs more energy released due to combustion and tends to decrease the rate of temperature increase due to combustion. The peak temperature may tend to increase or decrease depending upon which of these two effects is dominant. Higher heat capacity of the cylinder charge on the other hand would not have significant effect on the combustion duration.

iv. Increase in inlet charge temperature: Increase in inlet charge temperature subsequently raises the temperature of the cylinder charge at the end of compression stroke. As seen earlier higher in-cylinder temperatures at the start of fuel injection tend to decrease ignition delay. Increase in higher inlet charge temperature also results in higher peak temperatures.

v. Thermal throttling: Addition of EGR to the inlet manifold increases the temperature of the air and EGR mixture at the inlet to the cylinder. This decreases the density of the entering charge which in turn results in decrease in the inlet mass flow rate. Reduction in the inlet mass flow rate results in increase in temperatures as heat released by the combustion process is absorbed by reduced trapped mass. Higher combustion temperatures tend to decrease the burn duration.

6.4.2 Simulation results for the change in the EGR level

EGR sweeps are carried out to find out how simulation results reflect the various effects of EGR on engine combustion process. For theses results, all other input parameters are kept constant and EGR level is varied. Figures 43 – 47 show the results of the parametric sweeps of EGR on the pressure trace.

It is found that the simulation does not reflect all the effects of EGR mentioned earlier. The results show that the peak pressure reduces with the EGR as expected but the location of the peak pressure does not change. The rate of rise of pressure after the start of combustion slightly reduces which results in lower peak pressure.

Hence it can be seen that the simulation does not reflect the change in the ignition delay with change in EGR level. Simulation uses parameters such as combustion duration and Wiebe parameters to control the combustion process. As these parameters are unchanged in these EGR sweeps no changes in ignition delay can be observed. The reduced burning rates and lower peak pressures could be the result of increased equivalence ratio. Simulation includes the dissociation model for H_2O and CO_2 and hence takes into account the chemical effect. The simulation also calculates the instantaneous thermodynamic properties and accounts for the changes in the heat capacity of the charge. Hence it can be claimed that the simulation reflects the effect of dilution effect, chemical effect and thermal effect on temperature and combustion duration. But it does not take into consideration the effect on ignition delay. The inlet charge temperature is a user input and hence its effect on the temperature is incorporated in the simulation. But from these results it can be seen that the simulation does not reflect the effect of EGR on the ignition delay, and hence proper selection of burn duration and Wiebe parameters is necessary to reflect this effect. But at the same time this limitation offers an opportunity to study the effect of mode of combustion as, as far as simulation results are concerned the ignition delay is characterized by the Wiebe parameters and burn duration instead of EGR level specification. This idea is explained in detail in section 8.

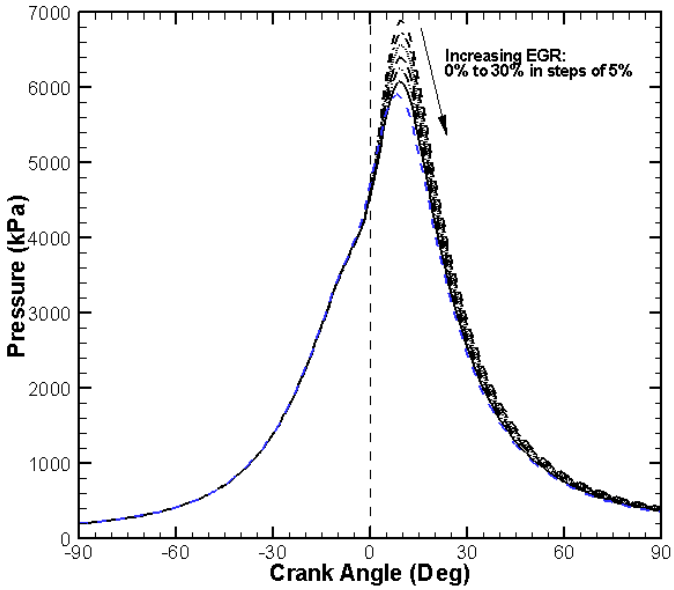

Fig. 43 Variation in pressure trace with change in EGR level for Best BSFC case.

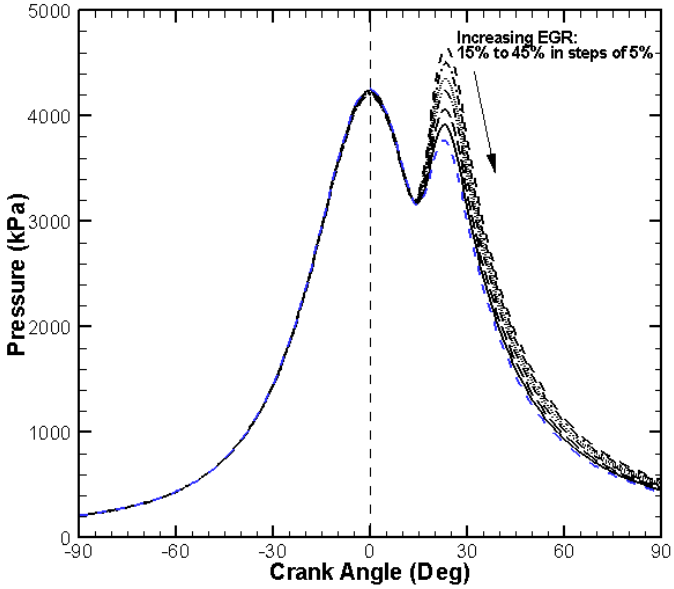

Fig. 44 Variation in pressure trace with change in EGR level for LC_3.

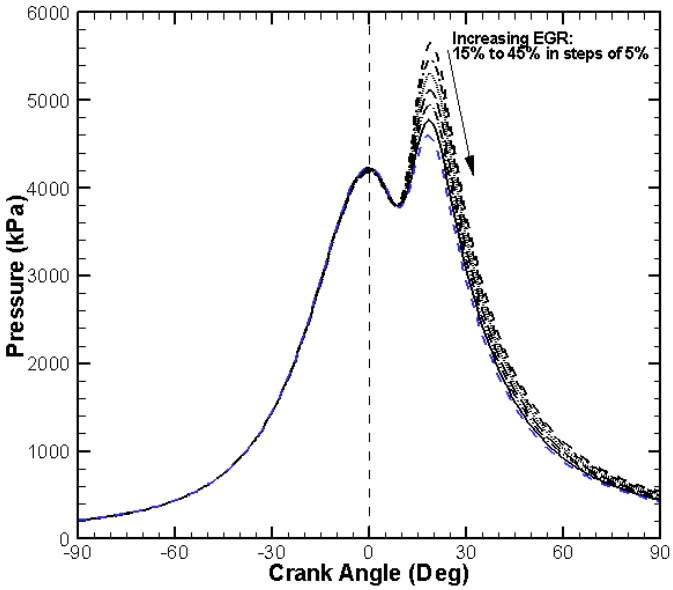

Fig. 45 Variation in pressure trace with change in EGR level for LC_5.

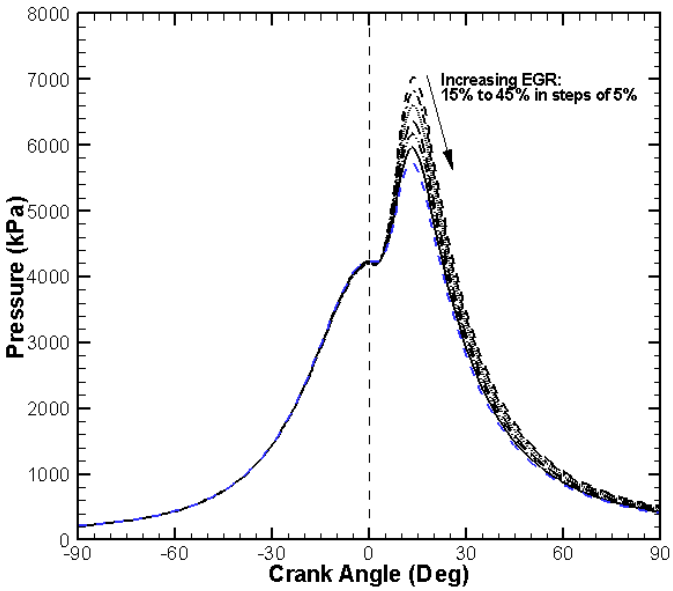

Fig. 46 Variation in pressure trace with change in EGR level for LC_10.

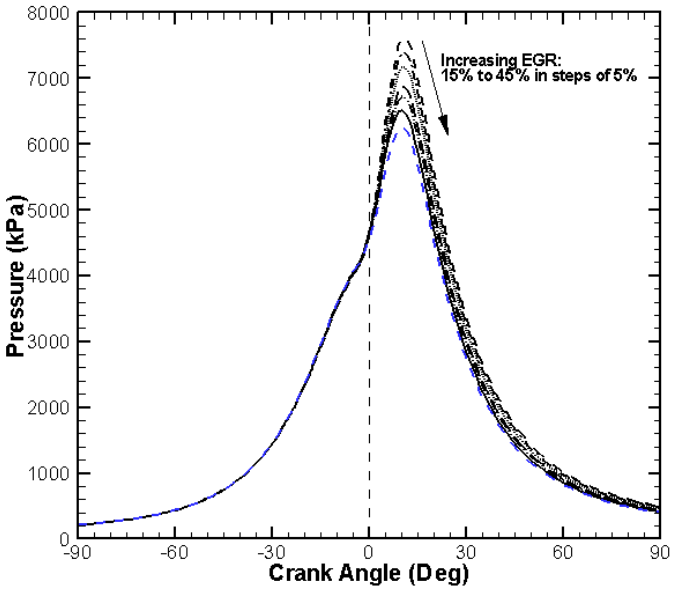

Fig. 47 Variation in pressure trace with change in EGR level for LC_15.

7. COMPARISON OF SIMULATION AND EXPERIMENTAL PRESSURE DATA

7.1 Introduction

Comparison of simulation and experimental data is an important step in the analysis of engine combustion using thermodynamic engine cycle simulation. It has been already demonstrated that the actual mode of combustion and the combustion model used by the simulation are different and hence differences exist between simulation and experimental results even after optimizing different input parameters (such as Wiebe parameters, combustion duration etc.) These differences are highlighted by comparing the experimental pressure traces with the corresponding "best fit" simulation pressure traces. Best fit simulation pressure traces are obtained using a set of optimum parameters. The list of the set of optimum parameters for different cases is provided latter in this section.

7.2 Comparison results

7.2.1 Best BSFC case

Figure 48 shows the comparison of experimental pressure trace with corresponding best fit curve for Best BSFC case. It is seen that closer agreement exists between these two traces for the portion of the cycle corresponding to the compression stroke. After the start of combustion, however, experimental pressure increases more rapidly than simulation pressure. Experimental pressure shows rapid increase in pressure

followed by more gradual decrease. On the contrary, simulation pressure trace shows almost equal rate of rise and fall in pressure. The difference arises due to difference in the mode of combustion. Simulation being based on the homogeneous model tends to give more "symmetric" heat release rate which is reflected in pressure trace by the equal rate of rise and fall of pressure after the start of combustion.

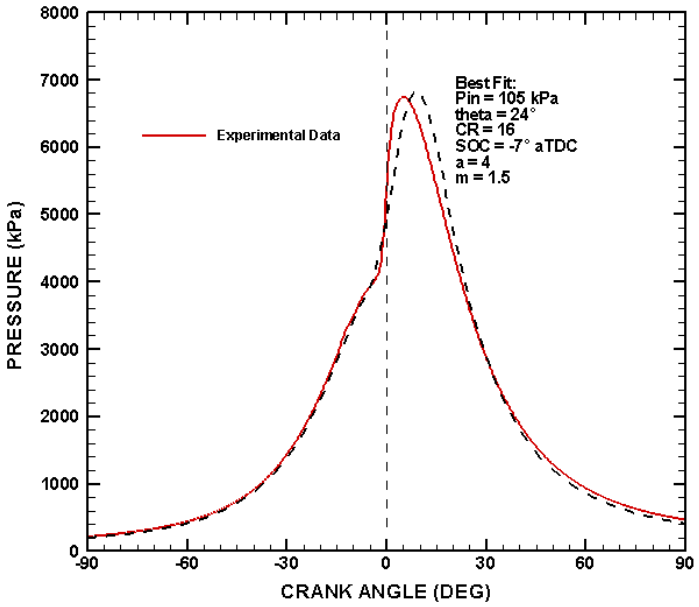

Fig. 48 Comparison of experimental pressure trace and best fit curve for Best BSFC case.

7.2.2 LC cases

Figures 49 – 52 show the comparison of experimental pressure traces with corresponding best fit curves for LC cases. The above discussion made in the context of Best BSFC case seems to be applicable in LC cases as well.

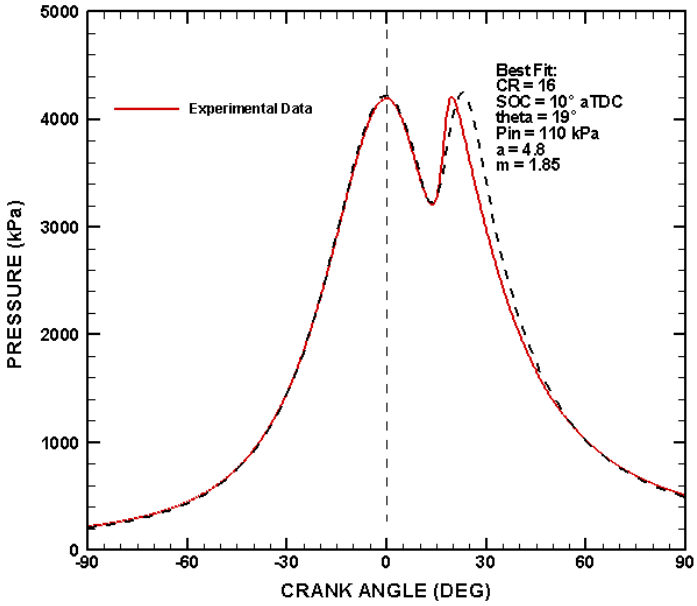

Fig. 49 Comparison of experimental pressure trace with best fit curve for LC_3.

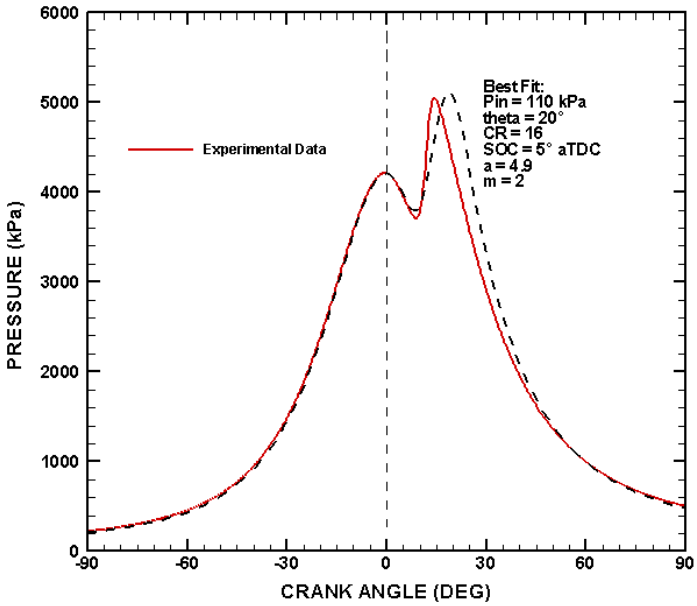

Fig. 50 Comparison of experimental pressure trace with best fit curve for LC_5.

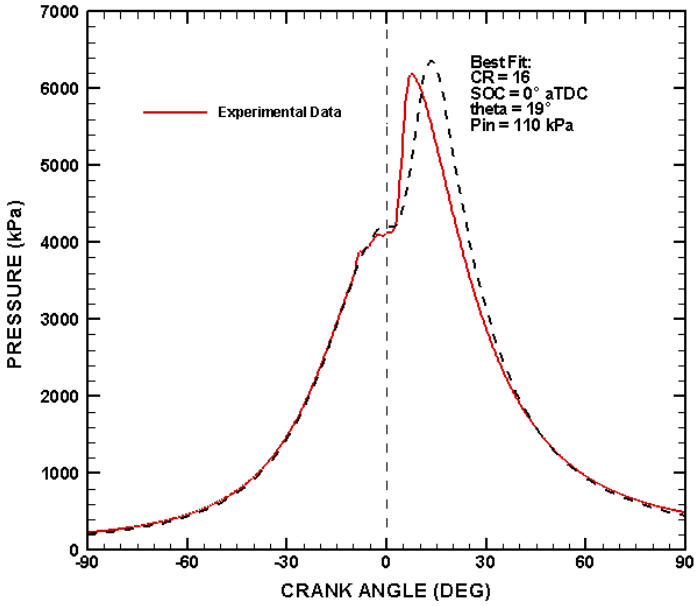

Fig. 51 Comparison of experimental pressure trace with best fit curve for LC_10.

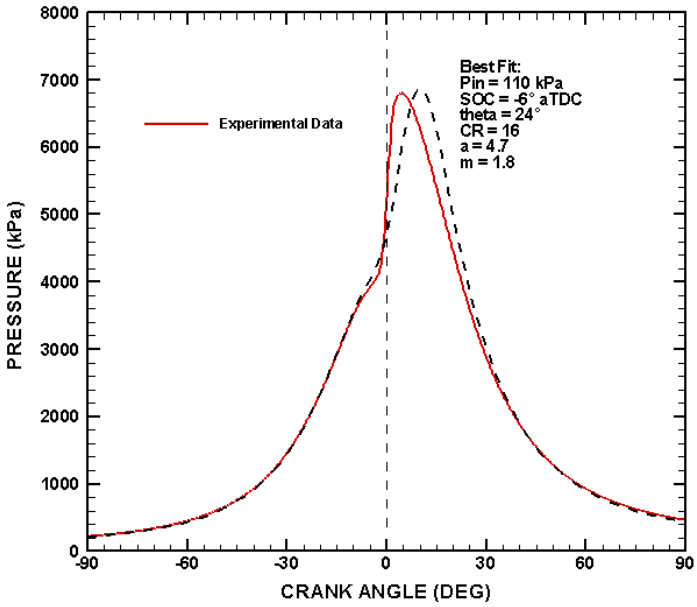

Fig. 52 Comparison of experimental pressure trace with best fit curve for LC_15.

7.2.3 PCI cases

Figures 53 – 67 show the comparison of experimental pressure traces with the corresponding best fit curves for PCI cases. The observations made above for Best BSFC and LC cases hold true for these cases also. In addition to that, the effect of fuel vaporization is seen distinctly in the experimental pressure traces. The experimental pressure traces show a small dip followed by a small hump before combustion starts. These are related to longer ignition delays associated with PCI combustion mode. Longer ignition delays cause more fuel to be injected into the cylinder before the start of combustion. Consequently more fuel is injected at lower cylinder temperatures and pressures. The injected fuel absorbs energy required for vaporization from the surrounding mixture, lowering the temperature slightly. This explains the presence of slight dip in the pressure traces observed for this mode. The injected fuel initially burns at low temperature as a result of cool flame reactions. These cool flame reactions manifest themselves through a slight hump seen in the pressure traces. The simulation on the contrary, assumes homogeneous fuel-air mixture with fuel in vaporized state. Thus it does not account for the fuel vaporization effect (No dip can be observed in simulation pressure traces). Also simulation being based on the homogeneous combustion model does not account for the presence of cool flame reactions and thus no hump can be located in the simulation pressure traces.

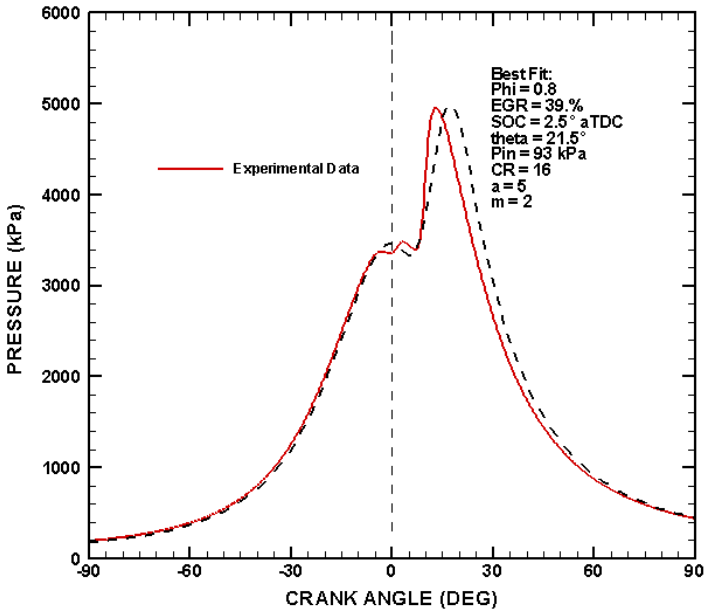

Fig. 53 Comparison of experimental pressure trace with best fit curve for PCI_39_9.

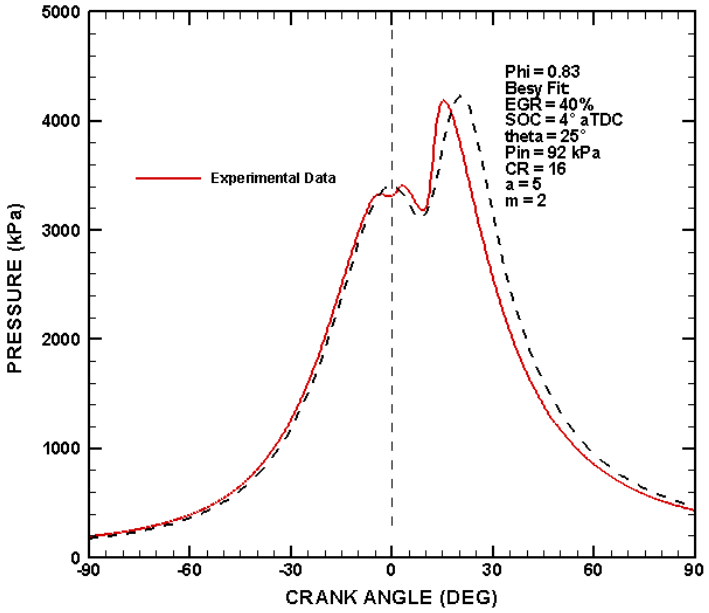

Fig. 54 Comparison of experimental pressure trace with best fit curve for PCI_40_9.

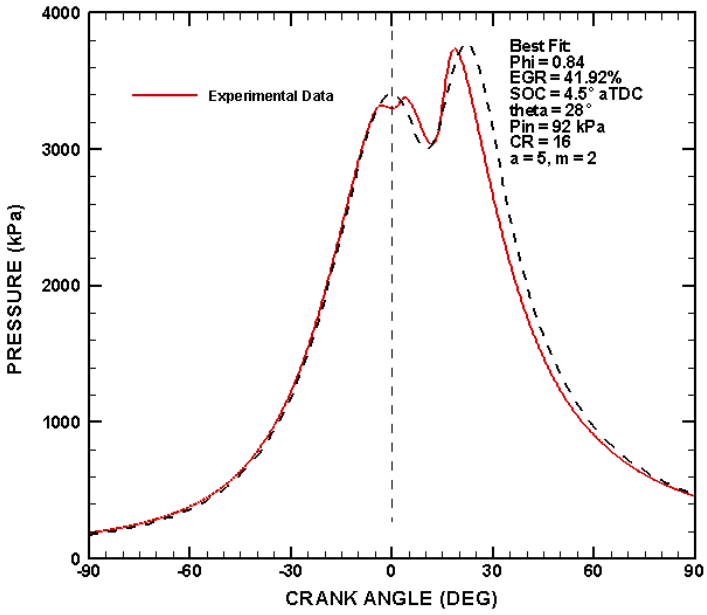

Fig. 55 Comparison of experimental pressure trace with best fit curve for PCI_42_9.

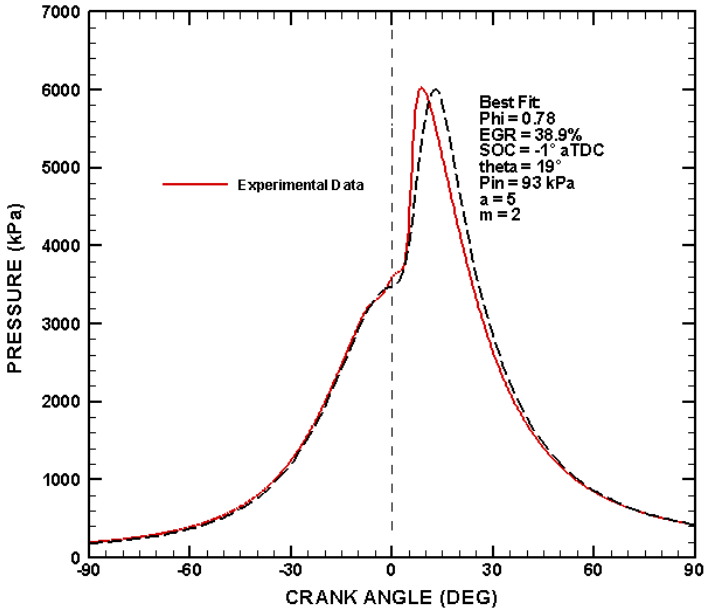

Fig. 56 Comparison of experimental pressure trace with best fit curve for PCI_39_12.

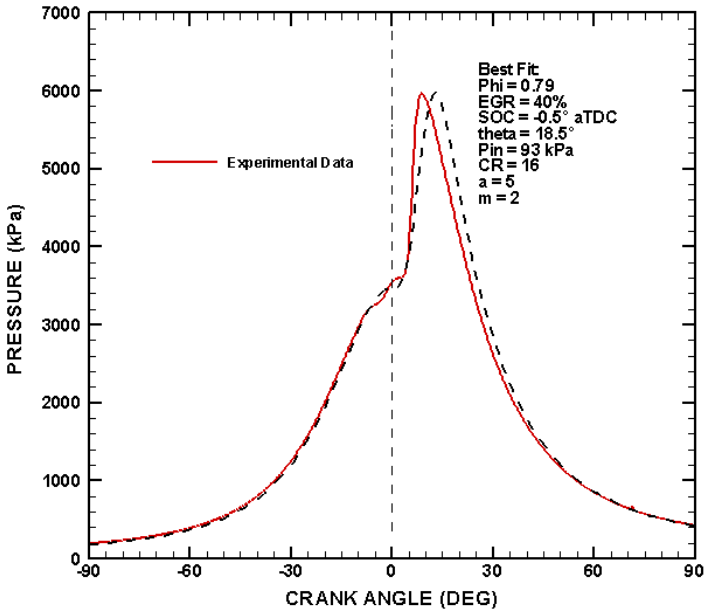

Fig. 57 Comparison of experimental pressure trace with best fit curve for PCI_40_12.

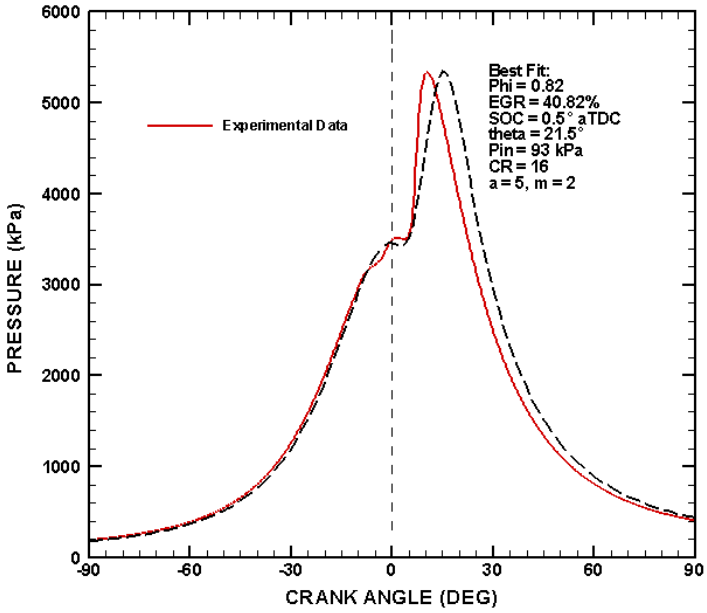

Fig. 58 Comparison of experimental pressure trace with best fit curve for PCI_41_12.

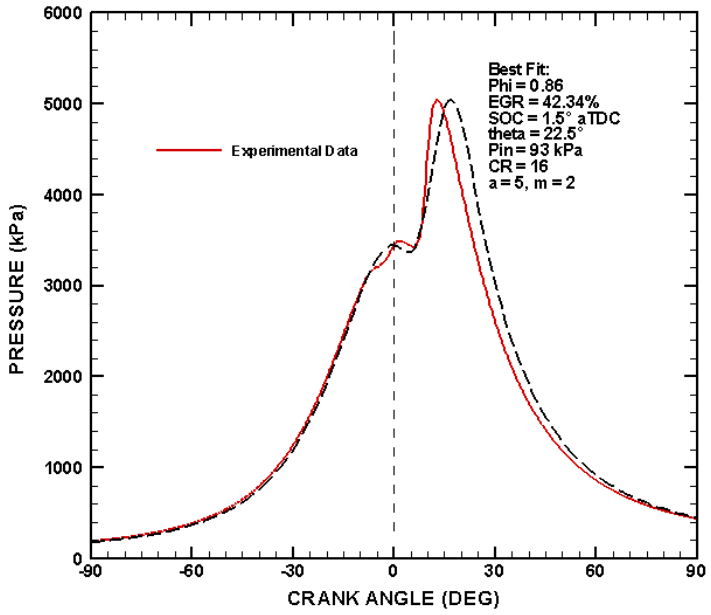

Fig. 59 Comparison of experimental pressure trace with best fit curve for PCI_42_12.

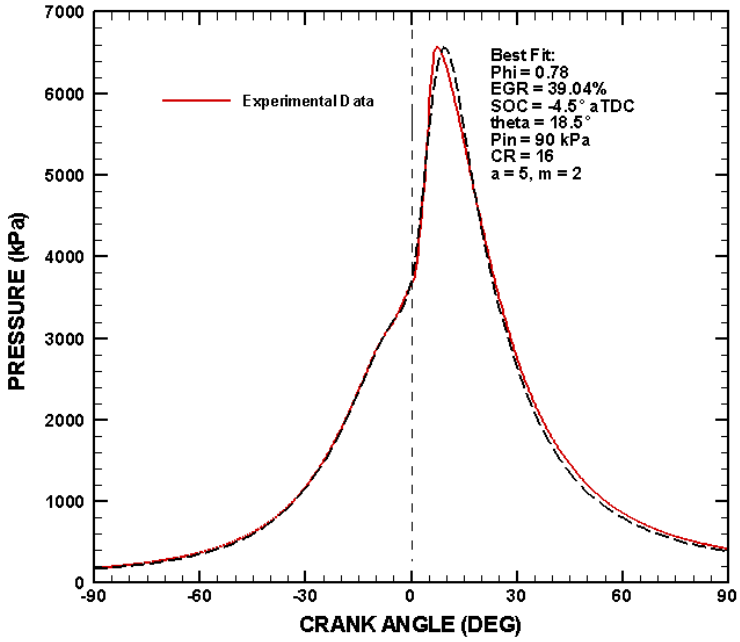

Fig. 60 Comparison of experimental pressure trace with best fit curve for PCI_39_15.

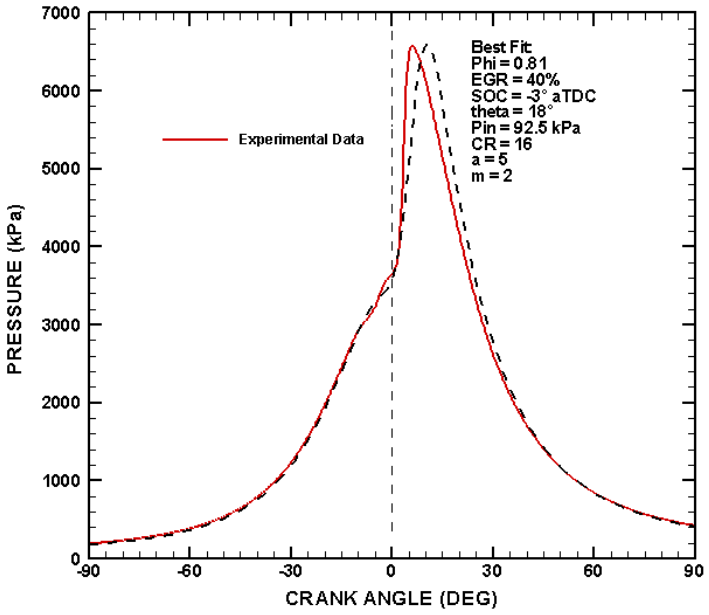

Fig. 61 Comparison of experimental pressure trace with best fit curve for PCI_40_15.

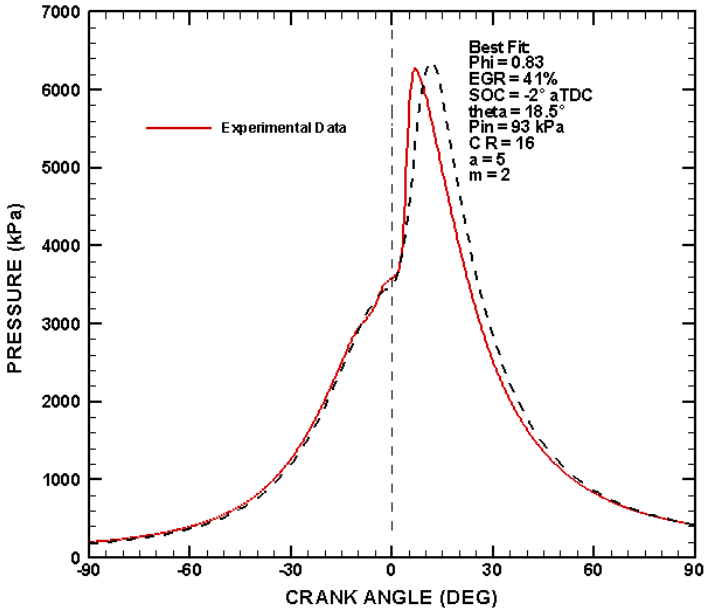

Fig. 62 Comparison of experimental pressure trace with best fit curve for PCI_41_15.

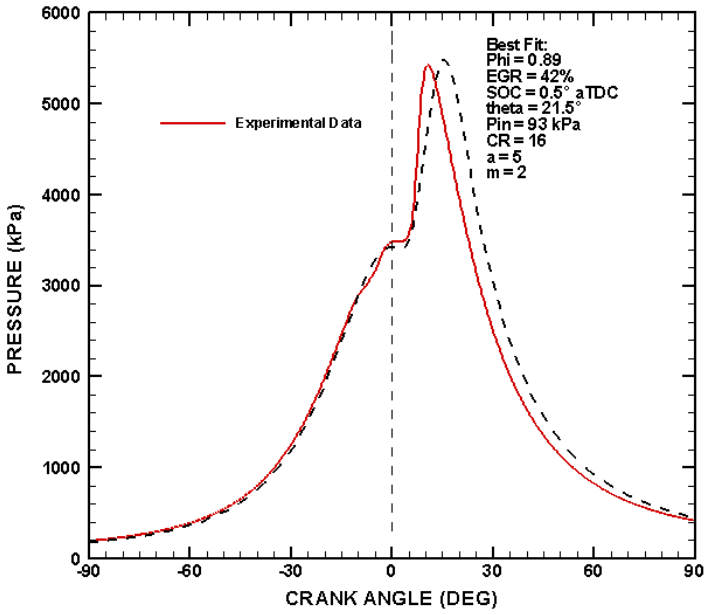

Fig. 63 Comparison of experimental pressure trace with best fit curve for PCI_42_15.

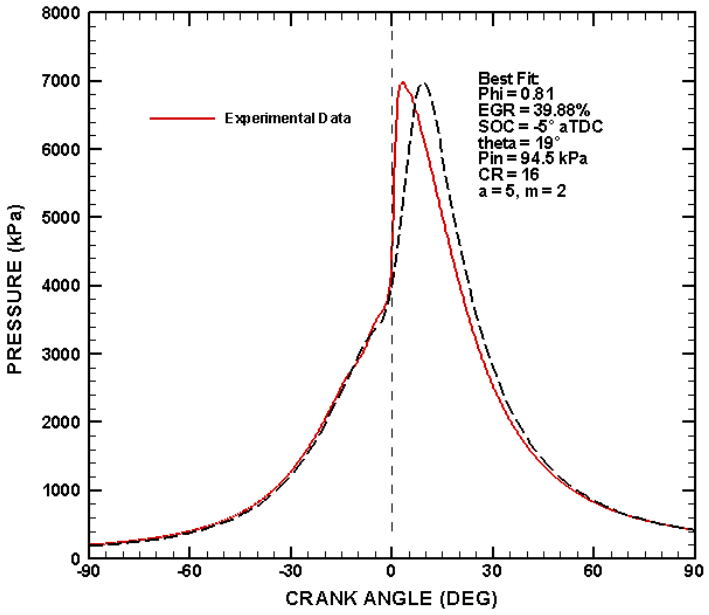

Fig. 64 Comparison of experimental pressure trace with best fit curve for PCI_40_18.

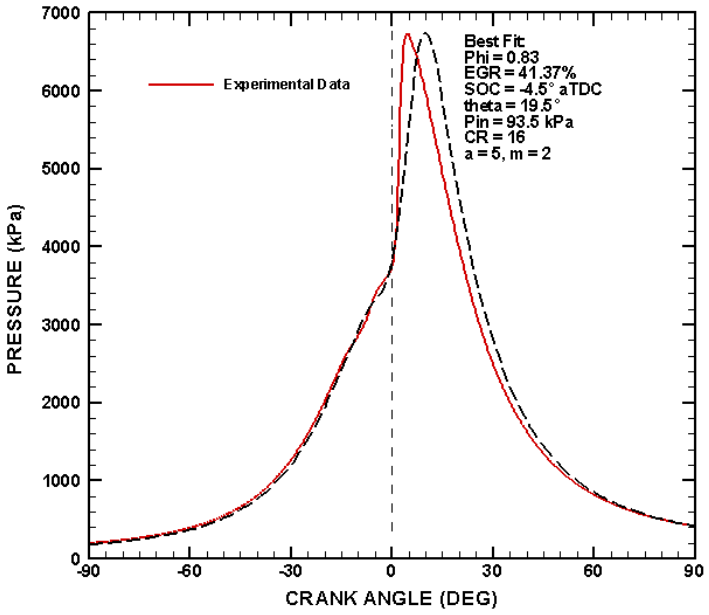

Fig. 65 Comparison of experimental pressure trace with best fit curve for PCI_41_18.

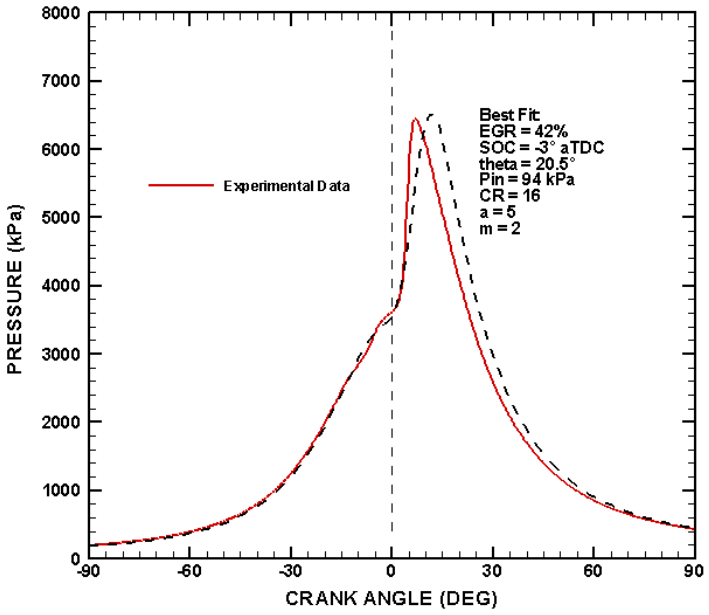

Fig. 66 Comparison of experimental pressure trace with best fit curve for PCI_42_18.

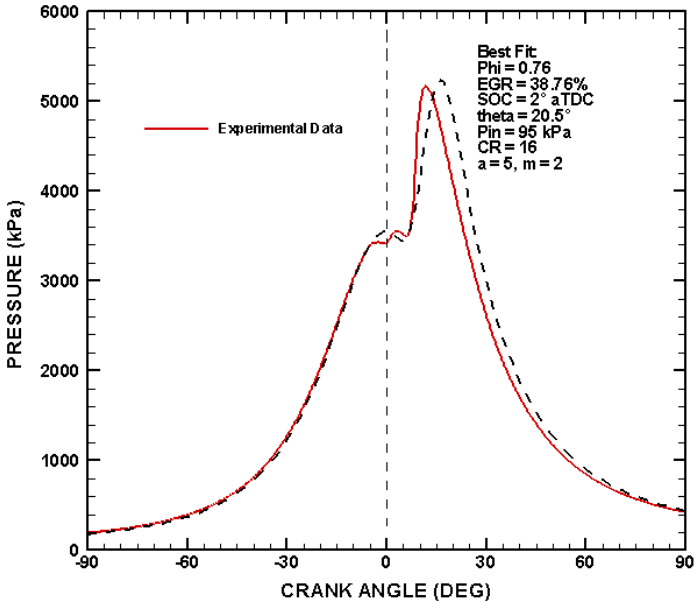

Fig. 67 Comparison of experimental pressure trace with best fit curve for PCI_38_9.

8. RESULTS AND DISCUSSION

Simulation results are obtained for the influence of mode of combustion, injection timing and EGR level on availability balance. Major sources of availability transfer and destruction are identified as availability transfer through heat transfer and exhaust, availability destruction due to combustion, availability destruction through intake mixing and availability unused due to unburned fuel. The remaining availability gets converted into indicated work. For the PCI cases the analysis is carried out to isolate the effect of start of combustion and EGR level on the availability balance. For LC cases, only the effect of start of combustion is analyzed.

Analysis of the influence of injection timing and EGR level is more straightforward compared to the analysis of mode of combustion. For injection timing effects, the cases with same mode of combustion are divided in groups with the same EGR levels. For the EGR level effects, the cases with same mode of combustion are divided in groups with same injection timing.

For the effects of the mode of combustion, both EGR level and the injection timing need to be maintained constant. But EGR level is used as a principal means to switch between the modes of combustion. This dilemma is resolved as described in the following section.

8.1 Influence of mode of combustion

8.1.1 Strategy for mode of combustion analysis

The simulation results for EGR sweeps were shown in Section 6. It was seen that the simulation does not account for the increased ignition delay achieved by higher EGR level. On the contrary, as demonstrated in Section 6, simulation uses Wiebe parameters and combustion duration to characterize combustion process. The only effects of EGR level changes accounted for by simulation are those triggered by the change in composition of the cylinder charge, change in the equivalence ratio and change in the inlet temperature.

Hence it is possible to change the EGR level and still simulate the same mode of combustion by holding Wiebe parameters, start of combustion and combustion duration constant. Even though this approach appears to result in hypothetical operating points, the practicality of achieving such operating conditions can not be eliminated. For example, same ignition delay can be achieved with changes in EGR level in reality with appropriate changes in swirl and combustion chamber modifications. The simulation on the other hand, offers a unique way of maintaining the same mode of combustion irrespective of the changes in EGR level.

Firstly, cases having different modes of combustion but the same injection timing are selected. This eliminates the effect of injection timing. Table 7 lists these cases. It is noted that the simulation does not consider injection timing; instead start of combustion is used as an input to the simulation. Appropriate start of combustion for a given case is determined by fitting the experimental pressure data with the simulation pressure data.

Hence start of combustion location is separated from the actual start of injection location by a few crank angle degrees. The start of combustion for different cases is also listed in Table 7.

Table 7 List of cases compared for the analysis of mode of combustion

Case	Mode	Injection Timing (°bTDC)	Start of Combustion (°bTDC)	EGR Level (%)
Best BSFC	Best BSFC	10	7	0
LC_10	LC	10	0	30
LC_15	LC	15	6	30
PCI_40_15	PCI	15	3	40

It is seen that the mode comparison can be made between Best BSFC and LC_10 if the EGR level is increased to 30% in Best BSFC case without changing the mode of combustion (i.e., all parameters except the EGR level are kept fixed). Similarly, mode comparison can be made between LC_15 and PCI_40_15.

This gives rise to two new simulated cases – Best BSFC_30 and LC_40_15. Best BSFC_30 indicates that this case has same input parameters used for Best BSFC case except for 30% EGR level. Similarly LC_40_10 is the case obtained by using the same input parameters as those used in LC_15 case except for higher EGR level.

It is essential to verify that the above strategy indeed represents three different modes of combustion. The Best BSFC_30 is supposedly having a lower ignition delay (simulated by delayed start of combustion) than that in LC_10. Similarly LC_40_15 is

expected to represent LC mode and thus anticipated to have less ignition delay (simulated by advancing the start of combustion) than PCI_40_15 case.

Table 8 shows the comparison of crank angles turned between injection timing and start of combustion. Even though injection timing is an experimental parameter and the start of combustion is a simulation parameter, this comparison is useful in the sense that the simulation parameters are optimized to represent actual cylinder combustion processes. And hence delayed start of combustion for the same injection timing reflects longer ignition delay in the corresponding experimental cases.

Best BSFC_30 and LC_10 have same injection timing, but the start of combustion has to be delayed in LC_10 case in order to simulate the experimental conditions. This indicates that the LC_10 has longer ignition delay than that observed in Best BSFC_30. Similarly, PCI_40_15 and LC_40_15 both have same injection timing but PCI_40_15 has more delayed start of combustion indicating the presence of longer ignition delay in PCI_40_15 as compared to LC_40_15.

Table 8 Comparison of crank angles revolved between start of injection and start of combustion for Best BSFC_30, LC_10, LC_40_15 and PCI_40_15.

Case	Start of Combustion (°bTDC)	Injection Timing (°bTDC)	Difference between start of combustion and injection timing (°CA)
Best BSFC_30	7	10	3
LC_10	0	10	10
LC_40_15	6	15	9
PCI_40_15	3	15	12

Another implication of the above strategy to analyze effects of mode of combustion is that only EGR level is varied to obtain new simulated cases (namely Best BSFC_30 and LC_40_15). The parameters such as inlet and exhaust port pressures, equivalence ratios are also kept constant, as used in the corresponding simulated original cases (Best BSFC and LC_15 respectively). As a result fuel mass flow rates and air mass flow rates are different in these cases. The comparison of these parameters is shown in Table 9. It is seen that the equivalence ratio increases as the mode of combustion is shifted from Best BSFC to LC to PCI. The differences in fuel mass flow rates and air mass flow rates must be taken into account before interpreting availability results for mode of combustion analysis. This is because, differences in the fuel flow rates effectively change the total fuel availability supplied to the engine per cycle. This point will be emphasized in next section in relation to the interpretation of availability results.

Table 9 Comparison of simulated mass flow rates, inlet and exhaust port pressure and equivalence ratios for Best BSFC_30, LC_10, LC_40_15 and PCI_40_15 cases.

Case	Equivalence ratio	P_{in} (kPa)	P_{out} (kPa)	M_{fuel} (g/cycle)	M_{air} (g/cycle)	T_{exh} (K)	T_{EGR} (K)
Best BSFC_30	0.387	105	103.34	0.0081	0.31	560	360
LC_10	0.552	110	112.03	0.012	0.32	583	364
LC_40_15	0.558	110	111.44	0.011	0.28	540	364
PCI_40_15	0.810	92.5	102.2	0.012	0.23	536	375

8.1.2 Simulation results

Figure 68 shows the influence of mode of combustion on availability balance by comparing results obtained for Best BSFC_30 and LC_10. Figure 69 compares the results obtained for LC_40_15 and PCI_40_15.

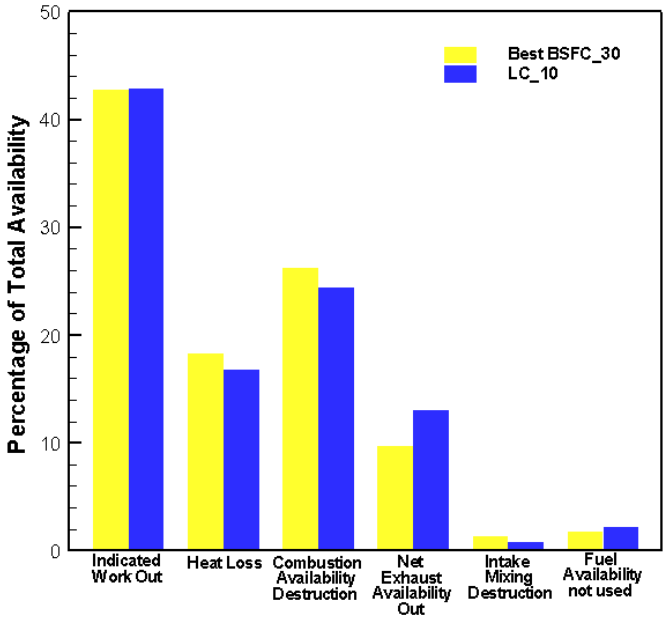

Fig. 68 Comparison of availability destruction and transfers during an engine cycle between Best BSFC and LC modes.

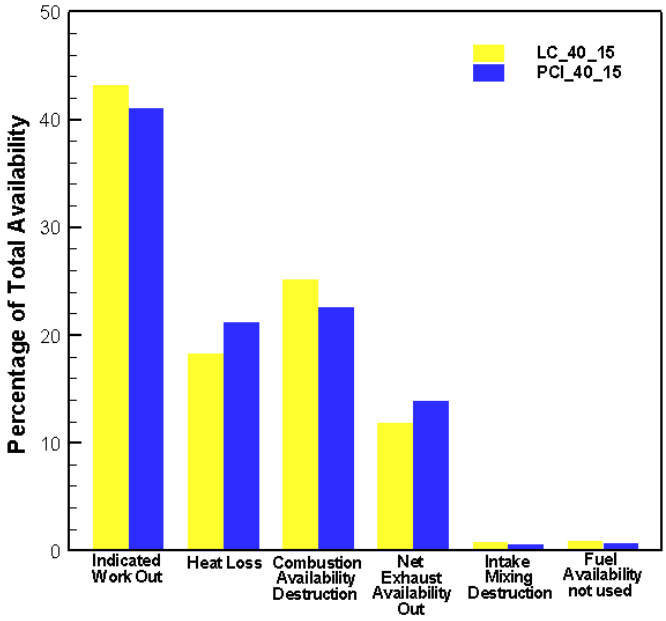

Fig. 69 Comparison of availability destruction and transfers in an engine cycle between LC and PCI modes.

8.1.3 Discussion

The change in the availability balance with the change in the mode of combustion as seen in the Figure 68 and Figure 69 is described below. The discussion highlights the changes occurring in different components of availability balance.

8.1.3.1 Indicated work out

It is seen that the percentage of the fuel availability converted into indicated work is almost the same in Best BSFC_30 and LC_10 cases. But the availability converted into useful work is less in PCI_40_15 case than that in LC_40_15. Indicated work is a function of many engine parameters such as injection timing, EGR level, equivalence ratio. As all these parameters are changing with the change in mode of combustion, the

individual factors responsible for above results can not be identified. But more optimized matching of these parameters could be achieved for higher percentage of availability conversion into indicated work.

8.1.3.2 Heat loss

It is seen from figure 68 that the availability transfer due to heat transfer decreases as the mode of combustion changes from Best BSFC_30 to LC_10. Figure 69 shows that the availability transfer through heat transfer is higher in PCI_40_15 than that in LC_40_15. The bulk gas temperatures are thus compared to gain more insight into the obtained results. The comparison is shown in Figure 70 and Figure 71. Figure 70 shows that the bulk gas temperatures are much higher in LC_10 as compared to Best BSFC_30. This contradicts with the higher percentage of availability transfer due to heat transfer observed in Best BSFC_30. The corresponding heat transfer coefficients are thus compared to gain further insight into the heat transfer rates. Figure 72 shows this comparison. It is seen that the heat transfer coefficient is also higher in LC_10 as compared to Best BSFC_30. Higher heat transfer coefficient along with higher bulk gas temperature would cause the heat transfer rate to be high in LC_10 and thus the availability transfer through heat transfer would be expected to be higher in LC_10 instead of Best BSFC_30. This apparent contradiction can be resolved by comparing the mass flow rates, inlet and exhaust port pressures and equivalence ratios between these cases. As seen in Table 8 the fuel flow rates and air flow rates are different in these two cases. As a result the amount of energy released (or the total fuel availability) is different

in these two cases. At the same time, it is noted that the availability results represent percentage distribution of availability in various components as opposed to the absolute magnitude. Thus, there is a possibility that even though the heat transfer rates are higher in LC_10 due to higher bulk gas temperatures, availability transferred due to heat transfer is less in terms of percentage of total fuel availability transferred due to heat transfer. This notion is in fact, found to be correct after comparing the fuel availabilities for these two cases. Best BSFC_30 has an incoming fuel availability of 0.3521 kJ/cycle, which is smaller than 0.5263 kJ/cycle supplied in LC_10 case. The actual heat transfer rates for these cases are compared in Figure 73.

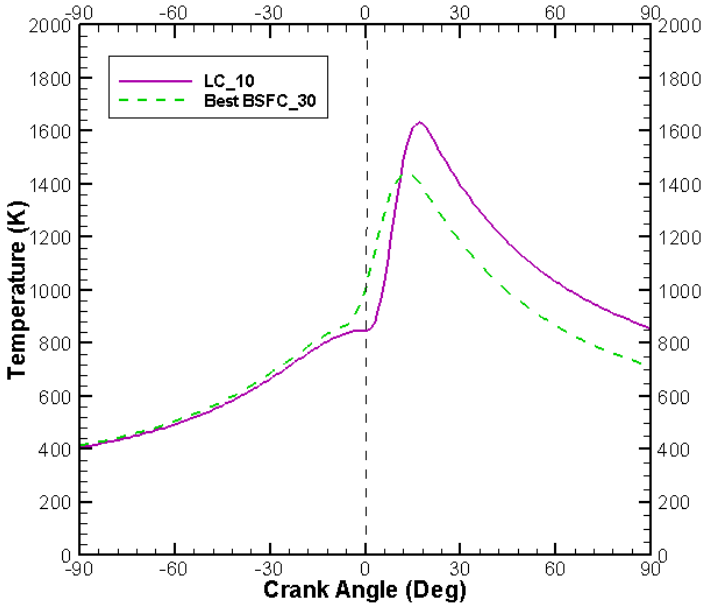

Fig. 70 Comparison of bulk gas temperatures between Best BSFC_30 and LC_10.

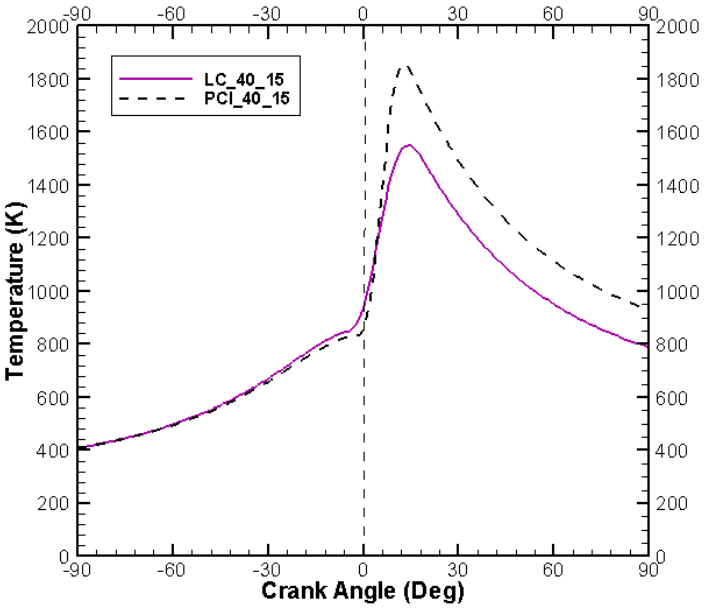

Fig. 71 Comparison of bulk gas temperatures between LC_40_15 and PCI_40_15.

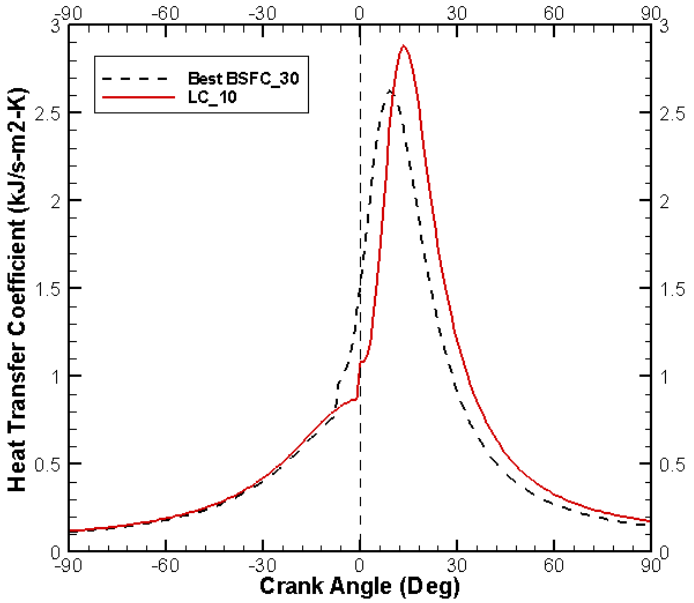

Fig. 72 Comparison of heat transfer coefficient between LC_10 and Best BSFC_30.

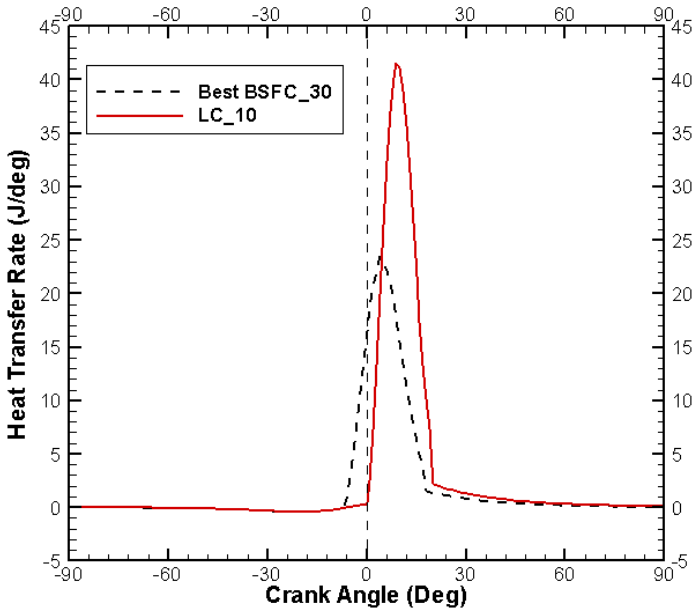

Fig. 73 Comparison of heat transfer rates between Best BSFC_30 and LC_10.

Comparison of mass flow rates between LC_40_15 and PCI_40_15 on the contrary, indicates that the fuel flow rate is almost the same in both the cases but the air flow rate is much smaller in PCI_40_15 than that in LC_40_15. As a result, there would be comparatively lesser cylinder charge available to absorb the energy released by combustion. As a result higher temperatures are expected to occur resulting in higher heat transfer rates. Figure 71 shows that the bulk gas temperatures are indeed higher in PCI_40_15 as compared to LC_40_15. Comparison of heat transfer coefficient shown in Figure 74 also indicates that the heat transfer rates would be higher in PCI_40_15. Figure 75 compares the corresponding heat transfer rates.

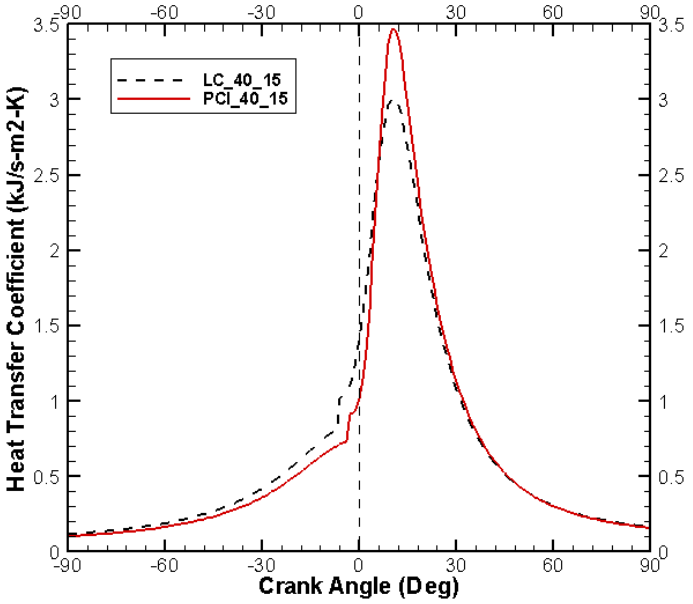

Fig. 74 Comparison of heat transfer coefficient between PCI_40_15 and LC_40_15.

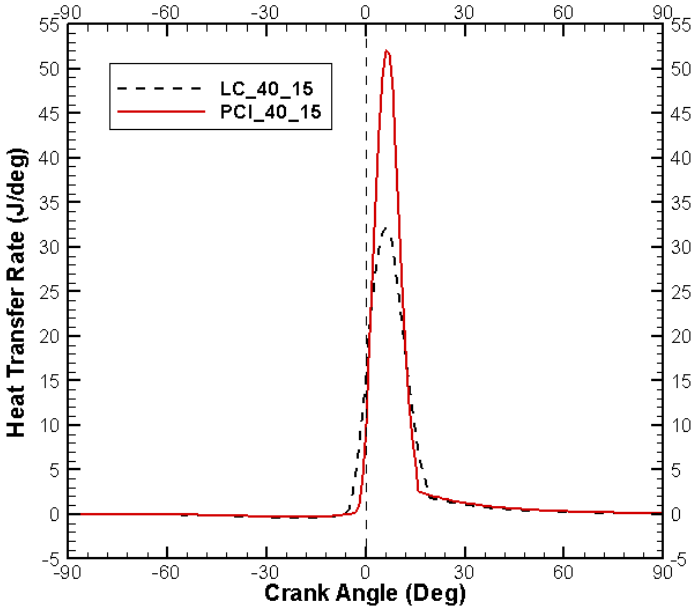

Fig. 75 Comparison of heat transfer rates between LC_40_15 and PCI_40_15.

8.1.3.3 Combustion availability destruction

It is seen from Figure 68 and Figure 69 that the combustion availability destruction decreases as the mode of combustion is shifted from Best BSFC to LC to PCI mode. It is seen earlier that the ignition delay increases as the mode of combustion changes from Best BSFC to LC to PCI. This would lead to higher degree of premixed burning in PCI cases. But the simulation being based on the homogeneous combustion model, does not consider the differences in fraction of premixed and diffusion burning in these modes of combustion. Hence combustion duration and Wiebe parameters for these cases are compared to understand the obtained trends in the combustion availability destruction. Table 10 shows this comparison.

Table 10 Comparison of combustion duration and Wiebe parameters between Best BSFC_30, LC_10, LC_40_15 and PCI_40_15

Case	Combustion Duration (°CA)	Wiebe parameter 'a'	Wiebe Parameter 'm'
Best BSFC_30	24	4	1.5
LC_10	19	3.8	1.5
LC_40_15	24	4.7	1.8
PCI_40_15	18	5	2

It can be seen that higher 'a' and 'm' values along with shorter combustion duration in PCI_40_15 gives the least availability destruction. LC_40_15 uses higher Wiebe parameters than those used in LC_10. But the combustion duration for LC_40_15 is longer than that in LC_10. These two factors have opposite effect on the combustion availability destruction. As a result, both these cases show the same percentage of availability destruction due to combustion. Best BSFC_10 on the contrary uses lower

values of Wiebe parameters along with longer combustion duration. Hence this case has the maximum combustion availability destruction among the four cases considered above.

The comparison of adiabatic zone temperatures also indicates the same availability balance trends observed. The adiabatic zone temperature increases as the mode of combustion is shifted from Best BSFC to LC to PCI. The comparison of adiabatic zone temperatures is shown in Figure 76 and Figure 77.

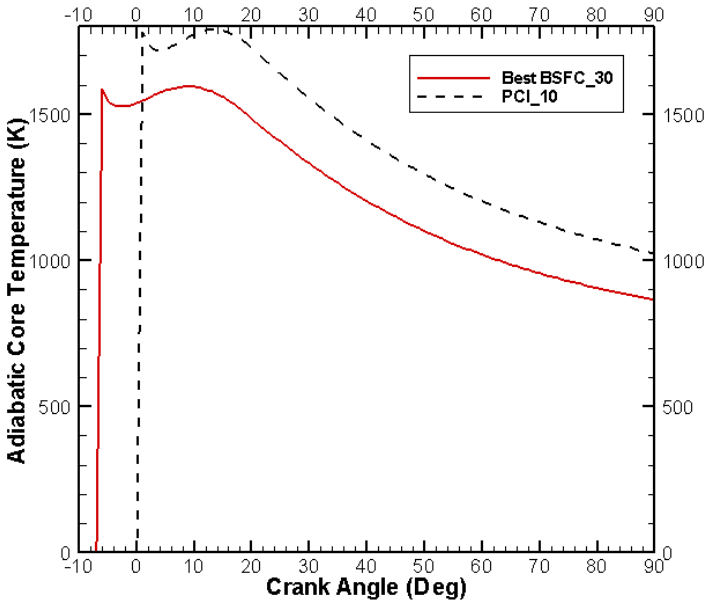

Fig. 76 Comparison of adiabatic core temperatures between LC_10 and Best BSFC_30.

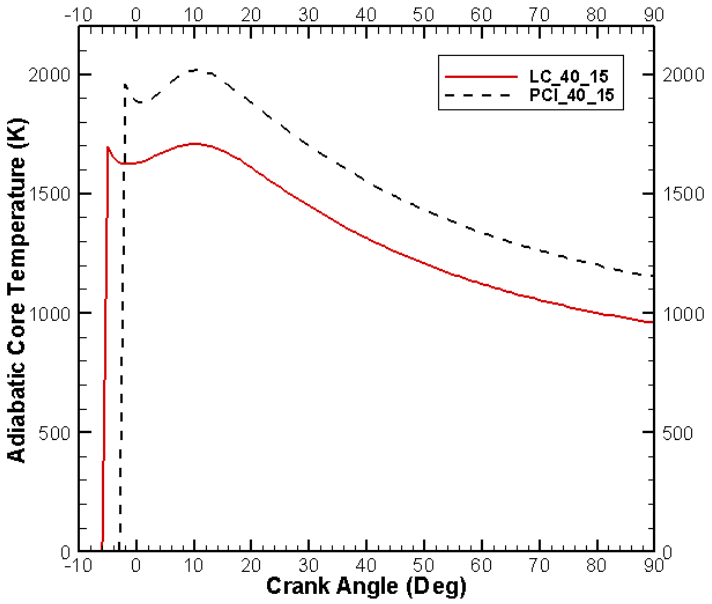

Fig. 77 Comparison of adiabatic core temperatures between LC_40_15 and PCI_40_15.

8.1.3.4 Net exhaust availability out

As expected, the availability transfer through the exhaust increases as the mode of combustion shifts from Best BSFC to LC to PCI mode (See Figure 68 and Figure 69). This could be attributed to the delayed start of combustion with shifting of mode of combustion from Best BSFC to PCI. More retarded start of combustion implies that the combustion continues late in the expansion stroke increasing the exhaust gas temperature. A delayed start of combustion also implies less thermodynamic expansion which further increases the exhaust availability transfer with change in mode of combustion from Best BSFC to PCI. Table 9 shows the comparison of exhaust gas temperatures between these cases. The increasing exhaust gas temperatures as

combustion mode shifts from Best BSFC to PCI further suggests the occurrence of delayed combustion.

8.1.3.5 Intake mixing destruction

Both Best BSFC_30 and LC_10 use 30% EGR. Hence the composition of the intake charge and the residual gases are expected to be approximately equal in both cases. Small difference exists between the inlet EGR temperatures as shown in Table 9. Similar EGR inlet temperature difference can be seen between LC_40_15 and PCI_40_15 cases. This explains the slight differences in the intake mixing destruction observed in Figure 68 and Figure 69.

8.1.3.6 Fuel availability not used

This component of availability balanced is exclusively influenced by the Wiebe parameters. Higher 'a' values result in more complete combustion while parameter 'm' does not affect the percentage of unburned fuel at the end of combustion. This follows from the Wiebe function (Equation 7):

In this equation, y is the extent of reaction. Hence at the end of combustion duration y = 1. Hence,

$$x_b = 1 - \exp(-a) \tag{12}$$

Hence as 'a' increases, x_b decreases. Or in other words, higher values of 'a' leave smaller fraction of fuel unburned at the end of the combustion process.

Wiebe parameters used for above four cases are summarized in Table 11. Hence the trends observed from Figure 68 and Figure 69 are congruent with the corresponding Wiebe parameters used.

Table 11 Summary of Wiebe parameters used for Best BSFC_30, LC_10, LC_40_15 and PCI_40_15.

Case	Wiebe parameter 'a'	Wiebe Parameter 'm'
Best BSFC_30	4	1.5
LC_10	3.8	1.5
LC_40_15	4.7	1.8
PCI_40_15	5	2

8.2 Influence of EGR

Fifteen PCI cases are analyzed for the influence of change in EGR level. The cases are grouped together as per the injection timing to eliminate the effect of injection timing. Figures 78 – 81 show the simulation results.

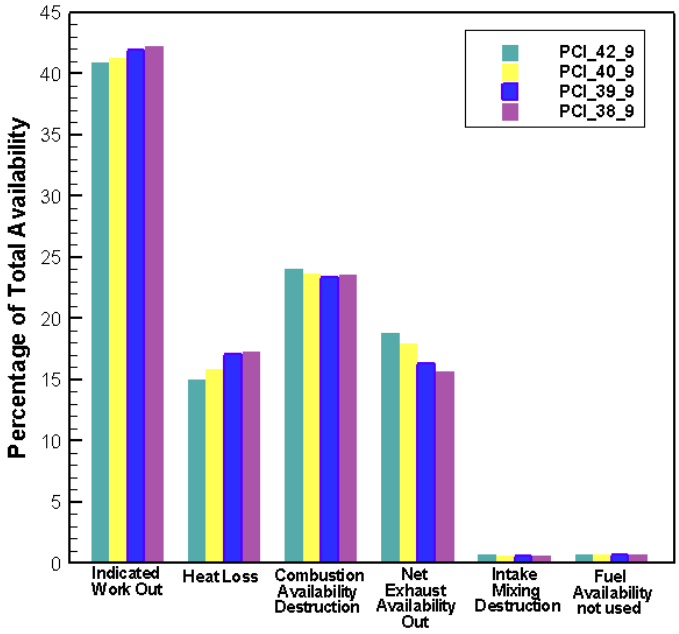

Fig. 78 Availability destruction and transfers during an engine cycle for PCI cases with injection timing 9° bTDC.

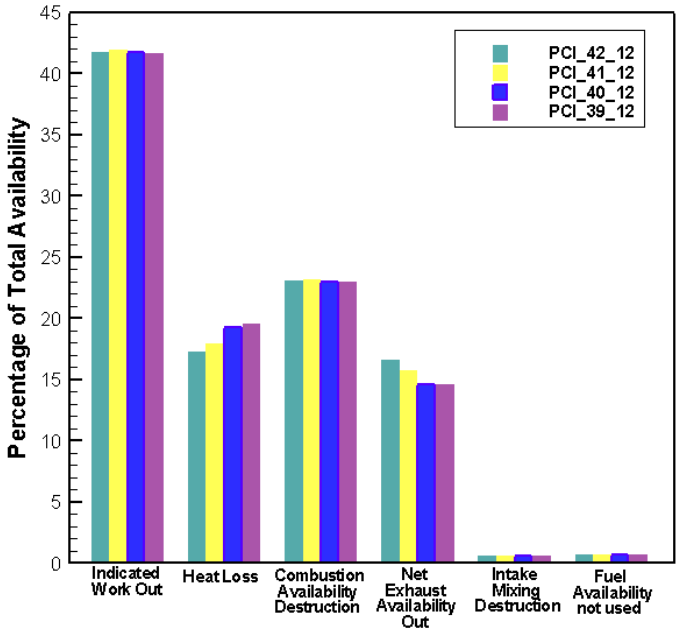

Fig. 79 Availability destruction and transfers during an engine cycle for PCI cases with injection timing 12° bTDC.

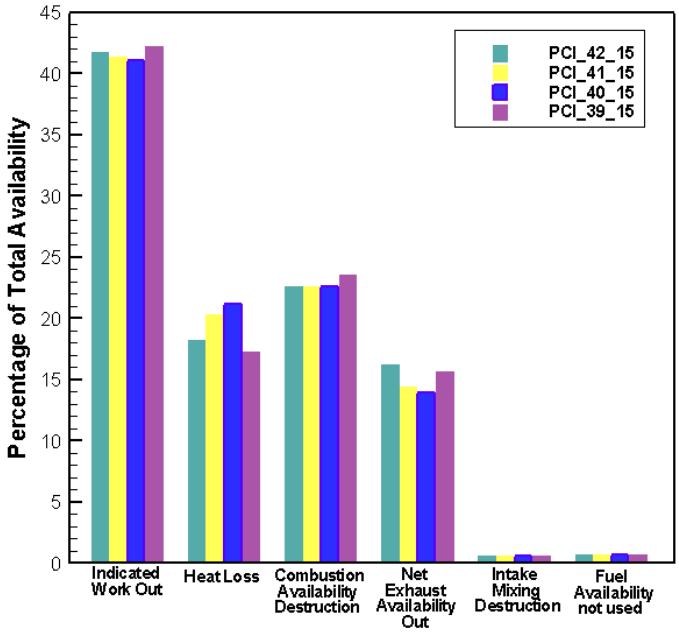

Fig. 80 Availability destruction and transfers during an engine cycle for PCI cases with injection timing 15° bTDC.

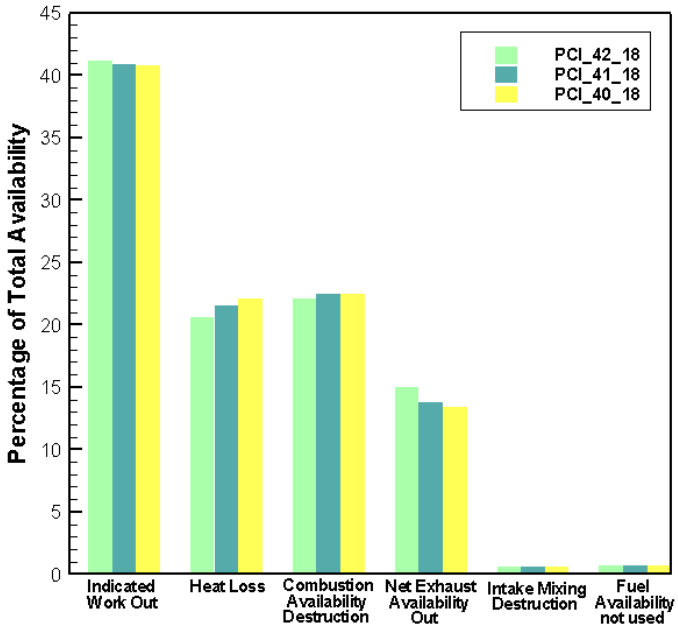

Fig. 81 Availability destruction and transfers during an engine cycle for PCI cases with injection timing 18° bTDC.

8.2.1 Indicated work out

There is no particular trend with changing EGR level observed in percentage of availability converted into work. This percentage is more or less the same for all the cases with change in EGR level.

8.2.2 Heat loss

Except for the injection timing of 15° bTDC (Figure 74), all other figures show a gradual decrease in the percentage of availability transferred through heat loss as the EGR level increases. This trend is expected as the EGR helps in reducing the combustion temperature, even though it increases the initial charge temperature. Thus, the heat transfer during and after the combustion event plays more dominant role in the total heat transferred in an entire engine cycle. A look at the bulk gas temperatures for these cases further supports this explanation. Figures 82 – 85 show that the bulk gas temperature indeed reduces as the EGR level increases. In case of PCI cases with 15° bTDC injection timing, there is no significant difference in bulk gas temperature with EGR and that is reflected in the availability balance of these cases. The trends in the heat transfer coefficient are also compared as shown in Figures 86 – 89, which indicate that the heat transfer coefficient decreases as the EGR level increases. This further reduces heat transfer with increasing EGR levels.

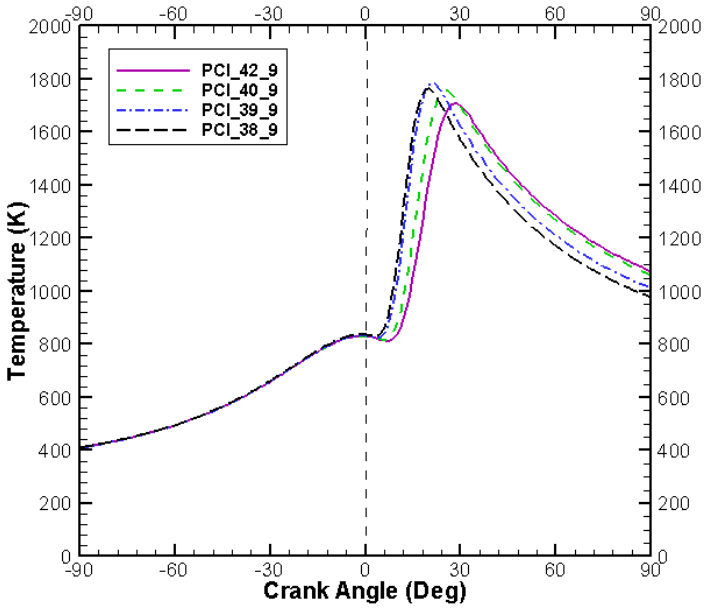

Fig. 82 Bulk gas temperature versus crank angle for PCI cases with injection timing 9° bTDC.

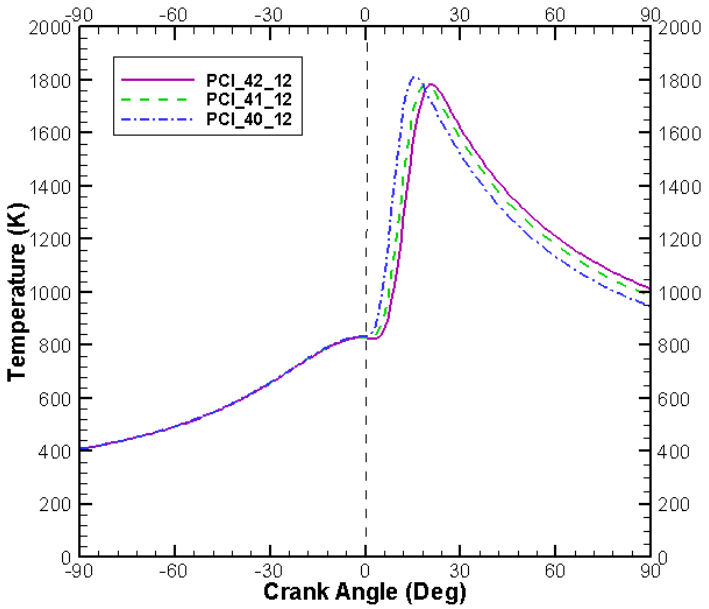

Fig. 83 Bulk gas temperature versus crank angle for PCI cases with injection timing 12° bTDC.

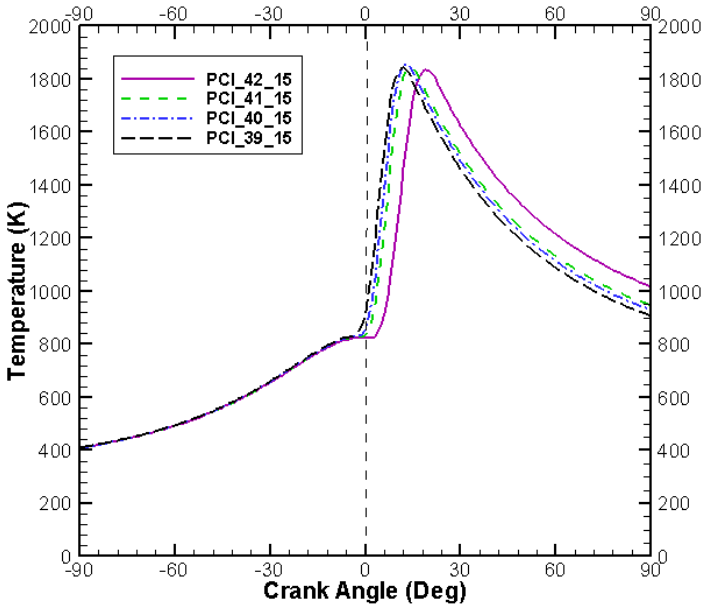

Fig. 84 Bulk gas temperature versus crank angle for PCI cases with injection timing 15° bTDC.

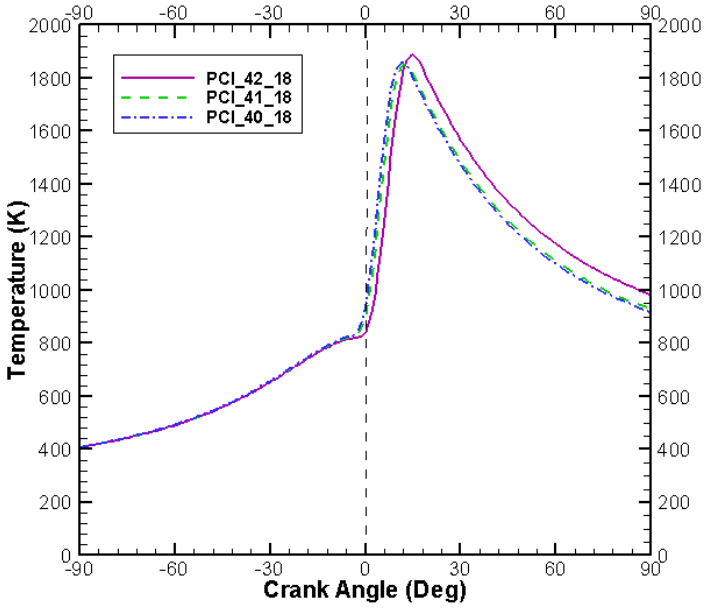

Fig. 85 Bulk gas temperature versus crank angle for PCI cases with injection timing 18° bTDC.

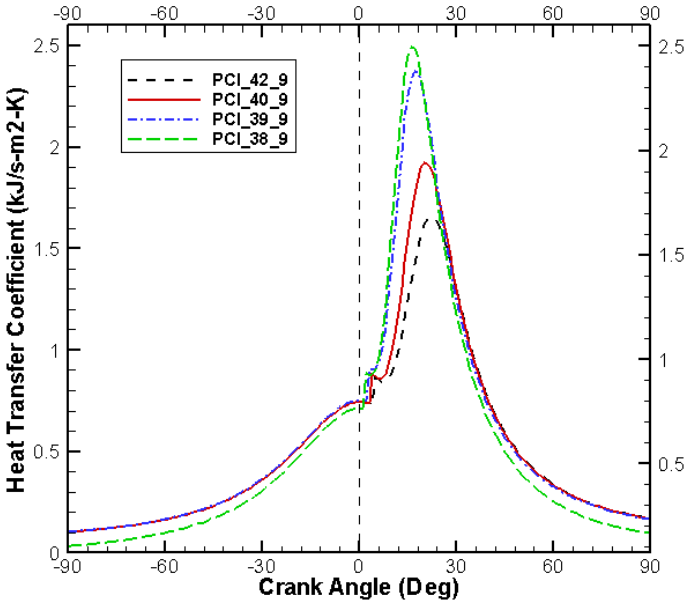

Fig. 86 Heat transfer coefficient versus crank angle for PCI cases with injection timing 9° bTDC.

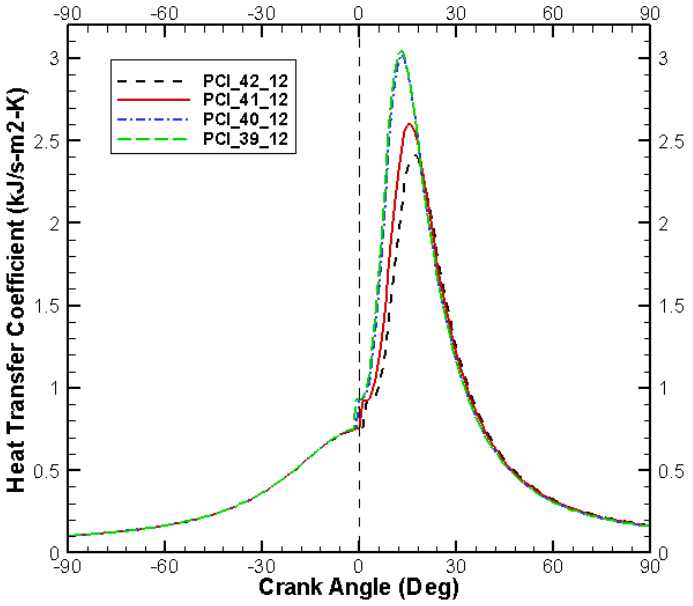

Fig. 87 Heat transfer coefficient versus crank angle for PCI cases with injection timing 12° bTDC.

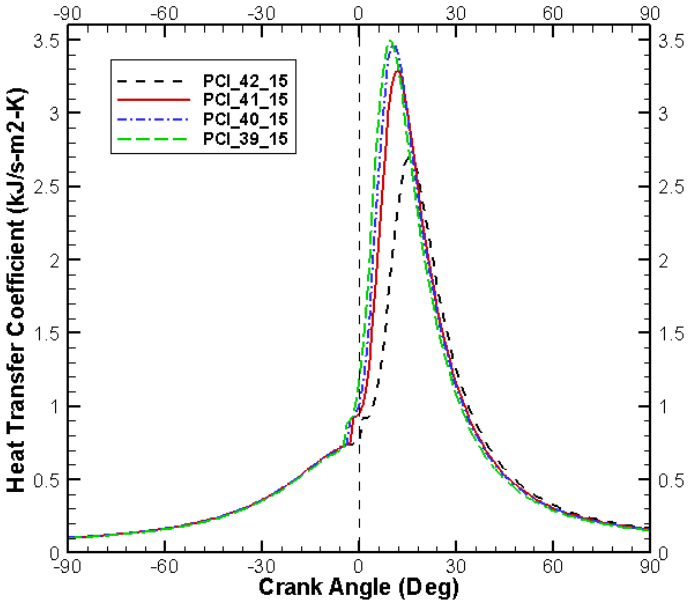

Fig. 88 Heat transfer coefficient versus crank angle for PCI cases with injection timing 15° bTDC.

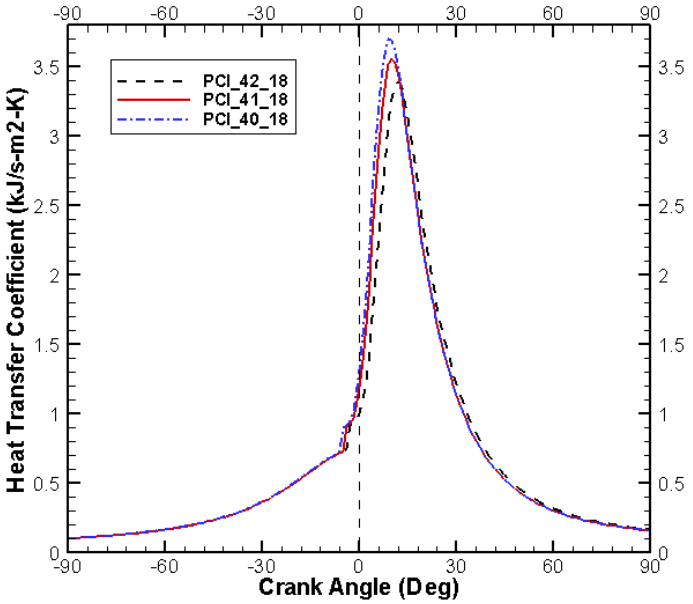

Fig. 89 Heat transfer coefficient versus crank angle for PCI cases with injection timing 18° bTDC.

8.2.3 Combustion availability destruction

It is observed that the percentage of availability destroyed in a combustion process is almost equal for different EGR levels. It was demonstrated earlier that the mode of combustion has a significant influence on the availability destroyed in a combustion process. Combustion temperature also affects this balance. But in all of the above cases, the EGR varies very slightly. The mode of combustion is essentially the same in all of the cases. Hence the components that are responsible for combustion availability destruction, namely, internal energy transfer, mixing and irreversible chemical reactions are equally influencing the availability balance in these cases.

8.2.4 Net exhaust availability out

The percentage of total availability transferred through the exhaust decreases with the decrease in the EGR level (except for the PCI cases with injection timing of 15° bTDC (Figure 80)). The increasing EGR level increases the ignition delay. This effect is incorporated in the simulation by delayed start of combustion. The delayed combustion in turn increases the exhaust gas temperature as combustion continues into the expansion stroke and there is less time for the heat transfer (this has been confirmed through the trend observed in availability destruction via heat loss). Less thermodynamic expansion of the cylinder charge associated with delayed combustion further augments the exhaust availability transfer with increasing EGR levels. The exhaust gas temperatures listed in Table 12 for these cases are in accord with the observed trends of the availability balance.

Table 12 Comparison of simulated mass averaged exhaust gas temperature for PCI cases.

Injection Timing degree bTDC	Case nomenclature	Exhaust Gas Temperature (K)
9	PCI_42_9	619
9	PCI_40_9	614
9	PCI_39_9	591
12	PCI_42_12	573
12	PCI_41_12	540
12	PCI_40_12	554
12	PCI_39_12	558
15	PCI_42_15	564
15	PCI_41_15	540
15	PCI_40_15	536
15	PCI_39_15	536
18	PCI_42_18	534
18	PCI_41_18	527
18	PCI_40_18	528

8.2.5 Intake mixing destruction

Intake mixing destruction largely depends on the temperature and compositional difference between the intake charge and the residual fraction. All the cases grouped as per the same injection timing use very similar EGR levels. This results in almost equal percentage availability destruction via intake mixing.

8.2.6 Fuel availability not used

This value is based on the Wiebe parameter ‘a’. As the same Wiebe parameters are used for the curve fitting of the PCI cases, the percentage of fuel availability not used

for all the PCI cases is around 0.66% irrespective of the EGR level and injection timing used.

8.3 Influence of injection timing

Fifteen PCI cases and five LC cases are analyzed for the effect of injection timing on availability balance. The cases using equal EGR levels are grouped together to eliminate the effect of EGR. Figures 90 – 94 show the simulation results.

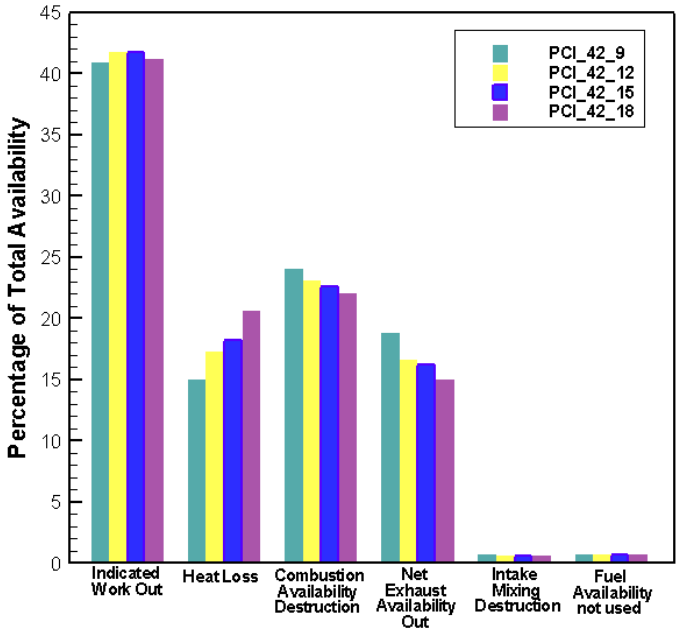

Fig. 90 Availability destruction and transfers in an engine cycle for PCI cases using 42% EGR.

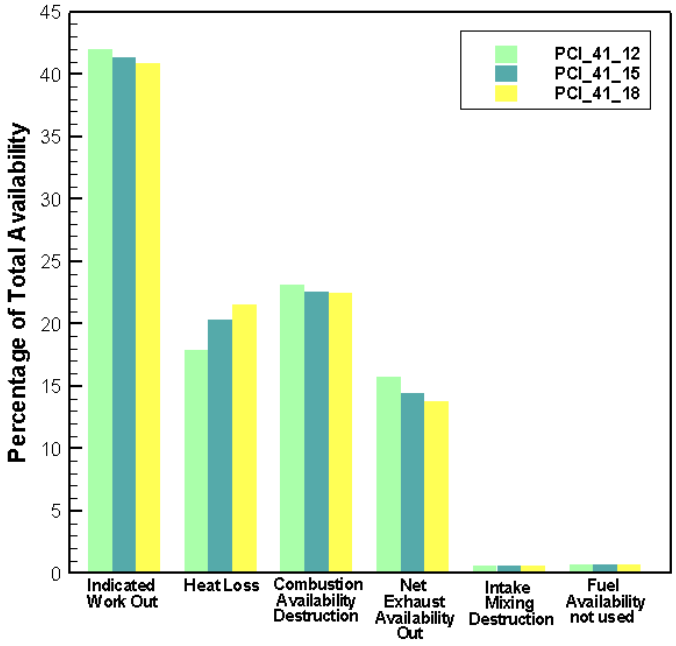

Fig. 91 Availability destruction and transfers in an engine cycle for PCI cases using 41% EGR.

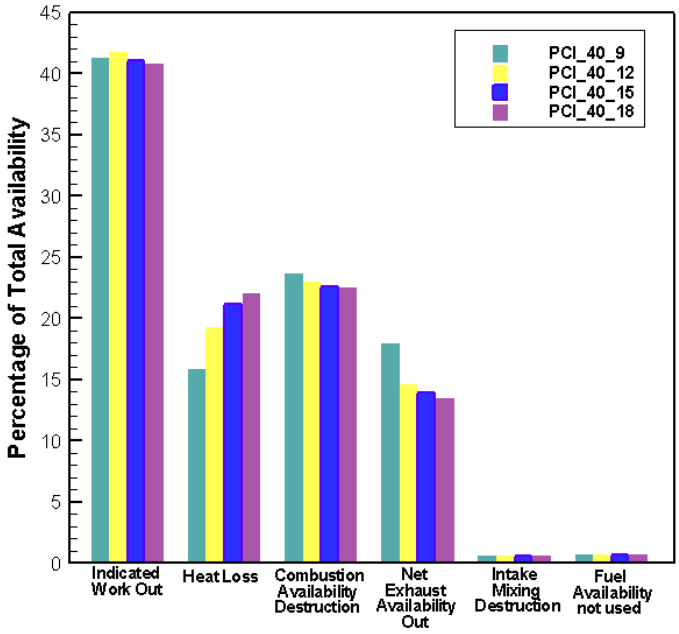

Fig. 92 Availability destruction and transfers in an engine cycle for PCI cases using 40% EGR.

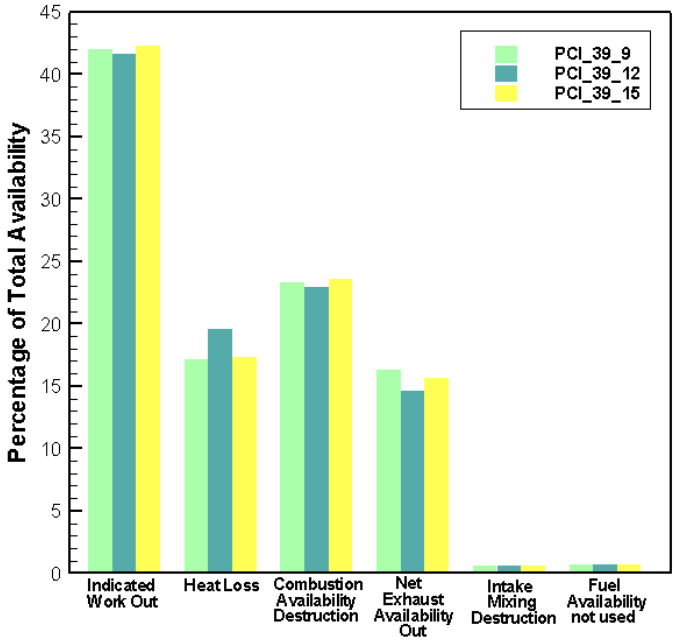

Fig. 93 Availability destruction and transfers in an engine cycle for PCI cases using 39% EGR.

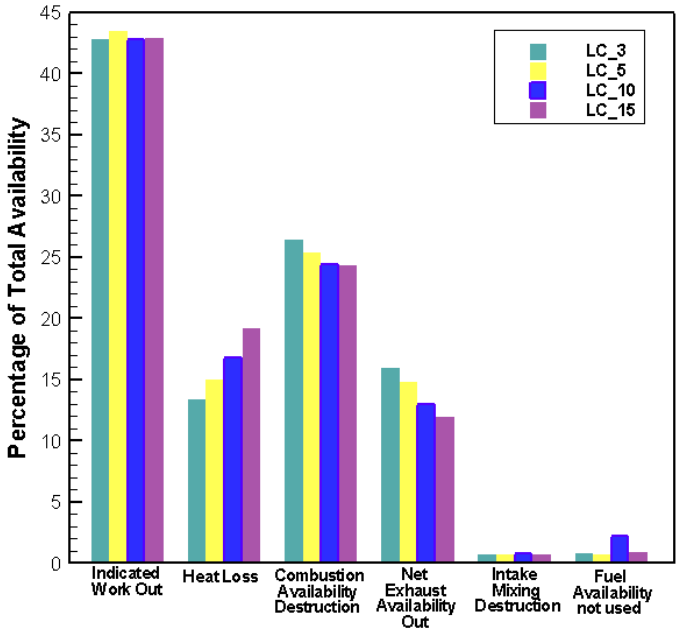

Fig. 94 Availability destruction and transfers in an engine cycle for LC cases.

8.3.1 Indicated work out

There is no particular trend with changing injection timing observed in percentage of availability converted into work. But from the figures 90 – 94, it is seen that this percentage is around the same irrespective of the injection timing used.

8.3.2 Heat loss

It is seen that the percentage of availability transferred through heat loss increases as the injection timing is advanced (except for the PCI cases using 39% EGR (Figure 93)). This might be due to two reasons: the advanced injection timing causes combustion to take place early. As the combustion occurs before or near top dead center, the combustion temperatures attained are higher than those attained with more retarded injection timing. This augments heat transfer. The second reason is that, as the combustion starts early in the cycle, there is more time available for heat transfer to take place. The bulk gas temperatures for these cases are compared to verify the rationale behind the observed trends. Figures 95 – 99 show the trend in bulk gas temperatures for these cases as the injection timing is gradually advanced. Figures 100 – 104 show the comparison of heat transfer rate. As expected, heat transfer rates increase as the injection timing is advanced.

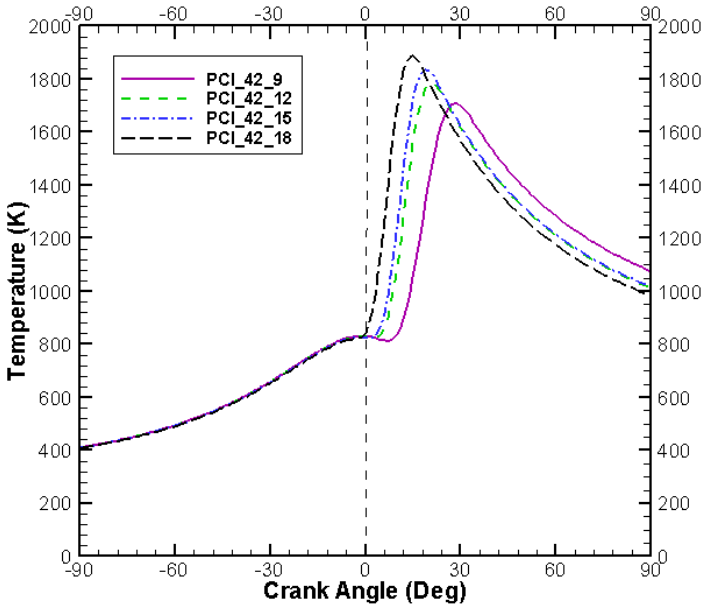

Fig. 95 Bulk gas temperatures versus crank angle for PCI cases with 42% EGR level.

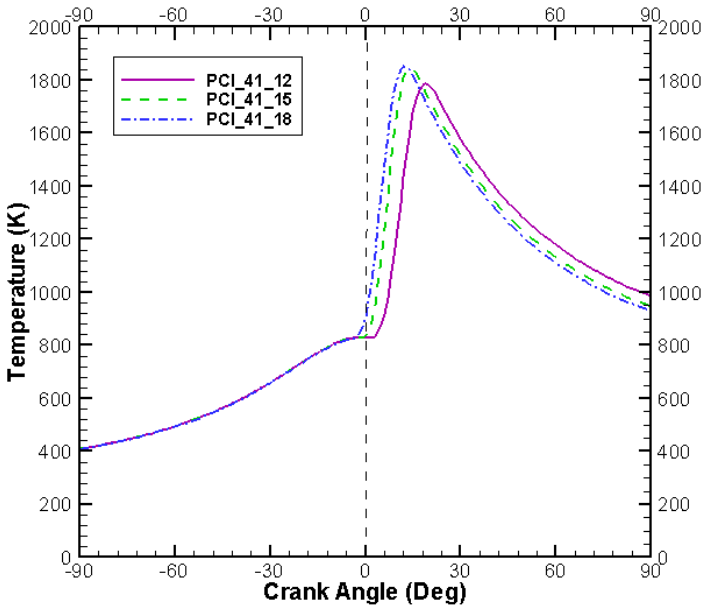

Fig. 96 Bulk gas temperatures versus crank angle for PCI cases with 41% EGR level.

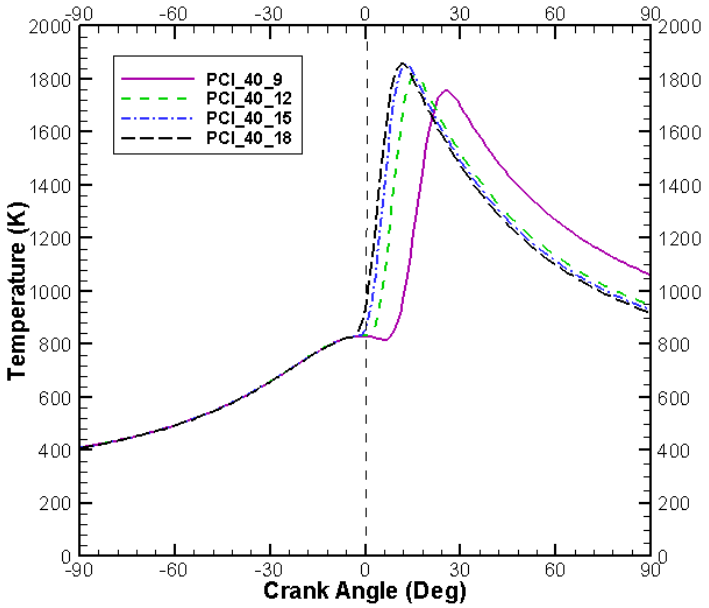

Fig. 97 Bulk gas temperatures versus crank angle for PCI cases with 40% EGR level.

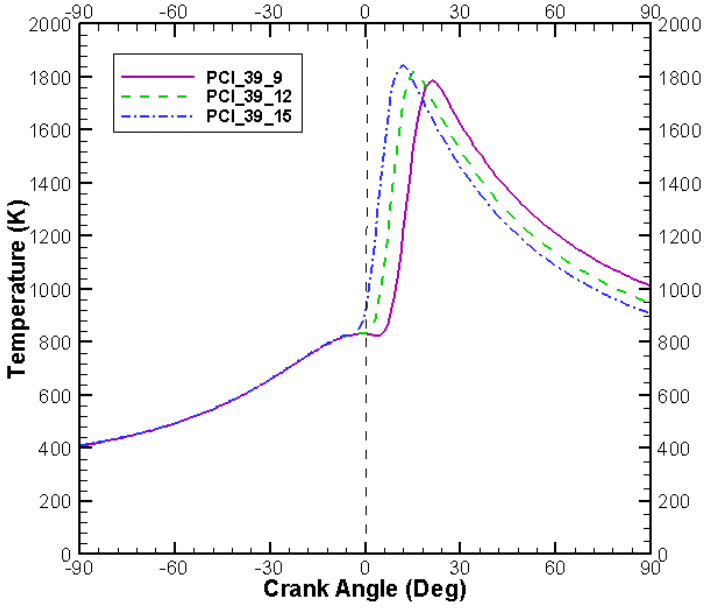

Fig. 98 Bulk gas temperature versus angle for PCI cases with 39% EGR level.

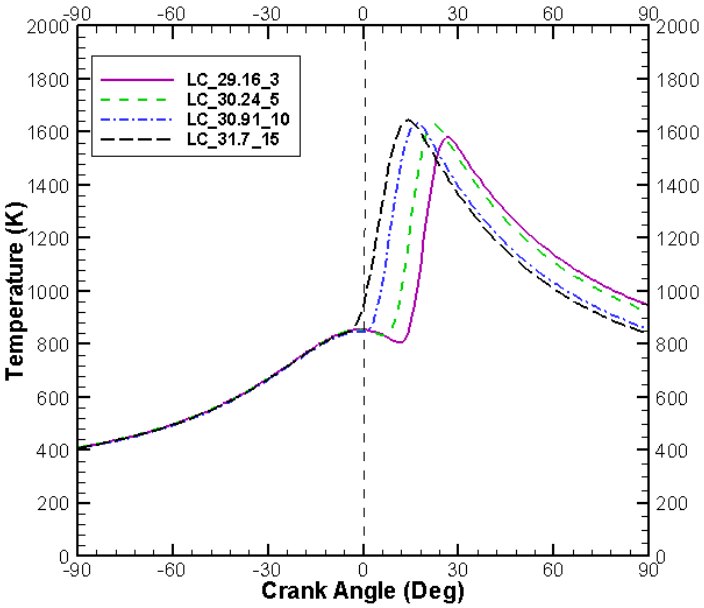

Fig. 99 Bulk gas temperatures versus crank angle for LC cases.

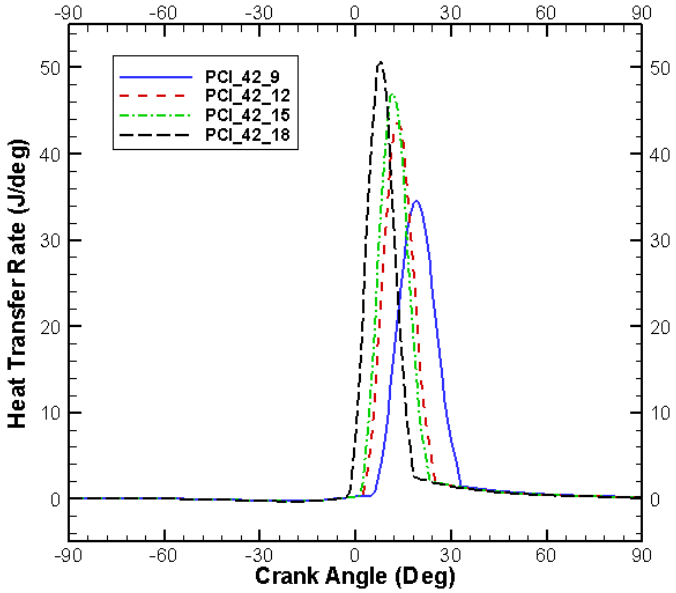

Fig. 100 Heat transfer rate versus crank angle for PCI cases with 42% EGR level.

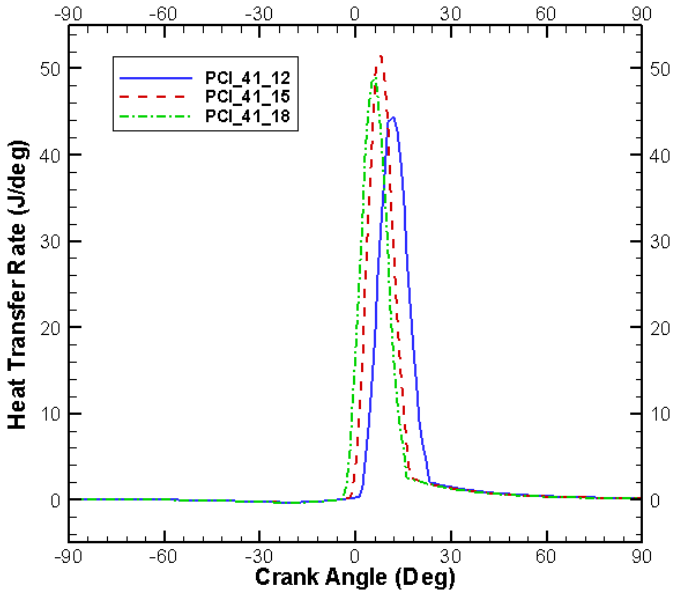

Fig. 101 Heat transfer rate versus crank angle for PCI cases with 41% EGR level.

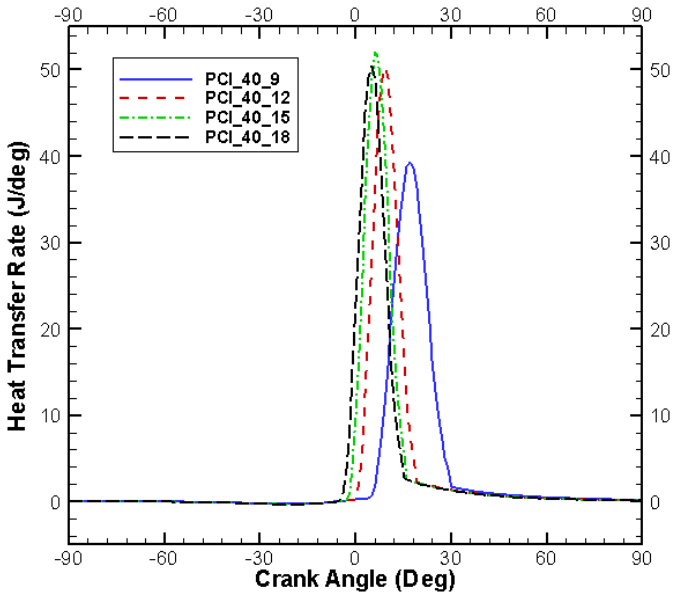

Fig. 102 Heat transfer rate versus crank angle for PCI cases with 40% EGR level.

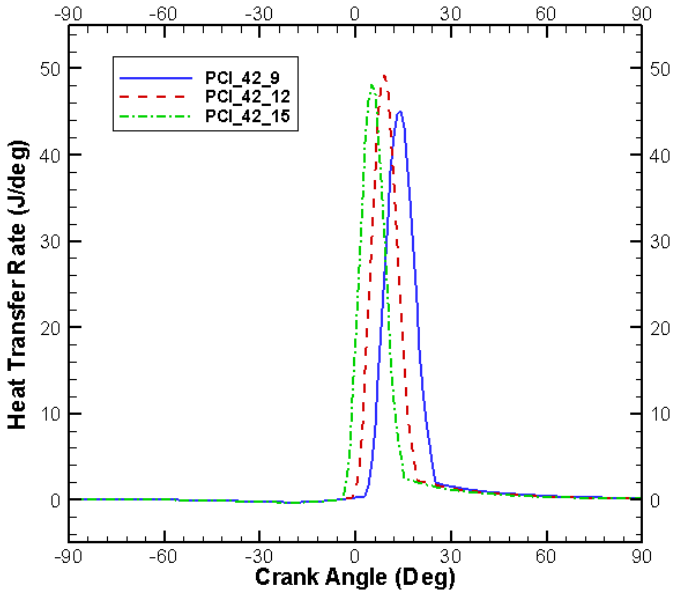

Fig. 103 Heat transfer rate versus crank angle for PCI cases with 39% EGR level.

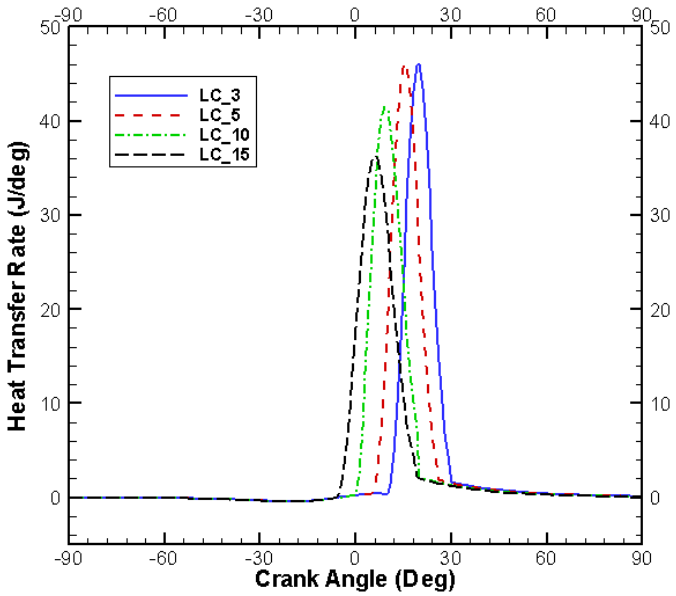

Fig. 104 Heat transfer rate versus crank angle for LC cases.

8.3.3 Combustion availability destruction

The percentage of availability destroyed in a combustion process decreases as the injection timing is advanced (except for the PCI cases using 39% EGR). This is unlike the trend observed for changing EGR levels. Combustion availability destruction was seen to be unchanging irrespective of the EGR level.

Even though the mode of combustion is same in all of the cases grouped together, the combustion temperature is significantly different because of the different injection timings used. Figures 105 – 109 show the comparison between the temperatures of the adiabatic zone for different injection timings. Higher temperatures are attained during advanced injection timing which cause reduced availability destruction via internal energy transfer. Higher temperatures are also maintained for a longer duration with the advanced injection timings. This further reduces combustion availability destruction.

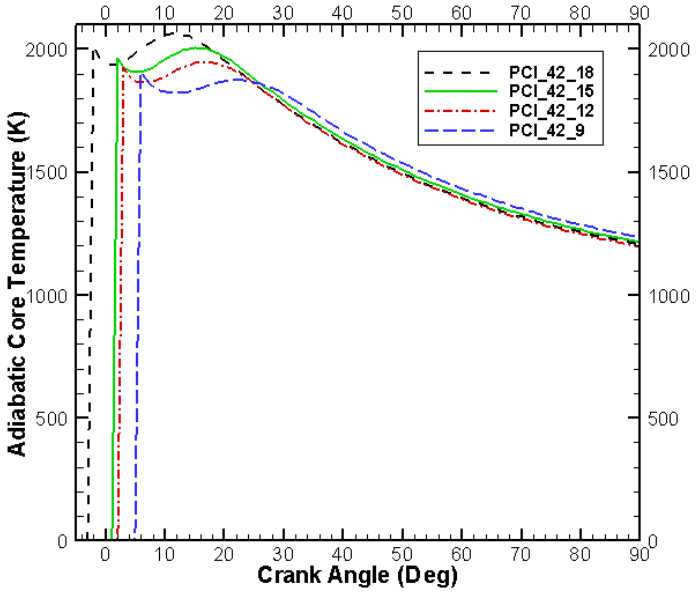

Fig. 105 Adiabatic core temperature versus crank angle for PCI cases with 42% EGR level.

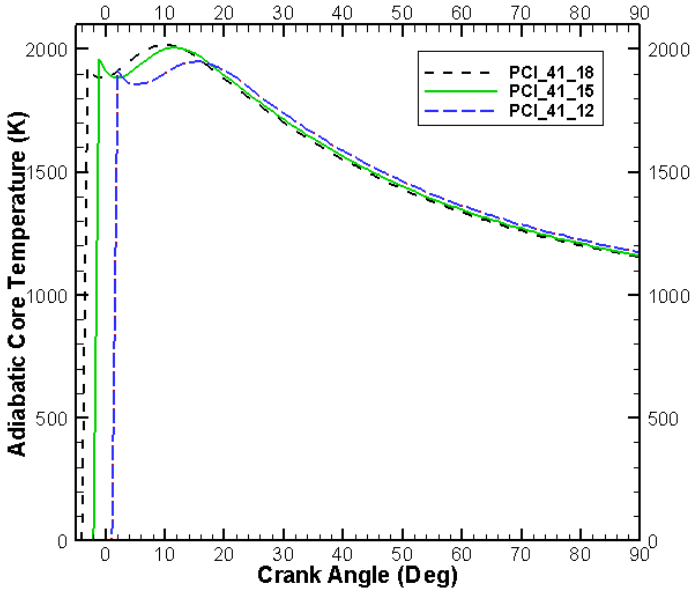

Fig. 106 Adiabatic core temperature versus crank angle for PCI cases with 41% EGR level.

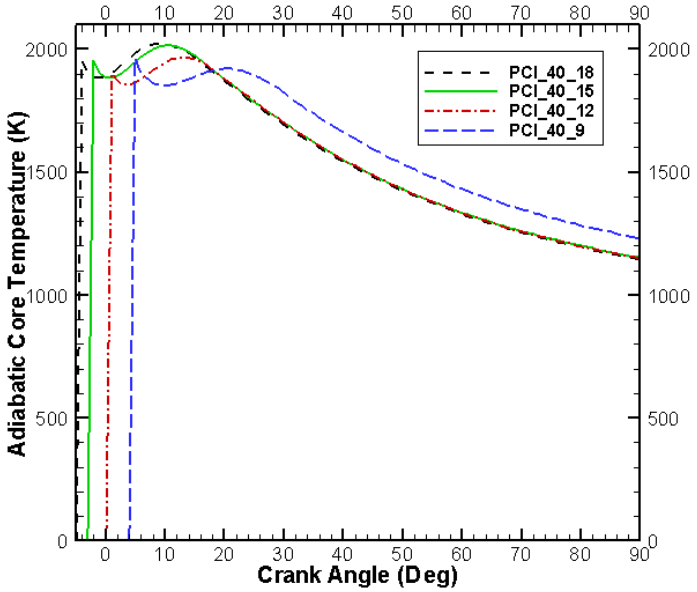

Fig. 107 Adiabatic core temperature versus crank angle for PCI cases with 40% EGR level.

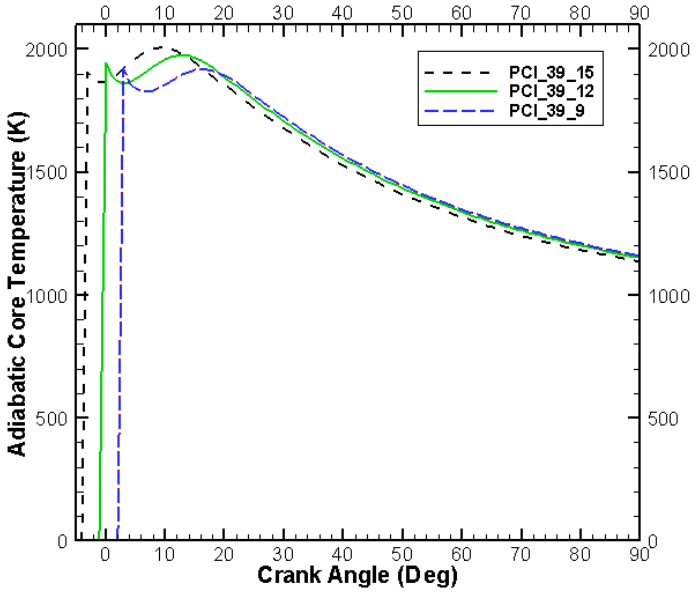

Fig. 108 Adiabatic core temperature versus crank angle for PCI cases with 39% EGR level.

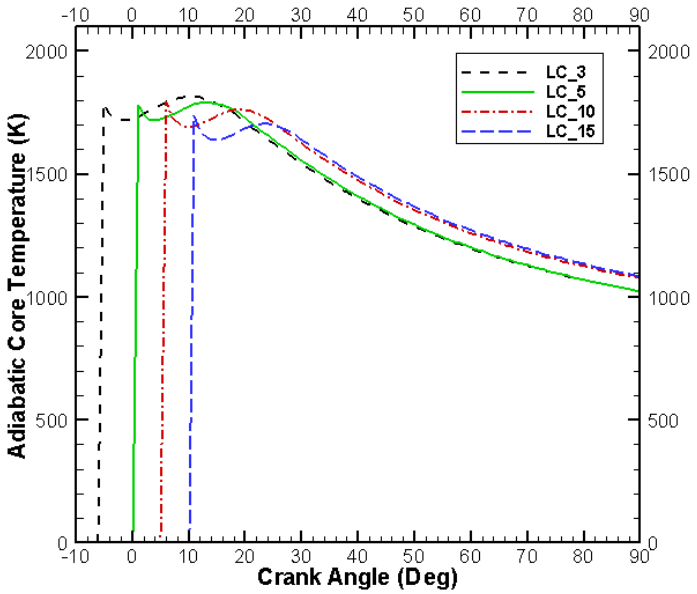

Fig. 109 Adiabatic core temperature versus crank angle for LC cases.

8.3.4 Net exhaust availability out

Percentage of net availability out decreases as the injection timing is advanced (except for the PCI cases using 39% EGR). With the retarded injection timing, and corresponding delayed start of combustion, the combustion takes place latter in expansion process. This may lead to less available time for heat transfer. There is also a less thermodynamic expansion with the delayed start of combustion. As a result, the temperature of the exhaust gas is expected to be higher for the delayed injection timing. The data gathered from the simulation runs, shown in Table 13, highlights this fact.

Table 13 Comparison of mass averaged exhaust gas temperature for PCI and LC cases

Injection Timing degree bTDC	Case nomenclature	Exhaust Gas Temperature (K)
9	PCI_42_9	619
12	PCI_42_12	573
15	PCI_42_15	564
18	PCI_42_18	534
12	PCI_41_12	567
15	PCI_41_12	540
18	PCI_41_18	527
9	PCI_40_9	614
12	PCI_40_12	554
15	PCI_40_15	536
18	PCI_40_18	528
9	PCI_39_9	591
12	PCI_39_12	558
15	PCI_39_15	536
3	LC_3	639
5	LC_5	618
10	LC_10	583
15	LC_15	567

8.3.5 Intake mixing destruction

As discussed earlier, this portion of the availability destruction depends primarily on the temperature and compositional changes between intake charge and residuals. The temperature difference is expected to be higher for the cases with delayed injection timing. But the same EGR levels used in these cases seems to have mitigated the differences. As a result, the percentage intake mixing destruction is almost equal in all the cases.

8.3.6 Fuel availability not used

As explained earlier, the percentage fuel availability not used is same for all PCI cases owing to the same Wiebe parameters used to simulate these cases. But different Wiebe parameters used in LC cases leads to variation in percentage fuel availability not used.

9. SUMMARY, CONCLUSIONS AND FUTURE SCOPE

A thermodynamic engine cycle simulation was used for the second law analysis of engine combustion processes. Simulation parameters were optimized to represent actual engine conditions as closely as possible. The influence of mode of combustion, injection timing and EGR level on the availability balance was examined. Even though the major components of availability balance were identified to be availability converted into indicated work, availability transfer through heat transfer, combustion availability destruction, availability transfer through exhaust, mixing availability destruction and fuel availability not used; only the first four components were seen to be more dominant and changes in those four components were more discernible with the parametric studies. The simulation results obtained are summarized below:

1. The percentage of availability converted into indicated work is nearly unchanged with changes in injection timing and EGR level. Even though the percentage of availability converted into indicated work was observed to be about equal for Best BSFC and LC mode of combustion, a significant drop in this percentage was observed in PCI mode as compared to LC mode.

2. Availability transferred through heat transfer decreased with increasing EGR levels and retarded injection timings. No trends could be identified for the mode of combustion; primarily because of the different fuel and air mass flow rates employed in

the cases studied for the mode of combustion analysis. The trends may be found out if these absolute values are matched while evaluating different modes of combustion.

3. Combustion availability destruction decreased with advanced injection timings. But it was unaffected by the changes in the EGR level. The mode of combustion was also seen to affect the combustion availability destruction. PCI mode showed the least while Best BSFC node showed the most combustion availability destruction suggesting that the PCI mode is more favorable for improving combustion efficiency.

4. Availability transferred through exhaust decreased with decreasing EGR levels and more retarded injection timings. Availability transfer through exhaust also decreased as the mode of combustion was changed from PCI to LC to Best BSFC.

An attempt is made to suggest an optimum strategy for efficient engine operations based on the above observations. These conclusions are summarized below:

1. Even though the availability converted into indicated work is unchanged by the changes in the EGR level, higher EGR levels are recommended. This is because of the fact that the availability transfer through heat transfer decreases while availability transfer through exhaust increases with increasing EGR levels. Higher EGR levels increase the exhaust gas temperatures. Higher exhaust gas temperatures are suitable for advanced aftertreatment devices. Higher EGR levels also tend to make combustion more premixed and thus would help in curbing the emissions formation.

2. Advanced injection timings (15° to 18° bTDC) are recommended as these are found to improve combustion efficiency.

3. PCI mode of combustion is recommended for better combustion efficiency. PCI mode also tends to make combustion more premixed and hence would aid in reducing emissions. There is a little penalty in switching the mode of combustion from Best BSFC to PCI in terms of reduction in percentage of availability converted into indicated work. But better matching of other operating variables such as injection timing, equivalence ratio can be sought to improve work output.

The activities recommended for future work are as follows:

1. As the simulation heat release model is fundamentally different from the actual modes of combustion, it is recommended to compare the results obtained for the second law parameters with standard tools intended for diesel engine combustion process.

2. Suggested strategy for optimum combustion processes can be verified and optimized through experiments. The suggested strategy does not take into consideration the implications on emissions formation. Hence the practicality of the suggested strategy can be evaluated based on emissions performance.

REFERENCES

1. **Jacobs, T.** Simultaneous Reduction of Nitric Oxide and Particulate Matter Emissions from a Light-Duty Diesel Engine Using Combustion Development and Diesel Oxidation Catalyst. PhD Dissertation, University of Michigan, Ann Arbor, 2005.

2. **Zhong L., Henein N.,** and **Bryzik W.** A New Predictive Model for Advanced High Speed Direct Injection Diesel Engines. Paper Presented at ASME Internal Combustion Engine Division 2004 Fall Technical Conference, Long Beach, California. ICEF2004-892.

3. **Desantes J., Arregle J.,** and **Molina S.** Influence of the EGR Rate, Oxygen Concentration and Equivalence Fuel/Air Ratio on the Combustion Behavior and Pollutant Emissions of a Heavy-Duty Diesel Engine. Paper Presented at SAE (2000) International Spring Fuels and Lubricants Meeting and Exposition, Warrendale, Pennsylvania. 2000-01-1813.

4. **Jacobs T., Assanis D.,** and **Filipi Z.** The impact of Exhaust Gas Recirculation on Performance and Emissions of a Heavy-Duty Diesel Engine. Paper presented at SAE (2003) World Congress, Detroit, Michigan. 2003-01-1068.

5. **Nitu, B., Singh I., Zhong L., Badreshany K., Henein N.,** and **Bryzik W.** Effect of EGR on Autoignition, Combustion, Regulated Emissions and Aldehydes in DI Diesel Engines. Paper presented at SAE International Congress and Exposition, Detroit, Michigan. 2002-01-1153.

6. **McTaggart-Cowan G., Rogak S., Hill P.,** and **Bushe W.** Effects of operating condition on particulate matter and nitrogen oxides emissions from a heavy-duty direct injection natural gas engine using cooled exhaust gas recirculation. *International Journal of Engine Research*, 2004, **5**, 499-511.

7. **Rakopoulos, C.D. and Giakoumis**, E.G. Second-law analyses applied to internal combustion engines operation. *Progress in Energy and Combustion Science*, 2006, **32** (1), 2-47.

8. **Flynn P. M., Hoag, K.L., Kamel, M. M.,** and **Primus, R. J.** A New Perspective on Diesel Engine Evaluation Based on Second Law Analysis. Society of Automotive Engineers, SAE Paper 840032, 1985.

9. **Primus, R. J.,** and **Flynn, P. F.** Diagnosing the Real Performance Impact of Diesel Engine Design Parameter Variation (A Primer in the Use of Second Law Analysis) International Symposium on Diagnostics and Modeling of Combustion in Reciprocating Engines, Tokyo, Japan. pp. 529-538, 1985.

10. **Van Gerpen, J.H. and Shripo, H. N.** Second law analysis of diesel engine combustion. *Trans ASME J Eng Gas Turbines Power*, 1990, **112**, 129-137.

11. **Gallo, W. L. R.,** and **Milanez, L. F.** Exergetic Analysis of Ethanol and Gasoline Fueled Engines. Society of Automotive Engineers, SAE paper 920809, 1992.

12. **Kyritis, D. C. and Rakopoulos, C. D.** Parametric Study of the Availability Balance in an Internal Combustion Engine Cylinder. SAE paper 2001-01-1263, 2001.

13. **Caton, J.** A Multiple-zone Cycle Simulation for Spark-Ignition Engines: Thermodynamic Details. Paper presented at 2001 Fall Technical Conference of the ASME-ICED, Argonne, IL.

14. **Waschni, G.** A Universally Applicable Equation for the Instantaneous Heat Transfer Coefficient in the Internal Combustion Engine. Society of Automotive Engineers, Transactions, SAE Paper 670931, vol. 76, pp. 3065-3083, 1967.

15. **Heywood, J.** *Internal Combustion Engine Fundamentals*, 1988, McGraw-Hill Inc., Singapore.

VITA

Name: Sushil S. Oak

Address: Texas A&M University, Department of Mechanical Engineering,
3123 TAMU, College Station, TX 77843-3123

Education: Bachelor of Engineering, Mechanical Engineering, Aug 2006
University of Mumbai, Maharashtra, India.

Master of Science, Mechanical Engineering, Aug 2008
Texas A&M University, College Station, Texas.